The PHILOSOPHICAL MAGAZINE

FIRST PUBLISHED IN 1798

. 2 Eighth Series No. 17 May 1957

A Journal of Theoretical Experimental and Applied Physics

PRICE £1 5s. 0d.
Annual Subscription £13 10s. 0d. payable in advance

ALERE FLAMMAM.
Printed and Published by
TAYLOR & FRANCIS LTD.
RED LION COURT, FLEET STREET, LONDON, E.C.4

The Thermal and Electrical Conductivity of Chromium at Low Temperatures†

By A. F. A. Harper, W. R. G. Kemp, P. G. Klemens, R. J. Tainsh and G. K. White‡

Division of Physics, Commonwealth Scientific and Industrial Research Organization, Sydney

[Received January 24, 1957]

Abstract

The electrical and thermal conductivities have been measured over a wide range of temperature of specimens of pure chromium, both in the ductile and embrittled states. It has been found that the low temperature conduction properties are very similar to those of other transition metals investigated. At low temperatures the electrical resistance is mainly due to the scattering of electrons from the s-band to the d-band, while (s–s) scattering contributes about 60% of the thermal resistance.

§ 1. Introduction

With the discovery that very pure chromium can be prepared in a ductile form (Wain *et al.* 1954–55), it has become possible to obtain specimens of the metal suitable for the accurate measurement of its thermal and electrical conductivities. These measurements are an extension of work on transition metals previously reported (Kemp *et al.* 1955, Kemp *et al.* 1956).

§ 2. Specimens

The specimens were supplied by Dr. H. L. Wain of the Aeronautical Research Laboratories of the Commonwealth Department of Supply in the form of rods, 8 cm long and 3 mm diameter. These had been prepared by forging high purity chromium in a sheath to form a bar of cross section 11 mm square, then grinding and electropolishing to size. A full description of the metallurgical properties of the metal are given in a series of papers by Greenway (1954–55). The purity of the metal is of the order of 99·998%.

The three specimens designated 1, 3 and 5 in the table, were supplied respectively in the cold worked condition, partially recrystallized and fully recrystallized. Recrystallization of ductile chromium leads to its embrittlement. After measurement specimens 1 and 3 were annealed *in vacuo* at 1050°C for 4 hours to become specimens 2 and 4.

† Communicated by the Authors.

‡ Now at the Division of Pure Physics, National Research Council, Ottawa.

The Specimens

Specimen number	Physical State	ρ_0 10^{-7} ohm cm	K_0/T W cm^{-1} deg^{-2}	$K_0\rho_0/T$ 10^{-8} W ohm deg^{-2}
1	Cold worked	2·55	$0{\cdot}092_3$	2·35
2	No. 1, annealed	1·81	0·135	2·44
3	Partially recrystallized	1·25	0·202	2·53
4	No. 3, annealed	0·90	0·275	2·48
5	Fully recrystallized	0·55	0·440	2·44
Theoretical Lorenz ratio		—	—	2·45

§3. Experimental Procedure and Results

The thermal conductivity measurements were made in a cryostat described previously (White 1953), and the electrical conductivities were measured simultaneously with the aid of a galvanometer amplifier (MacDonald 1947).

Fig. 1

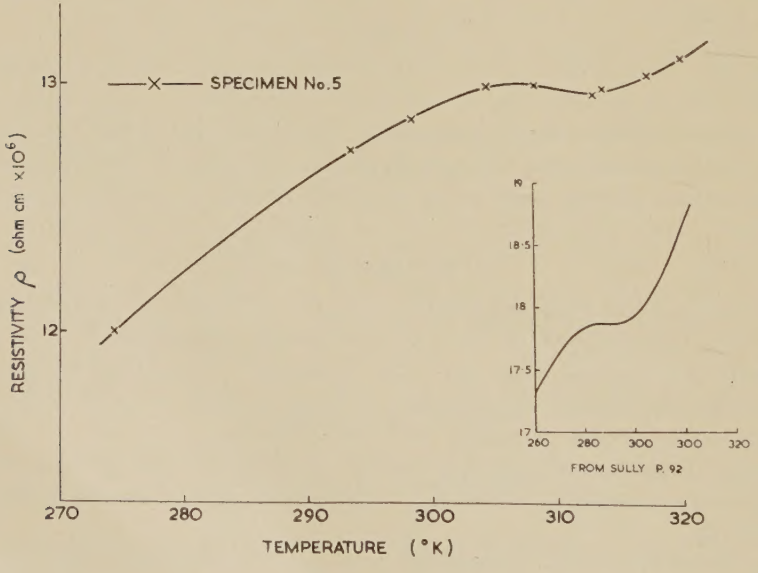

Resistivity of chromium.

Connections to the chromium were made by copper plating the ends of the specimens for a sufficient length to accommodate the end pieces and thermal and electrical connectors. These were attached by means of zinc–cadmium solder, which is not superconducting down to 2°K, the lowest temperature at which measurements were made.

Fig. 2

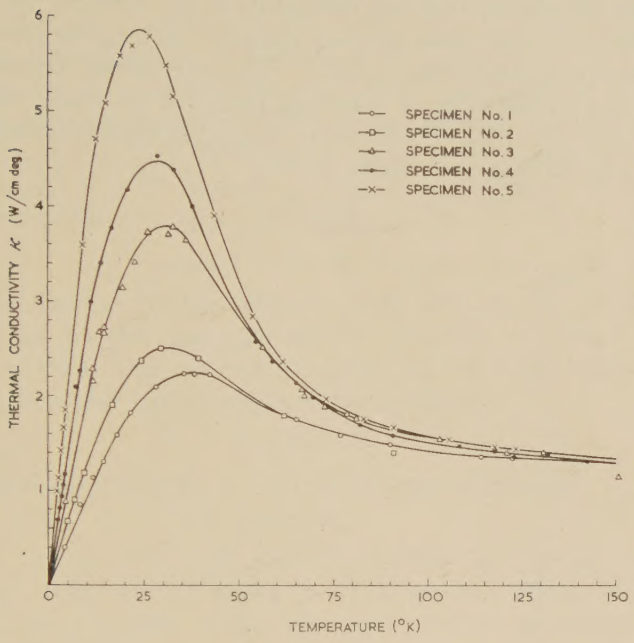

Thermal conductivity of chromium at low temperatures.

Fig. 3

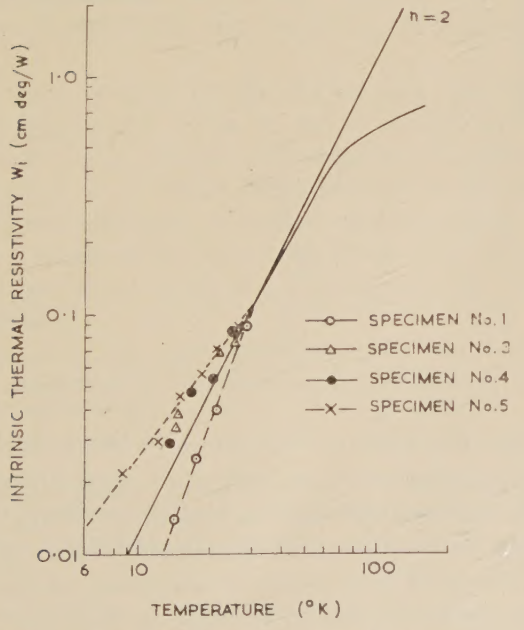

Intrinsic thermal resistivity of chromium

The electrical resistivity of specimen 5 above 273°K is shown in fig. 1. These results are similar to those quoted by Sully (1954, p. 92).

The thermal conductivities and the intrinsic thermal resistivities of all the specimens are shown in figs. 2 and 3. The intrinsic electrical resistivity of specimen 5 is shown in fig. 4. The high purity of specimen 5 is indicated by the low value ($4{\cdot}6 \times 10^{-3}$) of the ratio, ρ_0/ρ_{273}, of the electrical resistivity at lowest temperatures to its value at 0°C.

Fig. 4

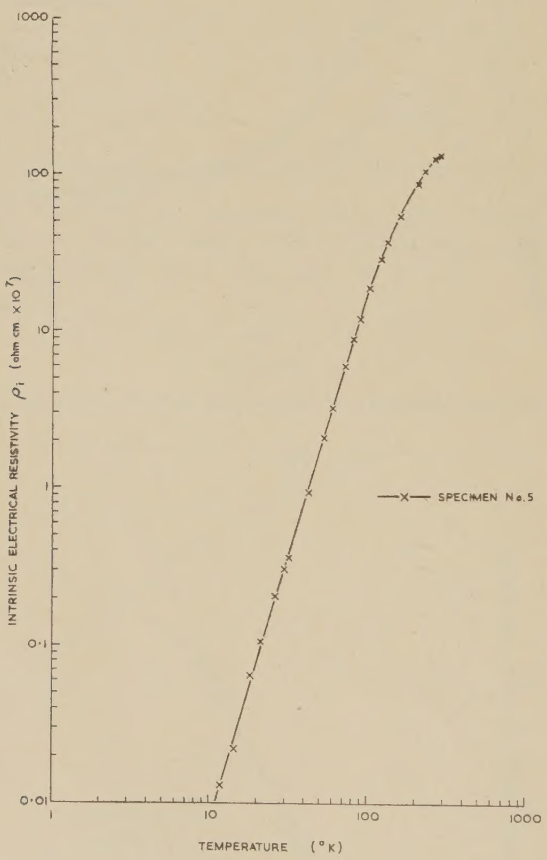

Intrinsic electrical resistivity of chromium.

§ 4. Analysis of Results and Discussion†

The electrical resistance is, to sufficient approximation, additively composed of the residual resistance ρ_0 and the intrinsic resistance ρ_i due to the scattering of electrons by static imperfections and lattice waves respectively :

$$\rho = \rho_0 + \rho_i, \quad . \quad . \quad . \quad . \quad . \quad . \quad . \quad . \quad . \quad (1)$$

† For a review of the theory see, for example, Klemens (1956).

ρ_0 is independent of temperature and ρ_i tends to zero at lowest temperatures. Thus ρ tends to a constant value at lowest temperatures. Values of ρ_0 thus obtained are given in the table. The intrinsic resistance ρ_i, shown in fig. 4 for specimen 5, which had the lowest value of ρ_0, varies as $T^{3\cdot2}$ between 10 and 100°K. This indicates that most of the intrinsic resistance is due to interactions taking electrons from states in the s-band into the d-band, for (s–s) scattering leads to a T^5 variation, while (s–d) scattering results in a T^3 dependence (Kemp *et al.* 1955). At about 30°K the intrinsic resistance is approximately given by

$$\rho_i \simeq 1{\cdot}1 \times 10^{-12} T^3 \text{ ohm cm.} \quad . \quad . \quad . \quad . \quad . \quad . \quad (2)$$

If heat conduction by the lattice can be disregarded, as seems most probable in the present case, the thermal resistivity is similarly composed of a residual and an intrinsic resistance due to the scattering of electrons by imperfections and lattice waves respectively.

$$W = W_0 + W_i \quad . \quad . \quad . \quad . \quad . \quad . \quad . \quad (3)$$

where W_0 and ρ_0 are related by the Wiedemann–Franz law

$$\rho_0 = L_0 W_0 T \quad . \quad . \quad . \quad . \quad . \quad . \quad . \quad . \quad . \quad (4)$$

and where $L_0 = 2{\cdot}45 \times 10^{-8}$ watt ohm deg^{-2} is the Sommerfeld value of the Lorenz ratio. This relation should hold irrespective of the details of the electronic band structure. From theory W_i would be expected to vary as T^2 for temperatures well below the Debye temperature (Klemens 1956) so that at lowest temperatures W_i should be negligible relative to W_0 and K should vary as T. This has been found to be so and in the table are given values of K_0/T, the low temperature limit of K/T, and of $K_0\rho_0/T$. The latter values do not differ significantly from L_0, as is required by eqn. (4).

Values of W_i deduced from (3) for the various specimens have been plotted in fig. 3. Above 30°K all points fall on a single curve, which from 30°K to 50°K, is a T^2 curve. Below 30°K there is a considerable scatter of the deduced values of W_i. Below about 10°K W_i is too small a fraction of the total thermal resistance to permit any conclusion to be drawn about the derived values of W_i, but from 10° to 30°K there is a definite trend for these values to lie above the T^2 curve except for specimen 1. Thus for all specimens

$$W_i = 1{\cdot}1 \times 10^{-4} T^2 \text{ cm deg } W^{-1} \text{ for } 30°\text{K} < T < 50°\text{K}. \quad . \quad . \quad (5)$$

and for all except specimen no. 1

$$W_i = 4{\cdot}3 \times 10^{-4} T^{1\cdot6} \text{ cm deg } W^{-1} \text{ for } 10°\text{K} < T < 30°\text{K}. \quad . \quad . \quad (6)$$

It is not clear whether the deviation from the T^2 relationship below 30°K is significant. A careful evaluation of the experimental procedures has failed to reveal any source of error which could account for the deviation. If it is real it would not seem possible to account for it on the basis of the (s–d) scattering, especially as there is no corresponding anomaly in the electrical resistance.

If expression (5) is taken to apply to lowest temperatures

$$L_i = \frac{\rho_i}{W_i T} = 0{\cdot}4 L_0. \quad . \quad . \quad . \quad . \quad . \quad . \quad . \quad (7)$$

In the case of transition metals the thermal resistance is due to (s–s) and (s–d) scattering, so that $W_i = W(s, s) + W(s, d)$, similarly

$$\rho_i = \rho(s, s) + \rho(s, d).$$

Now at low temperatures

$$W(s, s) \propto T^2 \text{ and } W(s, d) \propto T^2, \text{ while } \rho(s, s) \propto T^5 \text{ and } \rho(s, d) \propto T^3$$

see Klemens (1956). For (s–d) scattering the Wiedemann–Franz law should be satisfied, so that $\rho(s, d) = L_0 T W(s, d)$. Hence

$$L_i = \frac{W(s, d)}{W(s, d) + W(s, s)} L_0 \quad . \quad . \quad . \quad . \quad . \quad . \quad (8)$$

and in the present case $W(s, d)/W(s, s) = 0{\cdot}7$. This may be compared with a value of 0·5 for the corresponding ratio in the case of palladium (Kemp *et al.* 1955) and 0·8 in the case of nickel and iron (Kemp *et al.* 1956).

The high and low temperature values of W_i are related by

$$\frac{W_i(T_1)}{W_i(T_2)} \frac{\theta^2}{T_1^2} = C \quad T_1 \ll \theta < T_2. \quad . \quad . \quad . \quad . \quad . \quad (9)$$

From present value (6) of $W_i(T_1)$ and the high temperature limit of 1·54 watt^{-1} cm deg for $W(T_2)$ (Sully 1954, p. 103) $C = 29$, using for θ the value $\theta_D = 630°$K, the Debye temperature derived from the low temperature specific heat of chromium (Rayne and Kemp 1956).

Theoretically, for a single band of N electrons per atom, $C = 64\, N^{2/3}$ (Klemens 1954). If it is assumed that the ratio $W(s, s)/W(s, d)$ is independent of temperature, this value should also apply to (9), because the single band theory should apply to the component $W(s, s)$. Although there is gross disagreement (by a factor of order 4) between the theoretical and experimental values of C for the monovalent metals, in the case of palladium (Kemp *et al.* 1955) it was found that close agreement with theory was obtained if it was assumed that $N = 0{\cdot}6$ and a value of $1{\cdot}50\theta_D$ was used for θ to allow for longitudinal waves only being able to interact with conduction electrons in an s-band satisfying the results of the Bloch theory. In the present cases if the same values of N and θ/θ_D are used the theoretical value is about 30% less than the experimental one. When allowance is made for the uncertainties in the number of electrons in the s-band and in the appropriate values to use for θ and indeed for θ_D†, it may be concluded that, as with palladium, there is substantial agreement

† Other values for θ_D (Simon and Ruhemann 1927, Anderson 1937, Estermann *et al.* 1952, Wolcott 1956) are all lower than the value used here, the lowest being 418°K. A value of 538°K would give complete agreement between theory and experiment.

between the theoretical and experimental results, in support of the conclusion that the Bloch theory yields better results when applied to (s–s) transitions in these metals than when applied to the monovalent metals.

Acknowledgment

The authors wish to thank Dr. Wain, of the Aeronautical Research Laboratories, Department of Supply, for the specimens and for providing metallurgical advice.

References

Anderson, C. T., 1937, *J. Amer. Chem. Soc.*, **59**, 488.
Estermann I., Friedburg, S. A., and Goldman, J. E., 1952, *Phys. Rev.*, **87**, 582.
Greenway, H. T., 1954–55, *J. Inst. Met.*, **83**, 121.
Henderson, F., Quaass, S. T., and Wain, H. L., 1954–55, *J. Inst. Met.*, **83**, 126.
Kemp, W. R. G., Klemens, P. G., Sreedhar, A. K., and White, G. K., 1955, *Phil. Mag.*, **46**, 811.
Kemp, W. R. G., Klemens, P. G., and White, G. K., 1956, *Aust. J. Phys.*, **9**, 180.
Klemens, P. G., 1954, *Aust. J. Phys.*, **7**, 64.
Klemens, P. G., 1956, Thermal Conductivity of Solids at Low Temperatures—*Encyclopedia of Physics*, **14** (Berlin : J. Springer).
MacDonald, D. K. C., 1947, *J. Sci. Instrum.*, **24**, 232.
Rayne, J. A., and Kemp, W. R. G., 1956, *Phil. Mag.*, **1**, 918.
Simon, F., and Ruhemann, M., 1927, *Phys. Chem.*, **129**, 321.
Sully, A. H., 1954, *Chromium* (London : Butterworths Scientific Publications).
Wain, H. L., Henderson, F., and Johnstone, S. T. M., 1954–55, *J. Inst. Met.*, **83**, 133.
White, G. K., 1953, *Proc. Phys. Soc.* A, **66**, 559.
Wolcott, N. M., 1956, Conference de Physique des Basses Temperatures. Paris, p. 286.

On the Activation Energy of High Temperature Creep in Metals†

By Paul Feltham
The University, Leeds

[Received in revised form February 11, 1957]

Abstract

The temperature dependence of the activation volume or 'stress-concentration factor' q appearing in the expression

$$d\epsilon/dt = A \exp(-H/kT) \sinh(q\sigma/kT)$$

relating the equilibrium tensile creep rate $d\epsilon/dt$, the temperature T and the applied tensile stress σ has been studied in the case of several pure metals subject to creep above about $\frac{1}{2}T_m$, where T_m is the melting point. On writing $q=nb^3$, where b is the distance of closest approach of atoms in the lattice, the relation

$$n = n_0 \exp\left[-\frac{Q}{kT}\left(1-\frac{T}{T_m}\right)\right]$$

was found to be valid in all cases, with $Q=\alpha T_m$ and $\alpha=4{\cdot}9$ (cal/g atm)/°K, i.e. Q is equal to about twice the latent heat of melting. The increase of q with temperature is ascribed to the increase in the mean spacing between adjacent logs in screw dislocations, and Q appears to be the activation energy for the conservative motion of jogs along dislocations. In face-centred cubic metals large values of n_0 are found to be associated with low stacking fault energies, and *vice versa*.

§ 1. Introduction

In a recent paper Mott (1956) suggested that in cases of high temperature creep in metals in which the steady, second-stage, or equilibrium creep rate $d\epsilon/dt$ obeys a law of the form

$$d\epsilon/dt = A \exp(-H/kT) \sinh(q\sigma/kT),$$

where σ is the applied tensile stress, H the activation energy of volume self-diffusion, and where A may be regarded as approximately constant over considerable ranges of the temperature, the rate determining mechanism may be the migration of segments of screw dislocations impeded by jogs. One would then expect the activation volume q to be given by

$$q = \tfrac{1}{2}l\mathbf{b}^2 = \tfrac{1}{2}nb^3, \quad \ldots\ldots\ldots \quad (1)$$

† Communicated by the Author.

where $l(=nb)$ is the length of a segment of screw dislocation bordered on each side by a jog, and **b** is the Burgers vector. The jogs in the moving dislocations are assumed to form as the latter cut through other screw dislocation of the forest. Mott noted that l might depend upon the temperature ; as to the nature of this variability suitable data were not however available. The principal purpose of the present work was to obtain such data.

§ 2. The Effect of Microstructure on the Magnitude of q

The creep data compiled by Kauzmann (1941) and the recent results obtained with aluminium by Dorn (1956) seem to show that in the steady state of creep q increases with temperature, but is independent of the applied stress. Seeger (1955 a, b), who considered the temperature dependence of the inter-jog spacing qualitatively for certain types of deformation, also believes that, irrespective of the distance travelled by a screw dislocation through the forest, an average distance between jogs, corresponding to a dynamical equilibrium, should tend to establish itself. Further, a preliminary compilation of q-values obtained from data on the creep of a number of metals (Feltham 1953, 1956), shows that

(*a*) in pure polycrystalline metals q, measured in each case at the same fraction of the melting temperature T_m, is of the same order of magnitude, e.g. with $T/T_m \simeq 0{\cdot}6$ $q = 70 \pm 10$ (cal/g atm)/(kg/cm^2) in lead, aluminium and zinc.

(*b*) In annealed single crystals, in which essentially only one slip system operates during creep, q may be an order of magnitude greater than in polycrystals of the same metals flowing at the same respective temperatures.

(*c*) Still higher q-values are found with single crystals of exceptionally high purity, e.g. $q = 2 \times 10^4$ (cal/g atm)/(kg/cm^2) in the case of zinc of purity 99·999%, flowing at room temperature, but

(*d*) as the creep data on steels show (Feltham 1953), the effect of elements in dilute solid solution on the value of q is much less pronounced in polycrystals ; q decreases only slowly with increasing alloy content.

(*e*) In precipitation hardened dilute alloys q is about an order of magnitude smaller than in the corresponding pure polycrystalline parent metals.

(*f*) Finally, q does not appear to depend upon the grain size, provided of course the grains are sufficiently small in relation to the dimensions of the specimen to allow the latter to be regarded as truly polycrystalline. This conclusion is based on recent data on the creep of lead (Feltham 1956). Also, the general law of the temperature dependence of q, indicated by the parallelism of the lines in the figure, does not seem to be affected by the temperature dependence of the grain size, for the parallelism was maintained irrespective of whether the grain size was kept constant (as for copper), or was allowed to increase as the temperature increased (all remaining metals).

§ 3. The Temperature Dependence of q

In view of the observations listed above, particularly however because of (*a*), it was decided to consider the temperature dependence of q in polycrystalline metals of comparable high purity (99·99%), thus attempting to avoid complications such as might arise with alloys, or with single crystals sensitive to handling or very small differences in impurity content.

The results shown in the figure in which $\frac{1}{2}n$ (eqn. (1)) is plotted against T_m/T, where T_m is the melting temperature of the respective metal, except in the case of the body-centred alpha-iron (actually 0·4%C steel), for which T_m was taken to be the A_3-point. (850°C). As the lines in the figure are drawn parallel, the equation of any one of them is given by

$$n=N \exp(-Q/kT), \qquad (2)$$

with $Q=\alpha T_m$, and $\alpha=4{\cdot}9$ (cal/g atm)/°K. For a given metal N is a constant.

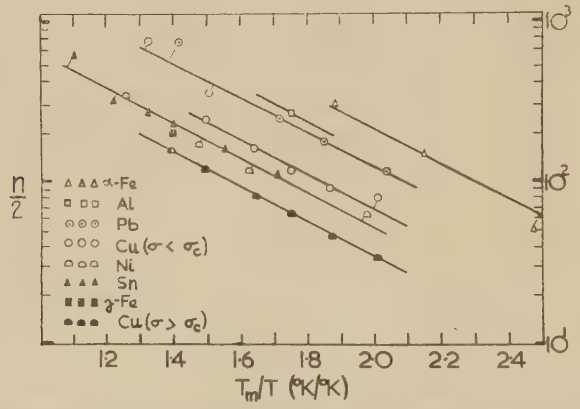

The relation between n (eqn. (2)) and the ratio T_m/T, where T_m is the melting point, except for alpha-iron for which T_m has been taken as the A_3-point (850°C). The data have been compiled from the following sources: Kauzmann (1941) (alpha-iron); Dorn (1956) (aluminium); Tyte (1938, 1939) (lead and tin); Meakin (unpublished) (copper); Weertman and Shahinian (1956) (nickel); Feltham (1953) (gamma-iron).

It should be noted that two separate lines are given for copper, depending on whether the applied stress σ falls below or above a critical stress σ_c. In so far as the equilibrium creep must be regarded as a recovery process, it must be affected by variations in the mechanism of work hardening. Now, preliminary results obtained by Meakin (1957), and the study of the modes of work-hardening in polycrystalline copper (Feltham and Meakin 1957 a) and of the creep of lead (Feltham 1956) seem to point to the conclusion that the mode of hardening in the creep of copper at stresses below σ_c is of the type treated theoretically by Friedel (1955), while above σ_c it is probably fine slip. The data relating to nickel were also obtained with $\sigma \gg \sigma_c$ (Meakin 1957), and this applies also to the remaining face-centred cubic metals.

§ 4. Discussion

The values of Q, of the latent heat of melting L, and of the ratio Q/L are given in the table. It can be seen that in the case of the face-centred cubic metals $Q/L \simeq 2{\cdot}0$, i.e. the activation energy Q is small, just sufficient for 'melting' a group of about two atoms. The absolute magnitude of Q, and the essential constancy of Q/L for all face-centred cubic metal for which data were available, suggest that the activation energy of the process described by eqn. (2) is that for the conservative motion of jogs along dislocations. The local derangement of atoms, being akin to melting, would however be expected to have an activation energy of the form

$$E = Q[1-(T/T_m)], \quad \ldots\ldots\ldots \quad (3)$$

involving the entropy of melting. It is probable, therefore, that in eqn. (2)

$$N = n_0 \exp(Q/kT_m), \quad \ldots\ldots\ldots \quad (4)$$

where, as is easily seen by substituting for N from eqn. (4) into eqn. (2), n_0 is the value of n when $T = T_m$, and is obtained from the figure by extrapolation of the lines to the left.

	Sn	Pb	Al	Cu	Ni	Fe (gamma)
Q $\frac{\text{kcal}}{\text{g atm}}$	2·5	2·9	4·6†	6·6	8·5	8·8†
L $\frac{\text{kcal}}{\text{g atm}}$	1·7	1·3	2·6	3·2	4·3	3·6
Q/L	1·5	2·2	1·8	2·1	2·0	2·4
$n_0 \times 10^{-3}$	1·2	9·0	1·4	1·6 and 0·8	1·2	1·2

† Values uncertain.

It can be seen that n_0 decreases in the order Al, Pb, Ni, Fe, Cu. Now, the stacking fault energies for aluminium, nickel and copper decrease in the order in which they are named (Seeger 1955 a). On the basis of Seeger's theoretical considerations one would also expect the stacking fault energies of the transition metals nickel and (gamma-) iron to be close together, similarly for the polyvalent metals aluminium and lead. Evidence in support of a high stacking fault energy in lead has also recently been obtained by Feltham and Meakin (1957 b) from experiments on the mode of work hardening of lead single crystals at low temperatures. Thus n_0 appears to decrease in the same order as the stacking fault energies. The full significance of the variability of n_0 from metal to metal is not, as yet, clear; from Seeger's (1955 b) treatment of the temperature dependence of the flow stress of close-packed metals n_0 would be expected to increase rather than decrease in the above order.

Acknowledgment

I am indebted to Mr. J. D. Meakin for the data relating to copper, and for assistance with the analysis of the data relating to nickel.

References

Dorn, J. E., 1956, *Symposium on Creep and Fracture of Metals at High Temperatures* (London : H.M. Stationery Office), p. 89.
Feltham, P., 1953, *Proc. Phys. Soc.* B, **66,** 865 ; 1956, *Ibid.*, **69,** 1173.
Feltham, P., and Meakin, J. D., 1957a, *Phil. Mag.*, **2,** 115 ; 1957b, *Acta Met.*, **5,** (in the press).
Friedel, J., 1955, *Phil. Mag.*, **46,** 1169.
Kauzmann, W., 1941, *Trans. Amer. Inst., Min. Met. Eng.*, **143,** 57.
Meakin, J. D., 1957, *J. Met.*, **9** (April).
Mott, N. F., 1956, *Symposium on Creep and Fracture of Metals at High Temperatures* (London : H.M. Stationery Office), p. 21.
Seeger, A., 1955a, *Defects in Crystalline Solids* (London : The Physical Society) p. 238 ; 1955b, *Phil. Mag.*, **46,** 1194.
Tyte, L. C., 1938, *Proc. Phys. Soc.*, **50,** 153 ; 1939, *Ibid.*, **51,** 203.
Weertman, J., and Shahinian, P., 1956, *J. Met.*, **8,** 1223.

Small Angle Scattering from Deformed Metals†

By H. H. Atkinson
Crystallographic Laboratory, Cavendish Laboratory, Cambridge

and R. D. Lowde
Metallurgy Division, A.E.R.E., Harwell, Berkshire

[Received January 29, 1957]

Recent experiments on the small angle scattering of x-rays of wavelength 1·54 A from pure metal foils have shown that the intensity measured in the range of scattering angles 1° to 6° is increased by cold working the specimen (Blin and Guinier 1953, Blin 1954). Blin (1954) has suggested that the effect is due to the formation in the metal of cavities with diameters of about 30 A, since the intensity of scattering was thought to be too great to be caused by dislocations (Dexter 1953). However, Beeman *et al.* (1957) have shown that at least part of the scattering at low angles is due to rays which have suffered two successive Bragg reflections. Surface irregularities also appear to contribute to the intensity (Robinson and Smoluchowski 1956). These two effects may have been present in Blin's experiments, and his interpretation is therefore open to doubt.

Both these sources of error can be avoided by studying instead the low angle scattering of slow neutrons. Firstly, it is possible to use wavelengths sufficiently long so that no Bragg reflections occur: secondly, for most metals the true absorption cross section for neutrons is very small, and therefore thick specimens can be used for which the surface effects are negligible. Such an experiment has been carried out on copper using a neutron beam (from the Harwell pile BEPO) which has passed through a bismuth filter (Egelstaff and Pease 1954). This filtered neutron beam had a mean wavelength of 8·7 A and contained less than 0·3% of neutrons capable of Bragg reflection in copper.

Polycrystalline copper specimens of commercial purity and 99·995% purity were used in the form of bars 0·6 cm thick. Recrystallized material and specimens deformed by an extension of 10% gave the same total intensity to within 0·003 barns steradian^{-1} atom^{-1} over the range of scattering angles 2° to 12°. This scattering cross section is equivalent to less than one hundredth of the x-ray scattering observed by Blin. It follows that at least 99% of the effect reported by Blin was due to processes other than true small angle scattering from defects in the volume of the metal.

A full account of the experiment will be published later.

---

† Communicated by the Authors.

References

Beeman, W. W., Kaesberg, P., Anderegg, J. W., and Webb, M. B., 1957, *Handbuch der Physik*, **32**, 440.
Blin, J., 1954, *Thesis*, University of Paris.
Blin, J., and Guinier, A., 1953, *C.R. Acad. Sci., Paris*, **236**, 2150.
Dexter, D. L., 1953, *Phys. Rev.*, **90**, 1007.
Eglestaff, P. A., and Pease, R. S., 1954, *J. Sci. Instr.*, **31**, 207.
Robinson, W. H., and Smoluchowski, R., 1956, *J. Appl. Phys.*, **27**, 657.

Electric Polarizability of Atoms and Molecules†

By J. A. Pople and P. Schofield
Department of Theoretical Chemistry, University of Cambridge

[Received November 12, 1956]

Abstract

Kirkwood's variation method for the calculation of the polarization of an atom or molecule in an external potential $V(\mathbf{r})$, uses a wave function

$$\Psi_0\left\{1+\mu\sum_i V(\mathbf{r}_i)\right\}$$

where Ψ_0 is the wave function in the absence of the perturbation, and the summation is over the electrons. The energy is varied with respect to the parameter μ. In this paper an extension of the method is presented using a wave function

$$\Psi_0\left\{1+\sum_i u(\mathbf{r}_i)\right\}$$

and varying the energy with respect to the function $u(\mathbf{r})$. The optimum form is found to satisfy a second order differential equation which involves the single and pair electron density functions.

This equation is solved numerically for argon, using the Hartree–Fock wave function. The form of u turns out to be nearly quadratic, and shows that almost the whole of the induced dipole moment is due to the outer shell of the electrons. An estimate of the dipole–dipole energy is made using the function u, which in the case of argon gives good agreement with that estimated by other means.

§ 1. Introduction

The theory of the electronic polarization of atoms and molecules proceeds by investigating the change in the energy and wave function under a perturbing electrostatic potential $V(\mathbf{r})$, the nuclei being held in fixed positions. In the particular case of polarization by a uniform field $\mathbf{E}$ the potential has the form $-\mathbf{E}\,.\,\mathbf{r}$ but other potentials may be of interest in dealing with problems of molecular interaction. It is possible to get a formal expression for the change in wave function due to $V(\mathbf{r})$ by perturbation theory. This is not the most convenient method in practice, however, as it requires detailed knowledge of the excited electronic states of the unperturbed system (including continuum states). Most work has therefore been based on variational methods.

† Communicated by the Authors.

An important method was evolved by Kirkwood (1932) who used a variation function

$$\Psi=\Psi_0\left\{1+\mu\sum_i V(\mathbf{r}_i)\right\}, \quad . \quad . \quad . \quad . \quad . \quad . \quad . \quad . \quad (1)$$

where Ψ_0 is the unperturbed wave function and the summation is over all the electrons. The parameter μ is varied to minimize the energy in the applied field. For an atom in a uniform field this leads to the expression

$$\alpha=(4/N)\left\{\int\Psi_0^*\left(\sum_i \mathbf{r}_i\cos\theta_i\right)^2\Psi_0\,d\tau\right\}^2 \quad . \quad . \quad . \quad . \quad (2)$$

for the molecular polarizability, where N is the number of electrons in the atom.

The chief disadvantage of a variation function of this type is its limited flexibility with only one variable parameter. Since Ψ_0 is multiplied by a function of V only, no allowance is made for the different polarizability of different parts of the molecule, or for the screening of the inner part of the molecule from the external field by the polarization of the outer. Later work has attempted to correct this in various ways mostly based on changes in individual orbital functions (Buckingham 1937, Sternheimer 1954). The aim of the present paper is to describe a method which is a simple generalization of the Kirkwood method and which gives direct information about the relative contribution of different parts of the molecule to the polarization. The variation function chosen is

$$\Psi=\Psi_0\left\{1+\sum_i u(\mathbf{r}_i)\right\}, \quad . \quad . \quad . \quad . \quad . \quad . \quad . \quad . \quad (3)$$

where $u(\mathbf{r})$ is a one-electron function. Since the modifying factor $\{1+\sum_i u(\mathbf{r}_i)\}$ is symmetric in the coordinates of all electrons, the total function is still antisymmetric. The form of $u(\mathbf{r})$ is then chosen to minimize the energy in the perturbed system. This leads to a simple partial differential equation.

§ 2. General Theory

We shall use a wave function of the type (3) and minimize the energy for the Hamiltonian

$$\mathscr{H}=\mathscr{H}_0+\sum_i V(\mathbf{r}_i). \quad . \quad . \quad . \quad . \quad . \quad . \quad . \quad . \quad (4)$$

It will be supposed that the perturbing potential V does not have the same symetry as $\mathscr{H}_0$.

Ψ_0 will satisfy the unperturbed equation

$$\mathscr{H}_0\Psi_0=\mathscr{E}_0\Psi_0 \quad . \quad . \quad . \quad . \quad . \quad . \quad . \quad . \quad . \quad (5)$$

and will be taken as normalized. It will be assumed that no magnetic fields are present so that all wave functions may be taken as real. It is convenient to choose the zero of energy so that

$$\int\Psi_0\left[\sum_i V(\mathbf{r}_i)\right]\Psi_0 d\tau=0 \quad . \quad . \quad . \quad . \quad . \quad . \quad . \quad (6)$$

the integration being over all electronic coordinates.

It can then be shown (Buckingham 1937) that the calculated second order change in $\mathscr{E}$ takes the form (using atomic units)

$$\mathscr{E}_2=\tfrac{1}{2}\int \Psi_0 \sum_i [\mathrm{grad}_i u(\mathbf{r}_i)]^2 \Psi_0 d\tau + 2\int \Psi_0 \Big[\sum_i u(\mathbf{r}_i)\Big]\Big[\sum_j V(\mathbf{r}_j)\Big]\Psi_0 d\tau. \quad . \quad (7)$$

This is the expression that has to be minimized by varying $u(\mathbf{r})$. It can be simplified if we define two density functions

$$\rho_1(\mathbf{r}_1)=N\int \Psi_0^2 d\tau_2 d\tau_3 \ldots d\tau_N\, ds_1$$

$$\rho_2(\mathbf{r}_1, \mathbf{r}_2)=N(N-1)\int \Psi_0^2 d\tau_3 d\tau_4 \ldots d\tau_N\, ds_1\, ds_2 \quad . \quad . \quad (8)$$

the integration $d\tau$ being over all but one or two of the N electrons. $\rho_1(\mathbf{r})$ is the electron density and $\rho_2(\mathbf{r}_1, \mathbf{r}_2)$ the density function in pair space. In terms of these functions, $\mathscr{E}_2$ can be written

$$\mathscr{E}_2=\tfrac{1}{2}\int (\mathrm{grad}\ u)^2 \rho_1(\mathbf{r}) d\mathbf{r} + 2\int \sigma(\mathbf{r}) u(\mathbf{r}) d\mathbf{r} \quad . \quad . \quad . \quad . \quad . \quad (9)$$

where

$$\sigma(\mathbf{r})=\rho_1(\mathbf{r})V(\mathbf{r})+\int V(\mathbf{r}')\rho_2(\mathbf{r}, \mathbf{r}')\, d\mathbf{r}'. \quad . \quad . \quad . \quad . \quad . \quad (10)$$

The integrals in (9) and (10) are now over the coordinates of a single electron. If the function $u(\mathbf{r})$ is varied in (9)

$$\delta\mathscr{E}_2=\int \rho_1\, (\mathrm{grad}\ u\ .\ \mathrm{grad}\ \delta u)\, d\mathbf{r} + 2\int \sigma \delta u\, d\mathbf{r}$$

$$=\int \delta u \{2\sigma - \mathrm{div}\ (\rho_1\, \mathrm{grad}\ u)\}\, d\mathbf{r} \quad . \quad . \quad . \quad . \quad . \quad . \quad . \quad (11)$$

since $\rho \to 0$ sufficiently rapidly at infinity. Hence the energy $\mathscr{E}_2$ is minimized if u satisfies the equation

$$\mathrm{div}\ (\rho_1\, \mathrm{grad}\ u)=2\sigma \quad . \quad . \quad . \quad . \quad . \quad . \quad . \quad . \quad . \quad (12)$$

with appropriate boundary conditions. The value of $\mathscr{E}_2$ is then given by either of the forms

$$\mathscr{E}_2=-\tfrac{1}{2}\int (\mathrm{grad}\ u)^2 \rho_1\, d\mathbf{r}=\int \sigma u\, d\mathbf{r} \quad . \quad . \quad . \quad . \quad . \quad . \quad . \quad (13)$$

$\rho_1(\mathbf{r})$ and $\sigma(\mathbf{r})$ are given functions if Ψ_0 is known and eqn. (12) is then equivalent to the general electrostatic problem of determining the potential in a field of variable charge density and dielectric constant. In practice only an approximate function Ψ_0 will be available, but this can be used to find approximations for ρ_1 and σ.

§ 3. The Polarization of Atoms and Ions in Uniform Fields

The simplest application of eqn. (12) is to find the function $u(\mathbf{r})$ for a spherically symmetric atom or atomic ion in a uniform field $\mathbf{E}$. If this is measured in atomic units

$$V=Er\cos\theta \quad . \quad . \quad . \quad . \quad . \quad . \quad . \quad . \quad . \quad . \quad (14)$$

using spherical polar coordinates with the direction of the electric field as polar axis. From the symmetry of the system σ and u will also have the form

$$\sigma=Es(r)\cos\theta,\ u=Eg(r)\cos\theta. \quad . \quad . \quad . \quad . \quad . \quad (15)$$

The Kirkwood approximation in this case corresponds to taking $g(r)$ proportional to r. The equation for its optimum form is

$$\frac{1}{r^2}\frac{d}{dr}\left(r^2\rho_1\frac{dg}{dr}\right)-\frac{2g\rho_1}{r^2}=2s. \quad . \quad . \quad . \quad . \quad . \quad . \quad (16)$$

The boundary conditions are that $g=0$ at $r=0$ since $g\cos\theta$ must be uniquely defined, and that $\rho_1 g^2 \to 0$ as $r\to\infty$ so that the wave function is small at large distances. The polarizability α is then given by

$$\alpha=\frac{4\pi}{3}\int_0^\infty\left\{2g^2+r^2\left(\frac{dg}{dr}\right)^2\right\}\rho_1 dr$$
$$=-\frac{8\pi}{3}\int_0^\infty sgr^2dr. \quad . \quad . \quad . \quad . \quad . \quad . \quad . \quad . \quad . \quad (17)$$

The simplest example is the hydrogen atom for which

$$\rho_1=\pi^{-1}\exp(-2r),\ s=\pi^{-1}r\exp(-2r). \quad . \quad . \quad . \quad (18)$$

The solution of (16) is then the familiar result

$$g=-(r+\tfrac{1}{2}r^2);\ \alpha=\tfrac{9}{2}. \quad . \quad . \quad . \quad . \quad . \quad . \quad . \quad (19)$$

Equation (16) can be solved for other atoms and ions if estimates of the functions $s(r)$ and $\rho_1(r)$ are obtained from Hartree–Fock wave functions. This has been carried out in detail for argon using the orbitals tabulated by Hartree and Hartree (1938). They give

$$U(r)=4\pi r^2\rho_1(r) \quad . \quad . \quad . \quad . \quad . \quad . \quad . \quad . \quad (20)$$

and $P_{ne}(r)$ where P_{ne} is r times the radial part of the orbital, the angular part being normalized to $(1/4\pi)$. Defining

$$F=U^{1/2}g \quad . \quad . \quad . \quad . \quad . \quad . \quad . \quad . \quad . \quad (21)$$

(16) becomes

$$\frac{d^2F}{dr^2}=\left\{\frac{2}{r^2}+U^{-1/2}\frac{d^2}{dr^2}(U^{1/2})\right\}F+2U^{-1/2}\Phi \quad . \quad . \quad . \quad . \quad . \quad (22)$$

where Φ is obtained from eqn. (10) and, after integrating over angle, becomes

$$\Phi=Ur-4\sum_{n=1,2,3}\sum_{n'=2,3}P_{n0}P_{n'1}\int_0^\infty P_{n'1}P_{n0}r\,dr. \quad . \quad . \quad . \quad (23)$$

Equation (22) was solved numerically by taking $F(0)=0$ and adjusting $F'(0)$ so that $F(r)\to 0$ as $r\to\infty$. A check on the solution is obtained by calculating α from both expressions (17).

The resulting function $g(r)$ is shown in fig. 1 together with the linear function $g(r)=-0{\cdot}61r$ obtained by the Kirkwood procedure. The significance of the difference between these functions is best illustrated by the corresponding function $M(r)$ defined so that $M(r)dr$ is the contribution of electrons in the shell $(r, r+dr)$ to the dipole moment in unit field.

The total dipole moment is given by

$$\int_0^\infty M(r)dr=-\int\Psi\sum_i r_i\cos\theta_i\Psi d\tau \quad . \quad . \quad . \quad . \quad . \quad (24)$$
$$=-\int\rho_1' r\cos\theta d\mathbf{r}$$

where ρ_1' is the perturbed electron density,

$$\rho_1'(r_1)=N\int \Psi_0^2\left\{1+E\sum_i g(r_i)\cos\theta_i\right\}^2 d\tau_2\ldots d\tau_N$$

$$=\rho_1(\mathbf{r}_1)+2E\{\rho_1(\mathbf{r}_1)g(r_1)\cos\theta_1+\int\rho_2(\mathbf{r}_1,\mathbf{r}_2)g(r_2)\cos\theta_2\,d\mathbf{r}_2\}+O(E^2). \quad . \quad . \quad . \quad (25)$$

In terms of the functions used in the calculation, the second term is

$$\frac{2E}{4\pi r^2}\left\{Ug-4\sum_{n=1,2,3}\sum_{n'=2,3}P_{n0}P_{n'1}\int_0^\infty P_{n'1}P_{n0}g\,dr\right\}\cos\theta \quad . \quad . \quad (26)$$

Fig. 1

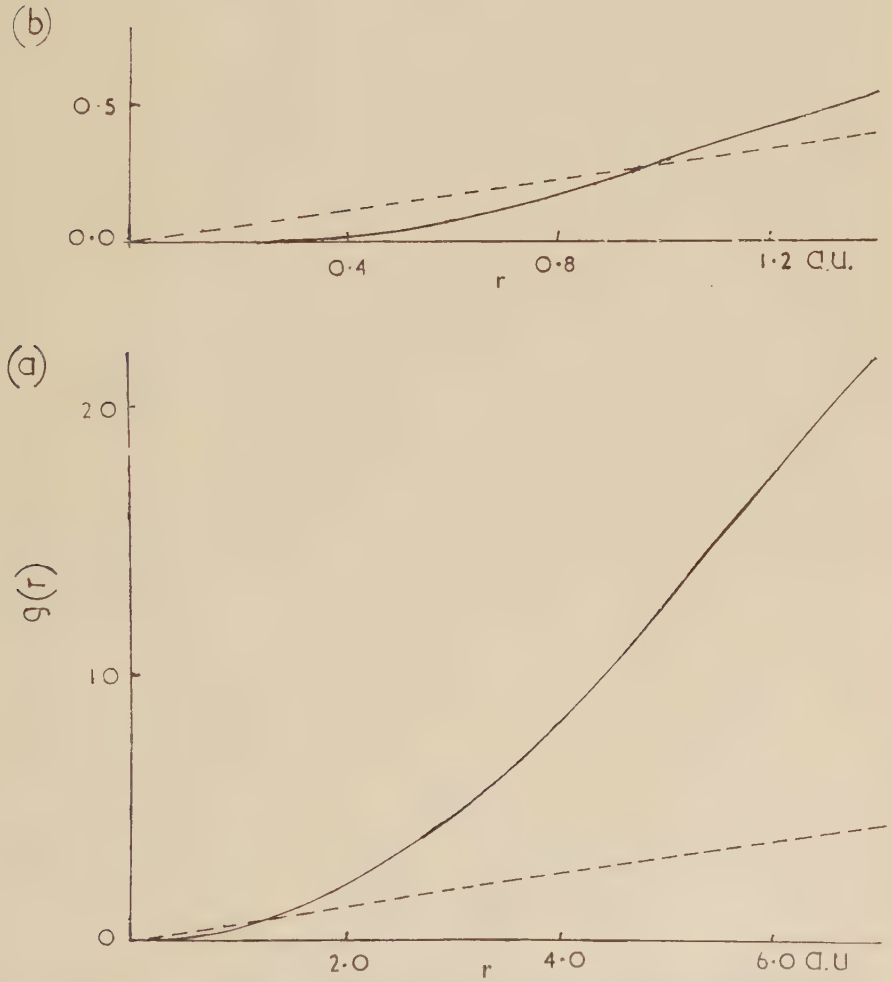

(*a*) The function $g(r)$ for argon. The continuous line shows the optimum form, and the broken line the best linear function, $g(r)=-0{\cdot}61r$. (*b*) shows the behaviour of $g(r)$ over the region of the ' inner shells '.

Fig. 2

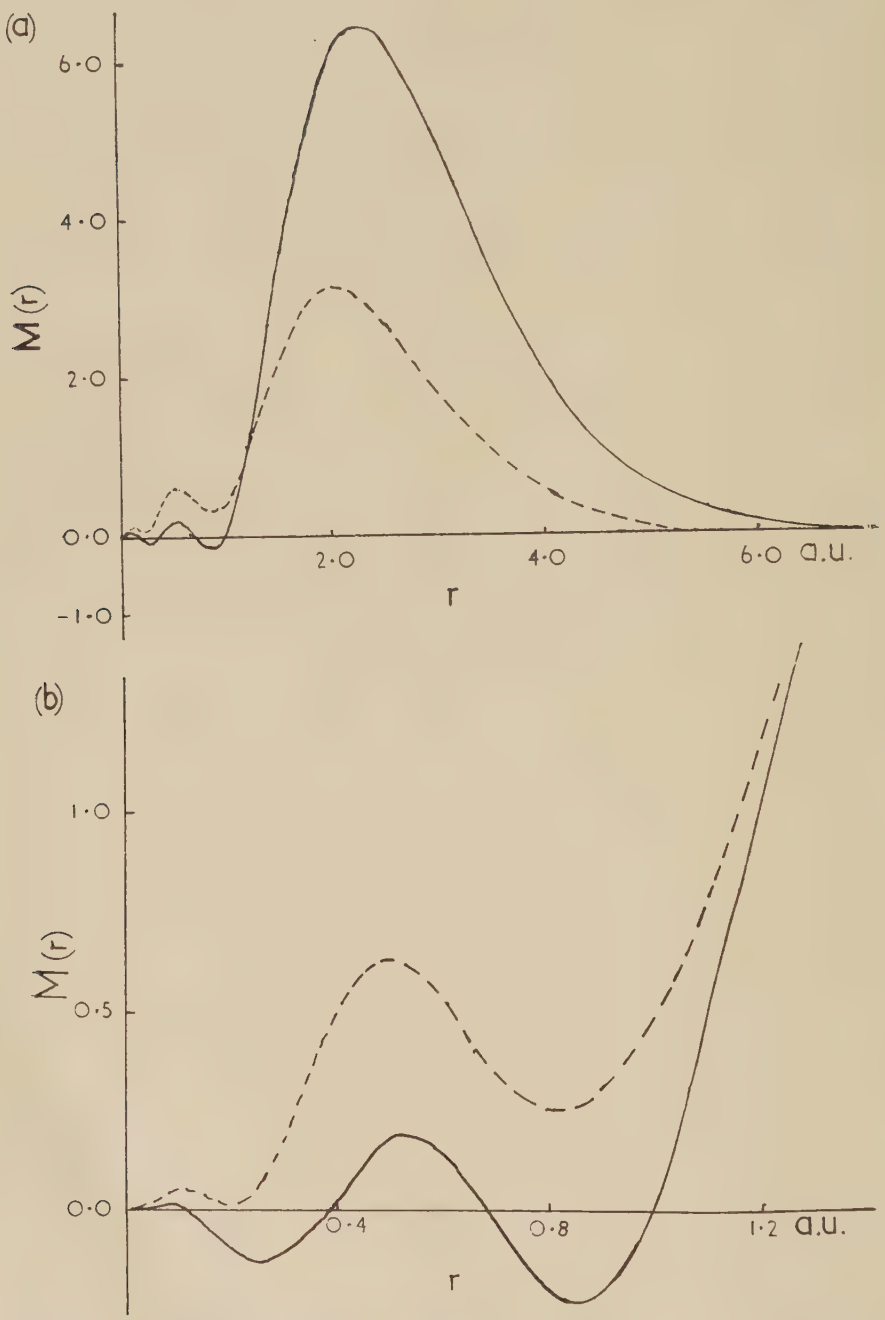

(*a*) The function $M(r)$ for argon. $M(r)dr$ is the contribution of electrons in the shell $(r, r+dr)$ to the dipole moment induced in unit field. The continuous line shows the function obtained with the optimum $g(r)$, and the broken line that obtained with the linear $g(r)$. (*b*) The behaviour of $M(r)$ over the region of the ' inner shells '.

so that

$$M(r)=-\tfrac{2}{3}\left\{Ug-4\sum_{n=1,2,3}\sum_{n'=2,3}P_{n0}P_{n'1}\int_0^\infty P_{n'1}P_{n0}g\,dr\right\}dr \quad . \quad . \quad (27)$$

$M(r)$ is shown in fig. 2.

From the general form of the functions it is clear that the Kirkwood method over-estimates the induced moment in the inner region of the atom but under-estimates it for the outer shell. The Kirkwood result is greatly improved if a variation function with two variable parameters,

$$g=\lambda r+\mu r^2 \quad . \quad . \quad . \quad . \quad . \quad . \quad . \quad . \quad . \quad (28)$$

is used. In fact the function $-0{\cdot}02r-0{\cdot}49r^2$, obtained in this way, is a very close approximation to the optimum form. The calculated values of α are compared with the experimental value in the table.

The polarizability of argon

Optimum $g(r)$	$2{\cdot}03\times10^{-24}$ cm^3
$g(r)=-0{\cdot}61r$	$0{\cdot}98\times10^{-24}$ cm^3
$g(r)=-0{\cdot}02r-0{\cdot}49r^2$	$1{\cdot}95\times10^{-24}$ cm^3
Observed	$1{\cdot}69\times10^{-24}$ cm^3

§ 4. The Dipole–Dipole Interaction of Two Atoms

An estimate of the dipole–dipole term in the van der Waals interaction between two atoms at large separation may be made using the function $g(r)$ calculated in § 3.

Let R be the internuclear distance and (x_i, y_i, z_i), (x_i', y_i', z_i') the coordinates of the electrons in the two atoms relative to their respective nuclei, with the z-axis along the line of centres. Then the dipole–dipole interaction is represented by the addition of a perturbing term to the Hamiltonian

$$V=R^{-3}\sum_{i=1}^{N_1}\sum_{j=1}^{N_2}(x_ix_j'+y_iy_j'-2z_iz_j') \quad . \quad . \quad . \quad . \quad (29)$$

where N_1 and N_2 are the numbers of electrons in each atom.

If R is sufficiently large for overlap between electrons on different atoms to be negligible, the wave function for the unperturbed system is

$$\Psi_0=\Psi_1\Psi_2 \quad . \quad . \quad . \quad . \quad . \quad . \quad . \quad . \quad . \quad (30)$$

where Ψ_1 and Ψ_2 are the ground state wave functions of the two atoms. Writing the perturbed wave function

$$\Psi=\Psi_0\{1+u(\mathbf{r}_i, \mathbf{r}_j')\} \quad . \quad . \quad . \quad . \quad . \quad . \quad (31)$$

the second order energy takes the form

$$\mathcal{E}_2=\tfrac{1}{2}\int\Psi_1\Psi_2\left\{\sum_{i=1}^{N_1}(\mathrm{grad}_i u)^2+\sum_{j=1}^{N_2}(\mathrm{grad}_j u)^2\right\}\Psi_1\Psi_2 d\tau_1 d\tau_2$$
$$+2\int\Psi_1\Psi_2 uV\Psi_1\Psi_2 d\tau_1 d\tau_2. \quad . \quad . \quad . \quad . \quad . \quad . \quad . \quad . \quad . \quad (32)$$

The variational function suggested is

$$u=\lambda R^{-3}\sum_{i=1}^{N_1}\sum_{j=1}^{N_2}\frac{g_1(r_i)g_2(r_j')}{r_i r_j'}(x_i x_j'+y_i y_j'-2z_i z_j') \quad . \quad . \quad . \quad (33)$$

λ being chosen to minimize the energy. Physically, this means that the field at atom 1 due to each configuration of electron in atom 2 is weighted as if atom 2 is polarized in some average field of magnitude λR^{-3}, and *vice versa*.

With the function (33),

$$\mathscr{E}_2=R^{-6}\{\tfrac{3}{2}\lambda^2(\alpha_1\beta_2+\alpha_2\beta_1)+3\lambda\alpha_1\alpha_2\} \quad . \quad . \quad . \quad . \quad . \quad (34)$$

where α_1, α_2 are the polarizabilities of the atoms, and

$$\beta=-\int_0^\infty M(r)g(r)r^{-1}dr. \quad . \quad . \quad . \quad . \quad . \quad . \quad (35)$$

The minimum value of $\mathscr{E}_2$ occurs when $\lambda=-\alpha_1\alpha_2(\alpha_1\beta_2+\alpha_2\beta_1)$ and gives for the dipole–dipole constant

$$c_{12}=\tfrac{3}{2}\frac{\alpha_1^2\alpha_2^2}{\alpha_1\beta_2+\alpha_2\beta_1}. \quad . \quad . \quad . \quad . \quad . \quad . \quad . \quad (36)$$

When $g(r)=\lambda r$, then this gives Kirkwood's formula (1932)

$$c_{12}=\tfrac{3}{2}\frac{\alpha_1\alpha_2}{\sqrt{(\alpha_1/N_1)}+\sqrt{(\alpha_2/N_2)}}. \quad . \quad . \quad . \quad . \quad . \quad (37)$$

For atomic hydrogen, where $g(r)=-r-\frac{1}{2}r^2$, (36) gives $c=6{\cdot}36$ a.u., compared with 6·00 a.u. given by (37). A more accurate variation treatment gives $c=6{\cdot}499$ a.u. (Pauling and Beach 1935).

For argon, using the optimum $g(r)$ and the calculated polarizability the result is $c=109\times10^{-60}$ ergs cm^6. This is expected to be larger than the true value since the polarizability is too large. In fact this value is close to the inverse sixth power coefficient in the Lennard–Jones 6–12 potential obtained from viscosity data, which contains contributions from induced quadruple and higher moments.

Acknowledgment

One of the authors (P.S.) wishes to acknowledge the receipt of a D.S.I.R. Maintenance Allowance during the tenure of which this work was carried out.

References

Buckingham, R. A., 1937, *Proc. Roy. Soc.* A, **160,** 94.
Hartree, D. R., and Hartree, W., 1938, *Proc. Roy. Soc.* A, **166,** 450.
Kirkwood, J. G., 1932, *Z. Phys.*, **33,** 57.
Pauling, L., and Beach, J. Y., 1935, *Phys. Rev.*, **47,** 686.
Sternheimer, R. M., 1954, *Phys. Rev.*, **96,** 951.

The Inter-Diffusion of Two Charged Particles (with particular reference to Ion-Exchange in Zeolites)†

By I. R. Beattie
Department of Chemistry, King's College, London

and

D. R. Davies
Department of Mathematics, The University, Sheffield

[Received January 2, 1957]

Summary

The general importance of ion exchange is mentioned, together with the work of previous investigators. The mechanism whereby two ions may change places is examined, and it is concluded that in many cases two ions diffusing in opposite directions in a charged substrate will diffuse independently of one another *apart from any space charge effects*. An equation is developed relating the amount of material exchanged during a reaction with the square root of the duration of the experiment. Practical applications of this equation are briefly discussed, as is the effect of immiscibility of solid solutions within the exchanger.

§ 1. Introduction

Ion exchange may be represented by the simple equation

$$ZA\ (s)+B^+\ (aq.) \rightleftharpoons ZB\ (s)+A^+\ (aq.),$$

where A and B are, for example, two unlike monovalent cations. The anionic framework (Z) of the solid exchanger (ZA) may be either organic or inorganic in nature. Both the kinetics of the exchange process and the final equilibrium position are of fundamental interest, although only the former will be discussed in this paper. In the case of zeolitic exchangers (aluminosilicates containing loosely held water), the material is usually available only as an irregularly shaped powder. Studies on the diffusion of ions in to and out of the zeolite are frequently carried out by immersing the solid in a well-stirred solution of known concentration. The mathematical treatment of the results is considerably simplified if the time is short enough, or the diffusion coefficient low enough, for the external surface area of the solid to be treated as a reasonably accurate representation of the cross sectional area into which diffusion has occurred. In this case the powdered zeolite may be regarded as a semi-infinite solid.

† Communicated by the Authors.

A further simplification is achieved if the concentration of the exchanging species in solution can be kept at a constant value throughout the duration of an experiment. The concentration at the interface may then be put equal to the equilibrium concentration at time infinity. The usual method of maintaining a constant concentration is applied by having two solid salts, each containing one of the exchanging species, in equilibrium with the solution.

Quantitative data on ion exchange in zeolites have been obtained by Barrer and others (1953, 1954, 1955, 1956), although in many instances the presence of two immiscible solid solutions has complicated any theoretical treatment of the results. Conduction processes in anhydrous analcites and chabazites ($M_2O \cdot Al_2O_3 \cdot 4\,SiO_2$) have been examined by Beattie (1954). In certain cases these zeolites constitute an ideal system where the alumino–silicate network remains unchanged throughout an ion exchange. Further, the possibility of cation–cation interactions other than through electrostatic forces is unlikely in a zeolite such as analcite. Each ion may then be considered to be uninfluenced by the nature of the neighbouring cations, apart from any stoichiometric requirements. A general understanding of ion exchange is essential for many purposes. Examples of ion exchange are to be found in biological systems, in soils, in water treatment, in the weathering of glasses, and in the separation of the rare earths. Fundamental studies on ideal exchanges are likely to be of particular importance in the interpretation of more complex cases. A formal mathematical treatment of ion exchange has not previously been given in the literature. It is the purpose of this paper to examine mathematically the process of ion exchange in a system in which the normal Fickian diffusion would occur in the absence of any effects due to an induced electric field.

There is a number of ways in which ion exchange may occur in crystals in general, and in zeolites in particular. These are considered separately below.

§ 2. Direct Exchange

This is essentially the simultaneous exchange of places by two ions A and B. It may be brought about in a number of ways, involving different numbers of ions. Any mechanism involving only two ions is unlikely for steric and energetic reasons. It may be noted that none of these processes is significant in relation to the conduction of an electric current. The exact significance of ion exchange rates from the point of view of individual diffusion coefficients is difficult to assess if simultaneous migration of two different species is a fundamental of the process.

§ 3. Independent Migration

A process involving the simultaneous migration of several ions is likely to be less favourable than diffusion by a defect mechanism. It has

recently been shown (Beattie 1955) that over part of the composition range both ions in a heteroionic crystal of analcite may migrate independently, apart from a certain necessary stoichiometry. In a case where ion exchange is occurring the two ions will diffuse independently *apart from any space-charge effects*. If two similarly charged particles are migrating in a structure, unless the diffusion coefficients of the two ions are equal, an electric field will be developed in such a direction that the rate of migration of the slower moving ion would be expected to increase, while that of the faster moving would decrease. In the steady state the two rates would be equal, with the measured rate of ion exchange dependent upon the diffusion characteristics of the two ions concerned.

Mott and Guerney (1950) give for the migration of an ion in an electric field the formula

$$J_1 = -D_1 \frac{\partial C_1}{\partial x} + EC_1 v_1 \quad . \quad . \quad . \quad . \quad . \quad . \quad . \quad (1)$$

where J_1=ionic current, D_1=diffusion coefficient, C_1=concentration, E=field strength, v_1=ionic mobility and x= distance in the direction of diffusion.

Suffix 1 refers to ion 1. Where two ions are migrating in opposite directions an exactly analogous expression may be written for ion 2. The elimination of E between these two equations, plus the use of the Einstein relationship between diffusion and conduction, yields eqn. (2).

$$\frac{J_1}{C_1 D_1} - \frac{J_2}{C_2 D_2} = \frac{\partial}{\partial x}[\ln (C_2/C_1)]. \quad . \quad . \quad . \quad . \quad . \quad (2)$$

The ionic current at x is J_1, while at $(x+\delta x)$ it is $J_1+(\partial J_1/\partial x)\,\delta x$. The rate of accumulation between the two planes defined by x and $(x+\delta x)$ is therefore given by

$$-(\partial J_1\ \partial x)\,\delta x = (\partial C_1\ \partial t)\,\delta x. \quad . \quad . \quad . \quad . \quad . \quad . \quad . \quad (3)$$

In order to proceed with this analysis it is necessary to make a simplifying assumption that the ionic flow in each direction is the same. This is equivalent to assuming the attainment of steady state conditions and can only be regarded as an approximation.

Putting $J_1 = -J_2$, and hence $\partial C_1/\partial x = -\partial C_2/\partial x$, eqn. (2) becomes

$$J_1 = \frac{\partial C_1}{\partial x}\left[\frac{C^* D_1 D_2}{C^* D_2 + C_1(D_1 - D_2)}\right] \quad . \quad . \quad . \quad . \quad . \quad (4)$$

with a corresponding expression for J_2. Here $C^* = C_1 + C_2$ = a constant.

Using eqn. (3) we obtain the result

$$\frac{1}{C^* D_1 D_2} \cdot \frac{\partial C_1}{\partial t} = \frac{\partial}{\partial x}\left[\frac{\partial C_1}{\partial x} \cdot \frac{1}{C^* D_2 + C_1(D_1 - D_2)}\right]. \quad . \quad . \quad (5)$$

For the case of the semi-infinite solid the boundary conditions are given below.

$C_1 = C_0'$ at $t=0$ for $x>0$.

$C_1 = C_\infty'$ at $x=0$ for $t>0$.

We first derive an approximate solution which is applicable in certain cases. Putting $C^*D_1D_2t=T$, and

$$\frac{C^*D_2+C_1(D_1-D_2)}{C^*D_2+C_0'(D_1-D_2)}=\exp(\theta_1)$$

then eqn. (5) may be written

$$\frac{\partial\theta_1}{\partial T}=\frac{\exp(-\theta_1)}{C^*D_2+C_0'(D_1-D_2)}\cdot\frac{\partial^2\theta_1}{\partial x^2}. \quad . \quad . \quad . \quad . \quad . \quad . \quad (6)$$

The new boundary conditions are

$$\theta_1=0 \text{ at } T=0 \text{ for } x>0.$$

$$\theta_1=\ln\left[\frac{C^*D_2+C_\infty'(D_1-D_2)}{C^*D_2+C_0'(D_1-D_2)}\right]=\theta_\infty' \text{ at } x=0 \text{ for } t>0.$$

If θ_1 is small, then this equation may be simplified to read

$$\frac{\partial\theta_1}{\partial T}=\frac{1}{C^*D_2+C_0'(D_1-D_2)}\cdot\frac{\partial^2\theta_1}{\partial x^2}. \quad . \quad . \quad . \quad . \quad . \quad . \quad (7)$$

Equation (7) will be valid for the conditions

(*a*) $T\to 0$, when $\theta_1\to 0$,

(*b*) D_1 is approximately equal to D_2 and

(*c*) C_1 is near to C_0'.

Although conditions (*b*) and (*c*) are not met with frequently, the solution of eqn. (7) may be of use in some particular cases. The appropriate solution of eqn. (7) may be expressed in the well known and easily computable form

$$\theta_1=\theta_\infty'[1-\text{erf}\{x\sqrt{[C^*D_2+C_0'(D_1-D_2)]}/2\sqrt{T}\}]. \quad . \quad . \quad (8)$$

It is of interest to note that Douglas and Isard (1949) approached this problem in a rather different manner. If J_1 were a function of x and C_1 only, then it would be possible to integrate eqn. (4) under suitable conditions. The relationship assumed by these authors is essentially $C_1=\exp(-bx)+a$, where a and b are constants. This assumption enables J_1 to be put equal to some constant value over the range $x=0$ to $x=d$. Proceeding in this manner these authors obtain a solution applicable when $C_\infty'=0$.

In this case

$$Q=C^*\sqrt{\left[t.\frac{2D_1D_2}{(D_1-D_2)}\left\{\frac{D_1}{(D_1-D_2)}\log_{10}\left(\frac{D_1}{D_2}\right)-1\right\}\right]} \quad . \quad . \quad (9)$$

where Q is the total flux that has crossed $x=0$ after time t.

An exact solution for all values of D_1 and D_2 can, however, be derived from the analyses of Fujita (1952 a, b) given in another context. Fujita has recently obtained a formal solution of the equation

$$\frac{\partial C}{\partial t}=\frac{\partial}{\partial x}\left(D\frac{\partial C}{\partial x}\right) \quad . \quad . \quad . \quad . \quad . \quad . \quad . \quad . \quad (10)$$

where

$$D=D_0/(1-\lambda C'). \quad . \quad . \quad . \quad . \quad . \quad . \quad . \quad . \quad (11)$$

D_0 and λ are both constants. Writing

$$\frac{C^*D_1D_2}{[C^*D_2+(D_1-D_2)C_0']}=D_0, \quad \ldots\ldots\ldots (12)$$

$$\lambda=\frac{(D_2-D_1)}{[C^*D_2+(D_1-D_2)C_0']}, \quad \ldots\ldots\ldots (13)$$

and $C'=C_1-C_0'$, eqn (10) becomes identical with eqn. (5), and the boundary conditions are now expressed in the form

$$C=0,\ x>0,\ t=0$$

$$C=C_\infty'-C_0'=C_0,\ x=0,\ t>0.$$

The solution given by Fujita (1952 a, b) is valid for $0<\alpha<1$, where $\alpha=\lambda C_0'$. This analysis is discussed fully by Crank (1956), the final solution being written as two parametric equations :

$$y=\frac{1}{\sqrt{(2\mu)}}\left[\{(\theta^2-\mu\ln\theta^2)^{1/2}-\theta\}\exp\left\{\int_0^\theta(\theta_1^2-\mu\ln\theta_1^2)^{-1/2}d\theta_1\right\}\right] \quad (14)$$

and

$$c=\frac{1}{[1-\exp(-\beta)]}\left[1-\exp\left\{2\int_0^\theta(\theta_1^2-\mu\ln\theta_1^2)^{-1/2}d\theta_1\right\}\right] \quad (15)$$

where

$$\beta=-\ln(1-\alpha)=2\int_0^1(\theta_1^2-\mu\ln\theta_1^2)^{-1/2}d\theta_1, \quad \ldots (16)$$

$C/C_0=c$ and $y=x/2\sqrt{(D_0t)}$. Now,

$$\alpha=\frac{(D_2-D_1)(C_\infty'-C_0')}{[C^*D_2+(D_1-D_2)C_0']}$$

where all the physical quantities are positive. Since C_x' must of necessity be less than C^*, it can be shown that α can only take values between $+1$ and $-\infty$. A solution for $-\infty<\alpha<1$ is therefore required for this paper. We find that the analysis by Fujita may be extended, with some modification, to cover the additional range $\alpha<0$. The final solution for this case may be rewritten

$$y=\frac{1}{\sqrt{(2\mu)}}\left[\{\theta+(\theta^2-\mu\ln\theta^2)^{1/2}\}\right.$$
$$\left.\times\exp-\left\{\int_0^\theta(\theta_1^2-\mu\ln\theta_1^2)^{-1/2}d\theta_1\right\}-2\exp(-\beta/2)\right]. \quad (17)$$

(so that $y\to 0$ as $\theta\to 1$ and $y\to+\infty$ as $\theta\to 0$),
and

$$c=\frac{1}{[\exp(\beta)-1]}\left[\exp\left\{2\int_0^\theta(\theta_1^2-\mu\ln\theta_1^2)^{-1/2}d\theta_1\right\}-1\right] \quad (18)$$

where in this case

$$\beta=+\ln(1-\alpha)=2\int_0^1(\theta_1^2-\mu\ln\theta_1^2)^{-1/2}d\theta_1. \quad \ldots (19)$$

The relationship between α and μ in eqn. (16) is given in graphical form in the paper by Fujita (1952 a, b), and also in Crank (1956), and the

corresponding relationship in eqn. (19) may readily be deduced from this. Only one numerical integration $\left(\text{of } \int_0^{\theta} (\theta_1^2 - \mu \ln \theta_1^2)^{1/2}\, d\theta_1\right)$ is required, since this expression occurs in all the final equations. It is then possible to write down values of y and c for appropriate values of θ, giving a parametric solution of the original equation, for $-\infty < \alpha < 1$.

It is frequently convenient to study ion exchange from the point of view of the total quantity of material exchanged during a reaction. For example, the change in weight of the sample may be followed. In such cases it is necessary to derive an expression for the total flux which has passed per unit area of the plane $x=0$ up to a time t.

In both the above instances ($\alpha<0$ and $0<\alpha<1$) the required solution is

$$Q = \int_0^t \frac{-C^* D_1 D_2}{[C^* D_2 + C_\infty'(D_1 - D_2)]} \cdot \left(\frac{\partial C_1}{\partial x}\right)_{x=0} \cdot dt\,,$$

where Q is the total quantity of material passing through the plane $x=0$ up to time t.

Now

$$\left(\frac{dc}{dx}\right)_{x=0} = \left(\frac{dc}{d\theta} \cdot \frac{d\theta}{dy} \cdot \frac{dy}{dx}\right)_{\theta=1}.$$

Using eqns. (17) and (18)

$$\left(\frac{dc}{dx}\right)_{x=0} = \frac{2^{1/2} \exp(\beta/2) t^{-1/2}}{[1 - \exp(-\beta)] D_0^{1/2} \mu^{1/2}} \quad \ldots\ldots (20)$$

while (14) and (15) yield

$$\left(\frac{dc}{dx}\right)_{x=0} = \frac{-2^{1/2} \exp(-\beta/2) t^{-1/2}}{[\exp(\beta) - 1] D_0^{1/2} \mu^{1/2}}. \quad \ldots\ldots (21)$$

The final expression for Q with $\alpha<1$ is then given by

$$Q = \frac{2^{3/2} A (C^* D_1 D_2)^{1/2} t^{1/2} [C^* D_2 + (D_1 - D_2) C_\infty']^{1/2}}{\mu^{1/2} (D_1 - D_2)}, \quad \ldots (22)$$

where A=surface area of the interface.

In the limit as $D_2 \to D_1$ (i.e. $\alpha \to 0$, $\beta \to 0$, and $\mu \to \infty$) it may be shown that

$$\mu^{1/2}(D_2 - D_1) \to \sqrt{(2\pi)} \cdot \frac{C^* D_2}{(C_\infty' - C_0')},$$

so that eqn. (22) then reads

$$Q = 2A(C_\infty' - C_0') \frac{\sqrt{(Dt)}}{\sqrt{\pi}}, \quad \ldots\ldots (23)$$

where $D = D_1 = D_2$. As expected, the expression is that found for simple Fickian diffusion in a semi-infinite solid.

In certain simplified systems ion exchange across a membrane is of interest in the steady state. Equation (4) may be written

$$J_1 = -\left(\frac{C^* D_1 D_2}{C^* D_2 + C_1 (D_1 - D_2)}\right) \cdot \frac{dC_1}{dx} \quad \ldots\ldots (24)$$

for the case of the steady state flow between the planes $x=0$ and $x=d$. Integration of eqn. (24) then yields the expression

$$J_1 = -\frac{C^*D_1D_2}{(D_1-D_2)d}\cdot\ln\left(\frac{(C^*D_2+C''_B(D_1-D_2)}{C^*D_2+C''_A(D_1-D_2)}\right)$$

since J_1 is a constant throughout the membrane. C''_A and C''_B are concentrations of C_1, at $x=0$ and $x=d$ respectively.

§ 4. Diffusion with Immiscibility present in the System

There are two main possibilities in the case of granular material, either diffusion of one ion is rate controlling in the outer layer, with diffusion of both ions independently present in the inner region, or conversely the migration in the outer layer is dependent on the diffusion of both ions, while diffusion in the inner region is rate controlled by one ion. Only the former case is at all amenable to calculation. There are effectively two fixed composition limits for the outer layer, the composition at the interface of the two solid solutions, and also the composition at the surface with the aqueous solution. Since the diffusion in this layer is controlled by one ion only, no electrical field will develop. It appears, therefore, that this is analogous to a tarnishing reaction and the equation of Danckwerts (1950) may be applied.

§ 5. Application

The major contribution in this paper is the formulation of an equation relating the quantity of material exchanged during an ion exchange reaction with the individual diffusion coefficients of the two migrating species. In the case of Fickian diffusion the solution obtained is

$$Q = \frac{2^{3/2}A(C^*D_1D_2)^{1/2}t^{1/2}[C^*D_2+(D_1-D_2)C_x']^{1/2}}{\mu^{1/2}(D_1-D_2)} \quad . \quad . \quad . \quad (25)$$

The most useful practical applications of the equation are likely to be when the diffusion coefficients differ by orders of magnitude, and where $C_0'=0$ or C^*.

When $D_2 \gg D_1$, eqn. (25) may be simplified to read

$$Q = \frac{2^{3/2}A[C^*(C^*-C_\infty')]^{1/2}}{\mu^{1/2}}\sqrt{(D_1t)}.$$

In the case where $C_0'=0$, α is found to have the value C_∞'/C^*. The observed diffusion coefficient is then equal to that of the slower moving ion multiplied by a constant dependent only on concentration. Where $C_0'=C^*$, α has the value $D_2(C_x'-C^*)/C^*D_1$, dependent on both diffusion coefficients.

Where experimental results yield only values of Q as a function of $\sqrt{t}$, it will in general be impossible to obtain individual diffusion coefficients.

References

Barrer, R. M., and Hinds, L., 1953, *J. Chem. Soc.*, 1879.
Barrer, R. M., and Raitt, J., 1954, *J. Chem. Soc.*, 4641.
Barrer, R. M. and Sammon, D., 1955, *J. Chem. Soc.*, 2838.
Barrer, R. M. and Falconer, J. D., 1956, *Proc. Roy. Soc.* A, **236,** 227.
Beattie, I. R., 1954, *Trans. Faraday Soc.*, **50,** 581 ; 1955, *Trans. Faraday Soc.*, **51,** 712.
Crank, J., 1956, *The Mathematics of Diffusion* (Oxford), p. 167.
Danckwerts, P. V., 1950, *Trans. Faraday Soc.*, **46,** 701.
Douglas, R. W., and Isard, J. O., 1949, *J. Soc. Glass Tech.*, **33,** 325.
Fujita, H., 1952 a, *Text. Res. J.*, **22,** 757 ; 1952 b, *Ibid.*, **22,** 823.
Mott, N. F., and Guerney, R. W., 1950, *Electronic Processes in Ionic Crystals* (Oxford), p. 256.

Irradiation Damage in Single Crystals of Magnesium Oxide†

By F. P. Clarke
Atomic Energy Research Establishment, Harwell

[Received January 23, 1957]

Summary

Single crystals of magnesium oxide have been subjected to ultra-violet x and neutron irradiation. The bands produced by these radiations, their optical and thermal bleaching and associated luminescence are discussed. Taking into account the data of other workers, schemes for ultra-violet activation and luminescence are proposed. The ultra-violet activation is attributed to the freeing of positive holes, perhaps with exciton formation as an intermediary process, and the subsequent trapping of both electrons and positive holes at negative and positive ion vacancies. The role of the various impurities is discussed and it is concluded that they do not directly give rise to the optical absorption bands observed. The luminescence scheme assumes an optical band width of over 7·0 ev. It is then shown that the various luminescence photon energies correspond to values which are to be expected on the assumption that the optical absorption energies represent the heights of bands measured from the top of the valence band.

§ 1. Introduction

Hibben (1937) was the first to report that periclase (single crystals of magnesium oxide) could be coloured by light from the 2537 Å mercury line. Subsequent to this Molnar and Hartmann (1950) gave details of certain absorption bands developed under x-irradiation and Weber (1951) showed that these bands could also be produced by additive coloration with the parent atoms. Day (1953) examined photoconductivity in neutron-irradiated crystals, and details of the luminescence and x-ray induced photoconductivity were given by Einstein (1954).

The present series of experiments fills in some of the gaps. Details of the ultra-violet induced activation are given and some of the effects of neutron irradiation examined. These results together with those of previous workers are then discussed in the light of an elementary model.

§ 2. Experimental Details

The magnesium oxide single crystals were obtained from the Infra-Red Development Company of Welwyn Garden City. Due to differences in

† Communicated by Dr. H. M. Finniston.

the optical absorption property between various specimens, a detailed spectrographic analysis was carried out to see whether these differences could be associated with differing impurity content. Typical analyses are shown in table 1. The specimens A and B show the order of variation typical of the crystals, and specimen C is of one kindly provided by Dr. B. Bleaney of the Clarendon Laboratory ; these figures are accurate to within a factor of two either way. An analysis and examination of about 30 different crystals show that no apparent correlation existed.

Table 1

	Impurity (parts per million)								
	Ni	Be	Fe	Mn	Al	Cr	Ca	Co	Si
A	10	10	100	10	100	10	500	10	10
B	10	10	100	50	100	10	700	100	400
C	10	10	700	10	100	100	1500	—	700

Thermal annealing of the crystals at 1200°C *in vacuo* did not make the absorption spectra more consistent and so the following method of standardizing the crystals was adopted. If the intensity of the light incident on one face and emerging from the opposite face of a crystal of thickness L be represented by I_0 and I then

$$\ln I = -\mu L + \ln KI_0 \quad . \quad . \quad . \quad . \quad . \quad . \quad . \quad . \quad (1)$$

where μ is the absorption coefficient and K is a constant related to the refractive index. Hence a plot of crystal thickness versus log transmission for any given wavelength should give a straight line of slope $-\mu$ and an intercept on the transmission axis of $\ln KI_0$. It was found that only certain of the crystals followed the straight line reasonably and gave a correct intercept of the transmission axis ; this intercept was calculated using the values of refractive index given by Strong and Brice (1935). The crystals which satisfied the relation were selected for the experiments.

Some of the crystals used were cleaved pieces, but where special thicknesses were required it was found necessary to grind the specimens on diamons impregnated lead and nylon laps, special precautions being taken to remove the lubricating layer subsequently.

The neutron irradiations were carried out in the Harwell BEPO pile, and at Windscale where higher fluxes were needed. In BEPO three separate facilities were used :

(*a*) Where the ambient temperature was 60°C–80°C and the fast-to-slow neutron flux ratio was 1 : 1.

(*b*) In the centre of a hollow uranium slug where the pile temperature was 20°C and the fast-to-slow flux ratio was 3 : 1.

(*c*) For irradiation times from 1 sec to 1 hour, in a pneumatic tube facility where the fast-to-slow flux ratio was 1 : 1, and the temperature 50°C–60°C. In this facility for short time irradiations the specimen does not have time to attain the pile ambient temperature, and so all specimens were raised to slightly above pile ambient before irradiation.

Absorption measurements in the range 6 ev (2060 Å) to 1·2 ev (1030 Å) were made on a Hilger 'Uvispek' spectrophotometer. Measurements in the infra-red were carried out by Mr. R. Wood of A.W.R.E. Aldermaston on a Unicam double-beam recording spectrophotometer, and in the range 5 ev (2470 Å) to 7·5 ev (1640 Å) on a vacuum spectrophotometer details of which will be given elsewhere. The thermal annealings were made in a vacuum furnace capable of being maintained within a temperature of ±2°C. Light intensities for the bleaching experiments were measured with a Schwartz thermopile, and where necessary the light was monochromated by passing it through a Hilger D222 quartz monochromator. Light at wavelengths of 2537 Å and 3650 Å were obtained from special lamps giving predominant lines at these wavelengths. Where luminescence photon energies are quoted, it means that the brightness was sufficient to allow inspection on a Beck pocket spectrometer.

The optical absorption figures given on graphs refer to the reflection corrected absorption. The actual transmission measurement made on the spectrophotometer is $I\ I_0$ where I_0 corresponds to 100% transmission and

$$I/I_0 = K \exp(-\mu L)$$

where

$$K = 16n^2(n+1)^{-4}$$

is the reflection correction, n being the refractive index at the wavelength of measurement. If after irradiation the absorption coefficient changes from μ to μ', corresponding to a transmitted intensity change from I to I', then

$$-(\mu'-\mu) = \{\ln(I'/I)\}/L.$$

This quantity has been called the "Irradiation Induced Absorption Coefficient". The number of defect centres contributing to any optical absorption band has been calculated from the "Irradiation Induced Absorption" versus "Photon Energy" curves using Dexter's (1956) formula

$$N_0 = 0{\cdot}821 \times 10^{17} n(n^2+2)^{-2} f^{-1} \int \mu(E)\, dE \text{ cm}^{-3}$$

where N_0 is equal to the number of centres per cm^3, E is equal to the photon energy in ev and f is the band oscillator strength. This has been taken as unity, so that N_0 will represent a minimum. It has been assumed that the refractive index, n, is not appreciably changed by irradiation. It was checked that irradiation did not alter the surface scattering properties of the crystal to ±1%.

§ 3. Purity of Crystals

As already stated crystals from different fusions showed variations in impurity content. These crystals always showed initial absorption bands with maxima at 4·3 ev (2880 Å), 5·6 ev (2200 Å) and 6·8 ev (1820 Å). The

heights of these bands varied slightly between the various crystals. but only the 6·7 ev band seemed to vary as the impurity content, becoming greater with larger amounts of impurity. This band was found to have an absorption maximum between 35 cm^{-1} and 25 cm^{-1} in the various crystals tested. The other bands which varied slightly between the crystals could be removed by heating at 1300°c in a vacuum better than 10^{-5} mm of mercury for 20 hours, but the 6·7 ev band still remained (fig. 1).

Fig. 1

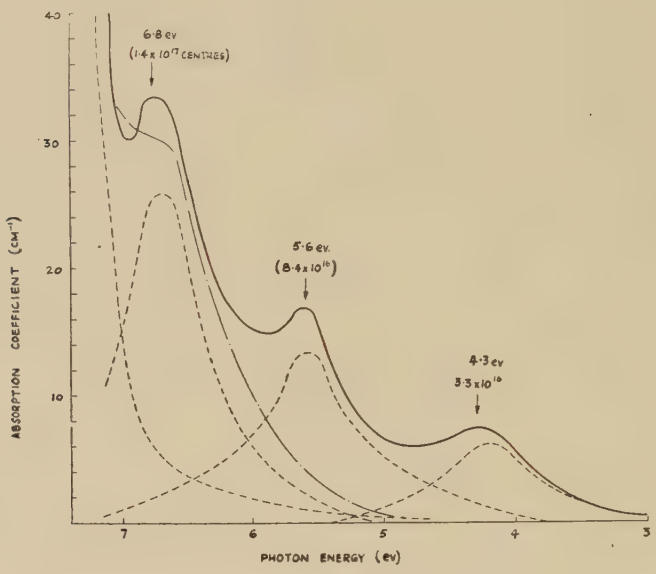

———— The optical absorption of an untreated crystal, with impurities corresponding to analysis A of table 1.

· —— · The optical absorption of a crystal heated *in vacuo* at 1300°c for 20 hours, and allowed to cool to 100°c in 4 hours.

— — — The suggested bands responsible for the profile of the untreated crystal.

The effect of irradiations on crystals with varying impurity content will be mentioned later, but it can be said here that the amount of impurity did affect the maximum values of ultra-violet (2537 Å) irradiation-induced absorption. In the crystals with the larger amounts of impurity the maximum attainable absorption was slightly lower. No compensating absorption band was observed anywhere in the region from the absorption edge to 0·2 ev (60 000 Å) where transmission begins to drop rapidly. For x-ray induced absorption however there seemed to be no such differences, the maximum absorption being the same within the limits of experimental error.

Using paramagnetic resonance techniques Bleaney and Orton (private communication) have established that iron, chromium and manganese

ions exist as Mn^{2+}, Cr^{3+} and Fe^{2+} or Fe^{3+}. In crystals which do not contain Fe^{3+} initially, ultra-violet irradiation produces Fe^{3+} ions which are then fairly stable, annealing on heating at around 600°C. In crystals which do contain Fe^{3+} initially the amount is either unchanged or decreased by irradiation. The Cr^{3+} ion is always present, and its amount may be changed either way by ultra-violet irradiation. These experiments make it probable that the impurities exist substitutionally but the charge compensation which would be expected in the case of the Fe^{3+} ion is not contained in the ions immediately surrounding the impurity.

The crystals having the highest impurity contents did not fit the straight line of eqn. (1) and so were not used for the other irradiation experiments.

§ 4. Experimental Results

4.1. *Ultra-Violet Irradiation*

Irradiation with light of 2537 Å (4·95 ev) wavelength produces bands with definite maxima at 4·3 ev (2880 Å), 4·95 ev (2500 Å) and 5·5 ev (2250 Å). In addition a shoulder appearing on the low energy side of the 4·3 ev band, may be shown to be due to a band having a maximum at 3·7 ev (3340 Å). and a broad band having a maximum somewhere between 2·4 and 2 ev may be broken down into two bands having maxima at 2·35 (5250 Å) and 2·05 ev (6000 Å). This irradiation-induced optical absorption due to ultra-violet light is shown in fig. 2, where the resultant curve is broken down into the various suggested bands. The minimum number of centres responsible for each band is also shown ; this has been calculated

Fig. 2

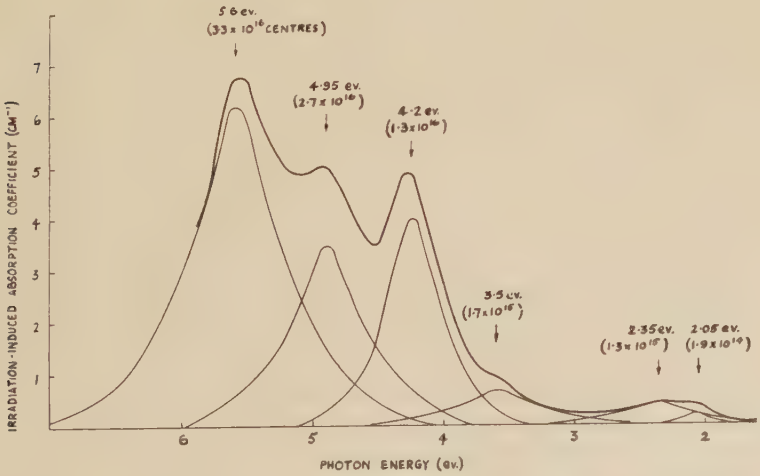

The full profile represents the irradiation induced optical absorption after exposure of the crystal to light of 2537 Å wavelength. This profile is broken down into suggested components, and these bands are shown by the lighter lines.

from Dexter's formula using an oscillator strength of unity. This particular curve does not represent fully developed absorption. The 4·95 ev band decays away in seconds at room temperature so that it does not show up clearly on the absorption profile. At around −50°c this decay is much less rapid, and it is possible to make a definite measurement of absorption. The other bands are unaffected by this lowering in temperature, and show no corresponding changes. This observation applies only to the visible and near ultra-violet regions of the spectrum and low temperature measurements in the infra-red and vacuum ultra-violet have not been made. The growth of optical absorption with time of ultra-violet irradiation is shown in fig. 3. It has been observed in some cases however that optical absorption has decreased after some minutes of irradiation and then it has increased again. Some thirty separate growth curves have been plotted and of these six showed abnormal variations under carefully controlled conditions. However fig. 3 shows the majority results, which agreed between different crystals to within $\pm 5\%$.

Fig. 3

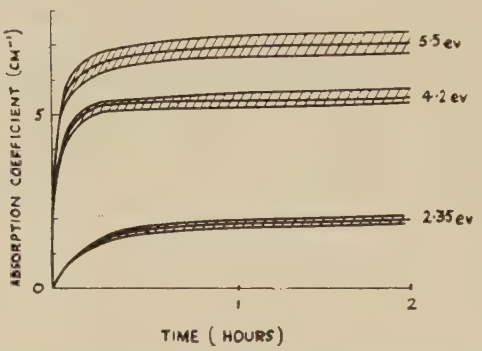

Growth of absorption coefficient at various photon energies, with time of irradiation with 10^{-3} watts cm^{-2} of light of 2537 Å wavelength.

These bands may be produced by light of smaller photon energies, but the efficiency in producing optical absorption decreases with the energy. Day (1953) has produced ultra-violet activation of MgO in respect of photoconduction at 2·1 ev, by light of as low an energy as 3·9 ev (3120 Å). This activation could not be reproduced in the present series of experiments for crystal which fitted the straight lines of eqn. (1). On crystals other than these, however, light of energy down to 3·5 ev (3500 Å) has produced appreciable absorption, and activation in respect of photoconductivity. Light of energies up to 7 ev (1760 Å) has been used for producing optical absorption, and though only a small amount of light was available at these energies, the quantum efficiency was very high. At several photon energies below 6 ev, the final saturation of absorption was found to depend only upon the total amount of irradiation incident on a given area, and was independent of dose rate. This also applies to photoconductivity (Day *loc. cit.*).

Hibben (1937) reported the complete decay in the dark of the visible bands. The present series of experiments showed that all bands at and below 4·3 ev initially decay quite rapidly in the dark, but stay fairly constant subsequently. For example an absorption coefficient starting at 2 cm^{-1} decayed to 1·1, 0·9, 0·86 cm^{-1} in 0·5, 18 and 66 hours respectively. Hence all measurements on 2537 Å activated crystals were made after at least half an hour, when the greatest rate of decay had passed.

Further irradiation with light anywhere in the region of absorption up to 4 ev (3090 Å) causes all dark-stable bands to bleach, the rate of bleaching being greater for the higher energy bands. This is shown in fig. 4 (*a*), (*b*) and (*c*), where the rates of bleaching with light of 6000 Å and

Fig. 4

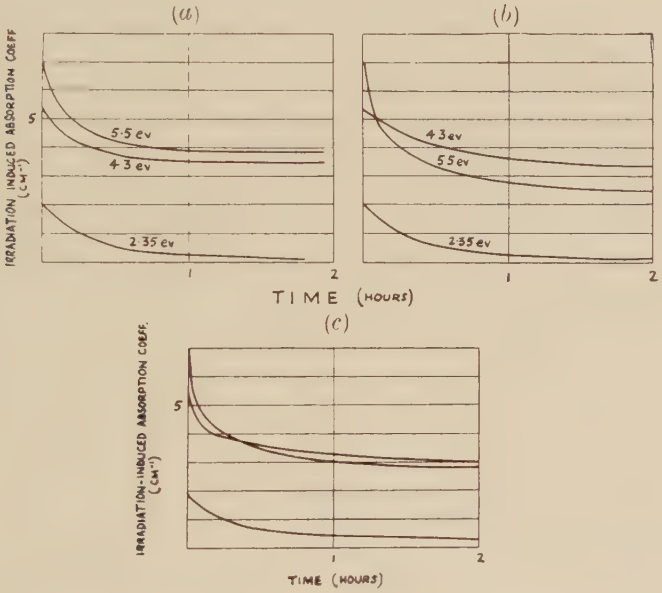

Change in absorption coefficient at various photon energies due to (*a*) heating at 220°c, (*b*) bleaching at room temperature with $5{\cdot}7 \times 10^{-4}$ watts of 6000 Å wavelength light, and (*c*) bleach at room temperature with 10^{-3} watts of 3650 Å wavelength light.

3650 Å wavelengths are compared with the rate obtained by heating at 220°c, at which temperature the absorption changes are of the same order. If it could be assumed that the oscillator strengths of the various bands were the same, then this would mean that more centres are disappearing at higher wavelengths and indeed this is the interpretation made by Molnar and Hartman (*loc. cit.*) in respect of x-irradiation damage. On this basis it would appear that for 6000 Å light or thermal bleaching (during most of the first two hours of treatment) the integrated drop in absorption coefficient of the 4·3 ev and 2·35 ev bands at any instant is approximately equal to that of the 5·5 ev band. This is not true for 3650 Å irradiation however.

In no case has all the ultra-violet induced absorption been caused to decay completely by optical bleaching, though after a week's irradiation under a high-pressure mercury arc lamp all bands except those at and above 4·3 ev had disappeared and these latter had been reduced to below 5% of the saturation absorption.

Thermal bleaching results are erratic and complicated. The absorption of all bands in the region 1·0 to 6·0 ev decreases initially. At temperatures below 100°c a partial recovery is sometimes observed after some minutes and then the decay continues. This behaviour has not been observed at temperatures above 100°c, and typical bleaching behaviour at 220°c is then shown in fig. 4.

This thermal bleaching is accompanied by a luminescence, though at 100°c the eye cannot detect it. At 220°c the luminescence last about two minutes. As far as can be ascertained with the aid of a small spectrometer the luminescence spectrum covers much of the visible spectrum with a predominance of red. Unfortunately this luminescence was detected only when the rates of decay of nearly all the bands was a maximum, and hence it could not be uniquely associated with the decay of any one band from these observations above.

If a crystal about $\frac{1}{2}$ cm thick be exposed on one face to 2537 Å wavelength light and the induced absorption along a section normal to the face examined, it is found that there is a region of darker absorption, followed by a uniform coloration over the rest of the section. This region of darker absorption covers about 2 mm and so all experiments in the growth and decay of ultra-violet induced bands were made on specimens less than 2 mm thick.

4.2. *Neutron Irradiation*

Neutron irradiation produces bands with apparent maxima at 1·2 ev (10 300 Å), 2·15 ev (5750 Å), 3·5 ev (3530 Å), 4·2 ev (2940 Å), 5 ev (2470 Å) and 5·5 ev (2250 Å). This irradiation-induced absorption is shown in fig. 5 where the resultant curve is broken down into various suggested components. This curve resulted from an integrated neutron flux of 2×10^{17} n.v.t.

In addition to the very apparent bands, the absorption between 3·5 ev and 2·15 ev may be broken down into two further bands at 3·0 ev (4120 Å) and 2·7 ev (4580 Å).

4.2.1. *The* 2·15 ev *band*

The 2·15 ev band has a shoulder on its low energy side, which does not appear convincingly for doses lower than 10^{17} n.v.t. ; a dose of 10^{20} n.v.t. makes the presence of this shoulder very definite however. For doses between 10^{17} and 10^{20} n.v.t. the shoulder rises and falls at the same rate as the 2·15 ev band maximum, and on thermal annealing both fall at the same rate.

Fig. 5

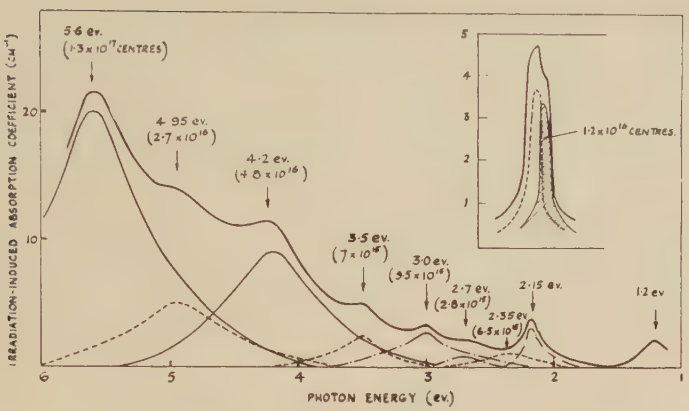

The optical absorption induced by a dose of 2×10^{17} n.v.t. In the profile analysis it has been assumed that the bands induced by ionizing radiation are present. The inset figure shows the suggested constitution of the 2·15 ev band : the absorption coefficient scale has been made larger, and the spectrum corresponds to a dose of over 10^{18} n.v.t.

Fig. 6

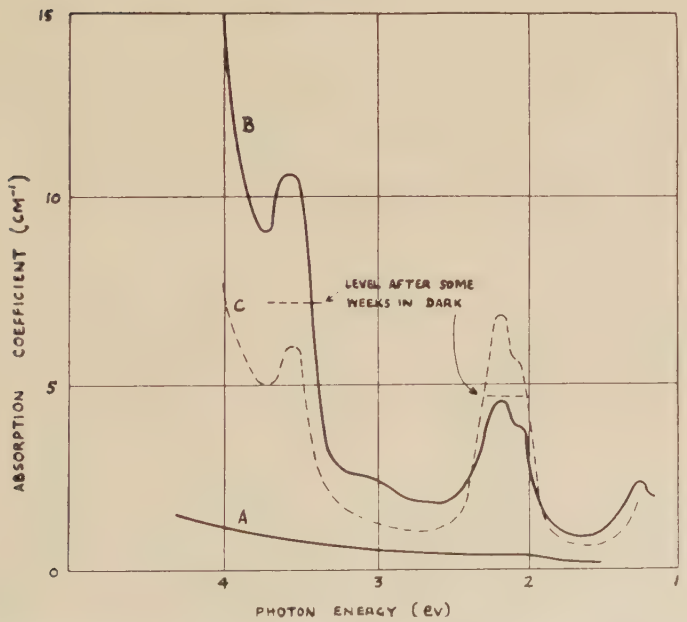

Curve A is of the unirradiated specimen. Curve B is after pile irradiation of 4×10^{18} n.v.t. Curve C is after subsequent optical bleaching. Temperature of irradiation $\simeq$ 21°c.

On optically bleaching with 3500 Å light, this band increases in its height, a typical increase being from 4·5 cm $^{-1}$ to 7 cm^{-1} as shown in fig. 6. this irradiation is accompanied by an intense red luminescence which lasts longer than the band change for any given 3·5 ev irradiation rate. If a neutron-irradiated crystal which has been subsequently irradiated with 3500 Å light to produce a greater absorption at 2·15 ev, is left in the dark for several weeks further absorption changes are observed. The absorption changes are shown in fig. 6.

The thermal stability of the 2·15 ev band is very neutron-dose dependent. Its rate of decay at 230°c, after optical bleaching, is shown in fig. 7, and this corresponds to a dose of $2{\cdot}2\times10^{18}$ n.v.t. Its behaviour

Fig. 7

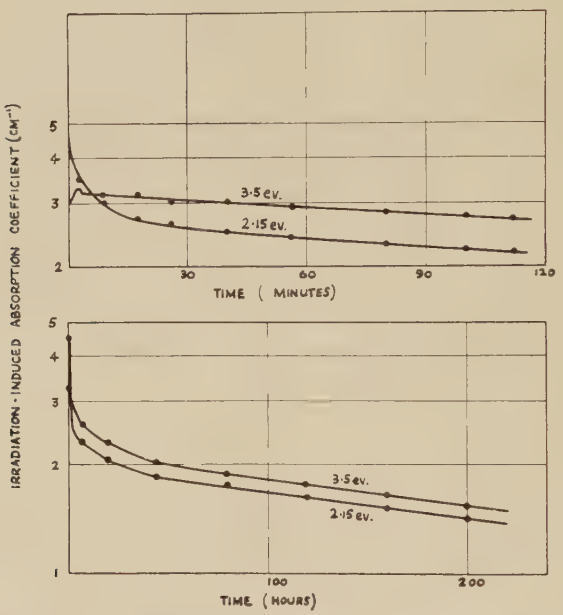

Decay of 2·15 and 3·5 ev bands with time, on heating at 230°c. The crystal had received a dose of $2{\cdot}2\times10^{18}$ n.v.t., and had then been irradiated with 3500 Å light before each anneal. The decay in a crystal not subjected to this latter treatment was found to be erratic.

after a dose of $2{\cdot}1\times10^{20}$ is shown in fig. 8. At 230°c there is a general instability in the band height, and this instability continues until a temperature of about 400°c when the absorption begins to rise. This rise continues until a temperature around 600°c is reached, when a rapid decay commences. Complete decay may be achieved in a few seconds at 1200°c. This behaviour has been observed in two crystals which were separately irradiated in the Windscale pile : here the ambient temperature was between 80°c and 100°c in the facility used, being slightly higher than the corresponding figures for the BEPO pile.

Irradiation with 2537 Å light at any stage in this thermal annealing process brought a slight rise in the height of the 2·15 ev band, but similar irradiation with 3500 Å light produced no detectable effect.

The shoulder on the low energy side of the 2·15 ev band, which rises and falls with the band maximum is not due to the tail of the 1·2 ev band. This is evident from an examination of the position and width of the 1·2 ev band (fig. 5). Some experiments on crystals which were rejected under the criterion expressed in eqn. (1), had previously been examined and in some of these, two distinct bands around 2·1 ev had been produced by 3650 Å irradiation. This suggests that the shoulder may be the result of superposing two bands very near each other, as shown inset in fig. 5.

4.2.2. *The* 3·5 ev *band*

As shown in fig. 7 for a 10^{18} n.v.t. dose this band initially shows quite different annealing behaviour to the 2·15 ev band, but after 20 min at 230 °C it settles down to a decay rate identical to that of the 2·15 ev band. Both of these decays are taken for crystals which contain oxygen excess before irradiation.

Fig. 8

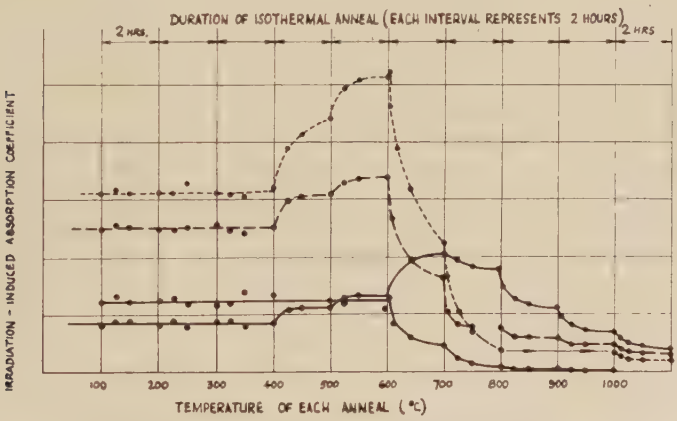

The isothermal annealing behaviour over a range of temperatures. Each isothermal is for a period of 2 hours. The curves are due to bands at 2·15, 3·5, 1·2 and 3·0 ev reading from top to bottom.

After a dose of 2×10^{20} however this band behaves in a very similar manner to the 2·15 ev band. The peak absorption rises until a temperature of around 600°C is reached when a rapid decay commences (fig. 8). The general variability in the absorption coefficient during heating from 100°C–400°C is also noticed for this band.

The effect of bleaching with 3500 Å light is to cause this peak absorption to decrease over a period of several hours when 10^{-3} watts cm^{-2} sec^{-1} (5×10^{15} photons cm^{-2} sec^{-1}) is falling on the surface of the crystal. The

shape of the band is not altered however, and on leaving the crystal in the dark for several weeks, the band peak partially regains its previous height as shown in fig. 6.

A crystal which has been the vacuum annealed prior to irradiation will show differences in the rate of decay of the band maxima as compared with the results of fig. 7 for doses of up to 10^{18} n.v.t. This is partly because in an 'excess-oxygen' crystal the width of the oxygen band at 4·2 ev measured 1 day after neutron irradiation is not changed sufficiently at the tail to affect the decay rate of the 3·5 ev band. Hence the contribution of the 4·2 ev band tail to the 3·5 ev absorption may be eliminated. In the vacuum annealed crystal, however, the whole of the 4·3 ev band is irradiation-induced and so decays with the 3·5 ev band, and affects the latter.

4.2.3. *The* 3 ev *band*

This band is very apparent for neutron doses in excess of 10^{18} n.v.t., and for a dose of 2×10^{20} its annealing curve is shown in fig. 8. It appears to be slightly more stable than the 2·15 ev and 3 ev bands since it commences to decay at a higher temperature and its decay rate is not so rapid.

In a crystal subjected to a dose of 10^{17} n.v.t. this band is barely apparent and may be optically bleached, until it is no longer apparent in the resultant spectrum. For a 2×10^{20} n.v.t. dose it is optically more stable, decaying by about 10% after prolonged exposure.

4.2.4. *The* 1·2 ev *band*

This band appears on neutron irradiation but differs from the other bands in that it does not show a consistent growth on annealing of heavy damage. Its behaviour is shown in fig. 8. Its reaction to heating up to 600°C is extremely erratic, and at this temperature it commences to decay. The decay between 600°C and 800°C can however be reversed by the action of 2537 Å light, but above 900°C the decay is irreversible and the band disappears completely after a few minutes at 1000°C.

After a dose of 2×10^{18} n.v.t. the band rate of decay at 300°C is very similar to the 3·5 ev band but there is a wide scatter of readings. At this dose the band may be 80% bleached by exposure to a high intensity mercury-arc source for about a day.

4.2.5. *Bands at and above* 4·2 ev

For doses of 10^{18} n.v.t. and upwards these bands absorb over 99·9% of the light incident at these photon energies; there is an accompanying fluorescence which makes absorption measurements less meaningful. This fluorescence is at least partly associated with radiation damage, and so even the use of a magnesium oxide crystal as a spectrophotometric standard does not assist in interpretation. Boyd *et. al.* (1947) have observed absorption above 4·3 ev for small neutron doses; from their analysis it appears that the 5 ev band may comprise two components,

one of which is very unstable decaying in a few minutes at 600 c. and the other following a first order decay process subsequently.

All these annealing results apply to heating in a vacuum better than 10^{-5} mm of mercury.

If the crystal has these annealings carried out in air, the results are similar to those mentioned above, up to 650°c. At this temperature the absorption decay rate lessens, and at 800°c a band at 4·2 ev begins to grow rapidly. Both the 2·15 ev and 3 ev bands will continue to decay however. These results apply to a crystal which has been vacuum annealed, prior to any irradiation treatments, to remove excess of oxygen in the lattice.

§ 5. Discussion

Attempts have been made to show thermodynamically whether Frenkel or Schottky defects exist in thermodynamic equilibrium in ionic crystals. Jost (1952) has made a calculation assuming the ion vacancy radius to be half the normal ion distance. This vacancy radius is critical however, and Mott and Littleton (1938) improved the argument by an exact determination of the vacancy radius. The application of these calculations to the alkali halides has shown that Schottky defects are expected to exist in equilibrium at all attainable temperatures, and experimental measurements have confirmed this. It is not so easy to make a similar estimate in the case of magnesium oxide however, since quantities such as the critical ion vacancy radius and lattice energy will depend upon the degree of ionic character, which is unknown. However following Mott and Littleton's arguments, Yamashita and Kurosatawa (1954) have shown the presence of Schottky defects is not energetically unreasonable, and experimental evidence to support their predominance in magnesium oxide will be mentioned in this text.

5.1. *Non-Stoichiometry and Impurities*

On heating crystals of magnesium oxide in the vapour of oxygen or magnesium, bands appear at various photon energies. It is important to arrive at some conclusion concerning the types of centre giving rise to these bands. In the case of magnesium addition, bands are produced at 2·35 ev, 3·6 ev and 4·95 ev. Bands having an identical profile with maxima at these same energies are also produced by potassium addition: hence it is clear that the spectrum is not due to resonance transitions at magnesium or potassium atoms because the resulting spectrum would be different in each case. It is probable that the spectrum arises from the added magnesium atoms becoming thermally ionized and thereby giving up their electrons to the interior of the solid. These would become trapped at existing centres. An examination of the absorption spectra produced in various planes at right angles to the direction of diffusion, shows that the spectrum does not fully develop in the crystal interior,

unless heating is carried out for a considerable time. One explanation of this is that the spectrum is due not only to electrons trapped at existing centres but also to those trapped at new centres which take time to diffuse inwards from the surface ; the electrons themselves would reach the centre of the crystal in a few seconds at 1200°c, because it is known from irradiation experiments that this type of centre is highly unstable at a few hundred degrees centigrade. The indication is that Schottky type defects are formed by the addition of magnesium to the crystal ; the absorption is due to electrons trapped at oxygen-ion vacancies. Varley (private communication) has suggested a reason for the electrons apparently not diffusing at a very fast rate into the crystal interior. After ionization of the added magnesium atoms, the electrons would be free to diffuse away. However the effect of a number of new positive ions near the surface would be the setting up of a space charge which would tend to localize the freed electrons, and keep them in traps near the space charge. As time progressed the ions forming the space charge would gradually diffuse into the crystal interior and so allow the electrons to do so too ; eventually the space charge would be homogeneously distributed throughout the crystal. Even on this scheme however the absorption is still due to electrons trapped at negative ion vacancies.

In the case of oxygen addition to the lattice, it is hard to distinguish from the data itself whether the absorption is due to neutralized magnesium ion vacancies or to interstitial oxygen atoms. The oxygen atom is about 1·2 Å diameter, smaller than the magnesium ion, and so size considerations favour a high mobility. Furthermore Weber has pointed out that the averaged frequency rates of certain groups of 2p–3s and 2p–3d transitions occurring in oxygen atoms in the gaseous state is the same as that of the two bands formed by oxygen addition to magnesium oxide. He suggests that the transitions behind these two bands may represent the same transitions as occur in the gaseous state but perturbed by the crystalline field.

The evidence from the production by ultra-violet irradiation of absorption at the same photon energies as the oxygen band is also relevant. It will be shown later that the ultra-violet irradiation produces free positive holes or electrons and that the trapping of these gives rise to the same absorption. Now if the absorption is due to resonance transitions at an interstitial oxygen atom, the oxygen must have been a singly charged negative ion in the vacuum annealed crystal. But this ion should itself give rise to absorption (an oxygen atom has an electron affinity of 2·2 ev for one electron) whereas none is to be seen.

Furthermore it seems rather unlikely that Schottky and Frenkel defects should occur together. It will therefore be assumed that additive coloration results in the formation of Schottky defects.

If the absorption is not due to the oxygen atoms as such, but rather to trapped positive holes generated as a result of the addition of oxygen, the question arises as to where the positive holes would be trapped. In

addition to the suggestion already made of a positive ion vacancy, the possibility of impurity ions acting as trapping centres must also be considered and in the ultra-violet irradiation case this does occur. But whereas the holes trapped at the iron or chromium ions may be removed by heating the crystal in air at 600°C, the ' excess oxygen ' bands are not changed by this treatment. Of the other impurities the Ca^{2+} and Be^{2+} ions already have the inert gas structure and so we would not consider the possibility of their trapping positive holes ; Mn^{2+} has been shown to remain stable under irradiation and crystals have been obtained without any detectable cobalt or nickel, but their physical properties have been unaffected. This leaves the aluminium and silicon impurities to be discussed.

Crystals with varying amounts of these have been obtained, but the saturation value of the optical absorption of the two bands under consideration has not varied.

It is therefore concluded that if these ions may trap positive holes, then they do not give rise to absorption spectra at the same wavelengths as those of the excess oxygen bands. The overall conclusion is that these bands are due to positive holes trapped at lattice inhomogeneities, and are not associated with impurity ions in the lattice.

5.2. *Ultra-Violet Irradiation*

The absorption spectrum arising from ultra-violet irradiation has a profile very similar to that arising from x-irradiation. In the case of x-irradiation Weber has showed that a superpositioning of the absorption spectra produced separately by magnesium and oxygen addition to the lattice, follow almost precisely the absorption profile produced by x-irradiation : this makes it highly probable that the absorption bands arise from the same types of centre in the two cases. A similar inference may be drawn here in respect of the ultra-violet induced bands.

Ultra-violet irradiation in the range 2000 Å 3000 Å will in general cause only electronic displacements in a virgin crystal. From Day's photoconductivity data a more precise idea of the exact type of displacement may be deduced, the experimental facts are there :

Ultra-violet irradiation in the range mentioned causes increased photon absorption at certain wavelengths. Part at least of the change is reasonably stable at room temperature in the dark. During irradiation the photocurrent decreases from its initial value by a factor of two, but subsequent irradiation with light of lower photon energies causes the photocurrent to increase by a factor of a thousand at these wavelengths.

The ultra-violet activating photon energy is about 4 ev (3120 Å) and the enhancement of photoconductivity occurs with peaks at 1·2 ev and 2·1 ev (10 500 Å and 5800 Å) ; this region of enhancement, may be shifted during its production, by the application of an electric field and it moves towards the negative electrode.

These experimental results mean that the 4 ev radiation has caused a positive charge to become free to move in the lattice. The trapping of

this charge gives rise to the centre which can be photoactivated by light of lower energy.

The positive charge is presumably a positive hole which is released by the excitation of an electron in a valence state of an ion, to a level where it becomes independent of the ion. Since the fundamental absorption edge lies at some photon energy greater than 7 ev, direct excitation of the electron to the conduction band by such a low photon energy as 4 ev is not reasonable.

Hence the electron excitation must somehow be associated with a lattice inhomogeneity which contains a trap level somewhere in the forbidden band of energy levels. There is initial absorption at the ultra-violet activating energy, but this shows no structure. This absorption appears to occur as long tail in the absorption edge in which case it is possibly due to exciton transitions. Any excitons formed may wander freely through the lattice and will either decay after about 10^{-8} seconds or become annihilated at imperfections or dislocations or in the region of an ion vacancy. The latter might occur if the exciton wave were to pass a trapping centre with an electronic state of lower energy than that of the exciton ; in this case the exciton electron could tunnel through to a stationary trapping state leaving a positive hole free to wander in the lattice. The occurrence of some such exciton mechanism is supported by the increase in efficiency in the process with increase in irradiating photon energy, and the fact that the photon energy responsible lies in the absorption tail. The direct excitation of an electron into the conduction band is not considered reasonable since there is good transmission up to 7·2 ev in the vacuum-annealed crystal.

Since the crystal is essentially in its virgin state there are three predominant possibilities for the trapping of an electron,

(i) at a negative ion vacancy,

(ii) at an interstitial positive ion or oxygen atom,

(iii) at an interstitial impurity ion or atom.

Following on the discussion under " Impurities " a centre of type (i) is preferred.

The hole which is released will jump from one lattice site to another very rapidly, making about 10^{13} jumps per second. The simplest trapping centre it might finish at would be a positive ion vacancy. An electron in a valence state of an ion adjoining such a vacancy, would have a higher energy than on an ion in a complete part of the lattice. And since a minimum photon energy of around 2 ev is necessary in order to cause the positive hole to be released, the state is presumably 2 ev or so above that of a normal valence electron. Hence we may represent the electrons adjoining a positive ion vacancy as being in a state 2·1 ev above the valence band. It will be shown that this simple scheme fits several other observations on ultra-violet activated crystals.

Alternatively the absorption at the irradiating ultra-violet photon energies could arise from centres with widely overlapping wave functions.

which would tend to destroy any fine structure. In this case the transitions would have to be to the conduction band, and the positive hole left behind would have to be free to wander about it in the lattice.

On either of these schemes the photocurrent caused by ultra-violet irradiation is due to the subsequent movement of positive holes released at negative ion vacancies to positive ion vacancies. It is observed (Day 1953) that this photocurrent decreases by a factor of 2 after continued irradiation ; this is due to the ' using up ' of the vacancies present and to increased optical absorption around 4 ev.

The decay of photocurrent at 2·1 ev takes place at a very slow rate occupying several hours. This is presumably due to the thermal activation required to take a positive hole up to a negative ion vacancy. Because of this the probability for recapture at a positive ion vacancy would be greater than for returning to the negative ion vacancy.

This scheme would mean that the level of activation made possible by ultra-violet light is proportional to the number of defect centres in the virgin crystals. This is experimentally supported by both photoconductive and optical absorption data. In the photoconductive case the activation level at photocurrent saturation is a factor of two lower after careful annealing ; this treatment would tend to reduce the number of defects (Day *loc. cit.*). The optical absorption level attainable by 4·85 ev (2537 Å) irradiation is reduced, by the factor of 4, after very slow annealing *in vacuo* from 1400°C.

Since the electron on an ion in the neighbourhood of a positive ion vacancy has a raised potential energy, we would expect luminescence to be associated with the 2·1 ev centre production. Nothing is visible to the eye, perhaps due to the high light background from the irradiating source. However, Eisenstein (1954) has observed a multiband luminescence spectrum on x-irradiation, with a long-time phosphorescence at 3·6 ev. After this phosphorescence was over the luminescence could still be stimulated by irradiation at around 2·1 ev. It is expected that x-irradiation would produce at least all the phenomena caused by ultra-violet irradiation, and so we would expect similar holes and electrons to be trapped. On the scheme under consideration then, the multiband spectrum during x-irradiation would be partially due to the hole trapping at positive ion vacancies, as well as simultaneous annihilation of F-type centres by other positive holes. The later stimulation of luminescence at 3·6 ev would then be the result of releasing the holes by 2·1 ev photons, and their recombining with electrons to give both luminescence and the observed optical absorption decay.

A possible explanation may be given for the enhanced decay of absorption at 2·1 ev by light irradiation plus simultaneous heating. Light irradiation alone may cause the holes trapped at positive ion vacancies to be released. These holes can either go to some impurity ion or to an occupied negative ion vacancy if they are to be trapped or annihilated without returning to a positive ion vacancy. However if the trapping

or annihilating centre carries an effective positive charge, the released positive hole will need a further energy to enable it to jump the resulting potential barrier. But many of the inhomogeneities supposed to exist may carry on effective positive charge, e.g. any impurity ion which may be capable of increasing its charge, Fe^{2+} etc., or a negative ion vacancy with one or perhaps even two electrons. Now the additional effect of temperature upon the kinetics or such a system would be to increase the rate of purely thermal release of both positive holes at positive ion vacancies and electrons at negative ion vacancies. In addition it would assist the rate with which released positive holes could surmount the potential barrier prior to trapping or recombination with trapped electrons.

Hence in thermal bleaching alone the factor limiting the rate is the effect which the temperature has upon the release probability of a hole. For optical bleaching the factor limiting the rate is the effect of temperature upon the combination probability of a positive hole with an ion in the neighbourhood of a negative ion vacancy. Levy and Varley (1955) have observed a similar enhanced rate of bleaching for vitreous silica.

5.3. *Cathodoluminescence*

Cathodoluminescence results have been reported by Gandy (1955), Saksena and Pant (1955) and Woods and Wright (1955). The process involved in the formation of this luminescence is that electrons bombarding the crystal cathode, penetrate the lattice and strip electrons off

Table 2

Source of information	Photon energy of luminescence (max.) (e.v)								
Gandy	1·7	1·9	2·1	2·2	2·4	2·7	3	3·6	5·1
Saksena and Pant			2·05	2·2		2·7		3·7	5·1
Woods and Wright		1·95	2·04	2·3		2·8	3·1		

ions. These electrons are given sufficient energy to reach the conduction levels where they are free to move until trapped at some centre. Part of the transition to this centre is non-radiative, because once the electron has left the ion, a lattice relaxation takes place. The remainder of the transition to a state of lower energy will possibly be radiative, and constitutes the luminescence.

Luminescence in MgO has been detected at various photon energies and these are detailed in table 2. The 5·1 ev band has been shown by Gandy and Saksena and Pant to be associated with excess oxygen and the 2 ev,

2·4 ev and 2·7 ev bands have been shown by Gandy, and Woods and Wright to be associated with excess magnesium.

In interpreting the luminescence energies we would expect to be able to tie each to a transition from the final energy state of the released electron to an empty defect state. In general this energy will be less than that required to get an electron directly into the conduction band, because of lattice relaxation ; the defect centre to which the electron moves will already be in a relaxed position. Hence each of the above emissive energies taken from the minimum energy of a released electron, in the conduction band, should represent the energy of various states measured from the top of the valence band.

There is some evidence (Johnson 1954) that the absorption edge lies above 7·3 ev, and if the luminescence energies are taken from 7·2 ev there is a reasonable correlation as shown in table 3.

Table 3

Absorption band energies (e.v)	1·2	2·1–2·35	3	3·5-3·7	4·3	4·8–4·9	5·6–5·7
Emissive energy (ev)		5·1		3·6	3	2·4, 2·2, 2·1	1·7
7·2–Emissive energies (ev)		2·1		3·6	4·2	4·8, 5, 5·1	5·5

The emissive energy of 2·7 ev is not accounted for. This is consistent with there being transitions between the two states at 4·95 and 2·35 ev associated with excess magnesium. The luminescence band at 2·1 ev could also be made up of direct trap to valence level transitions.

Saksena and Pant (1955 *loc. cit.*) have proposed a scheme for the observed cathodoluminescence in the case of an excess magnesium crystal based upon a conduction band width of only 5·9 ev. It is difficult to see how this can be so when it is possible to obtain good transmission in a stoichiometric crystal up to 7 ev. However some of the transitions which they propose would be valid for the radiative decay of excitons formed in the tail of the fundamental edge or for the band to band transitions associated with negative ion vacancies or other excess magnesium defects ; in this sense the present proposals supplement theirs by showing that the observed data and their proposals for band to band transitions are not inconsistent with assuming a forbidden band width of over 7 ev.

Garlick (1956) has pointed out that since the ratio of dielectric constants for low and optical frequencies is (9·7/2·95), and the high temperature activation energy for semiconduction is 2·1 ev, the absorption edge should be around 7 ev as suggested by optical studies.

5.4. *The Band Scheme Picture*

The band scheme picture which emerges is shown in fig. 9. If the optical transition width for the forbidden band be taken as 7·2 ev, then the positions of the 2·35 ev, 3·6 ev and 4·95 ev bands are unambiguously fixed relative to the top of the valence band. This is because transitions to the 4·95 ev, 3·6 ev and 2·35 ev levels from the top of the valence band are numerically the same as 2·35 ev, 3·7 ev and 4·95 ev transitions from these levels to the conduction band at 7·3 ev. Hence it has to be decided whether these transitions observed represent the movement of electrons to or from these levels. But since they have been associated with the trapping of electrons at negative ion vacancies, their representing transitions to the conduction band is preferred. Hence the action of ultraviolet light is to fill these levels.

Fig. 9

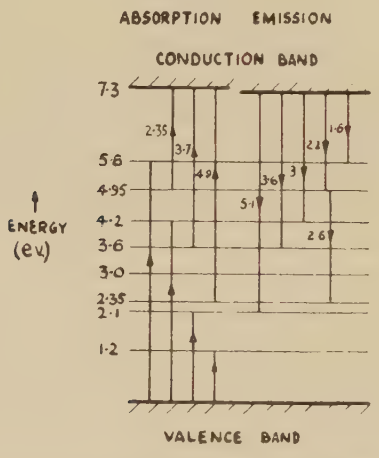

The suggested scheme for absorption and luminescence. All transitions are given in electron-volts.

Day's results make it certain that the 1·2 ev and 2·1 ev transitions are due to the excitation of electrons into levels at 2·1 ev, which are full in the unirradiated crystal. The instability of the 1·2 ev and 4·95 ev bands at room temperature may be associated. The thermal excitation of electrons into the 1·2 ev band frees positive holes which are trapped at the 2·35 ev level ; this reduces the number of electrons which can make up the 4·95 ev transition from this level.

The 4·2 and 5·6 ev absorption bands are associated with positive holes trapped at positive ion vacancies. Hence the transtion is one from the valence level of an ion further away from the centre, to a level very near the vacancy. In an unirradiated crystal the valence band level will become locally raised due to the perturbing effect of the doubly-charged vacancy. This is expressed in another way by noting that the lattice

relaxation will effectively change the ion–ion spacing locally, which will cause both the conduction and valence energy levels to be raised. Hence we would expect a transition to the perturbed 7·2 ev level to take place only if the ion was in a high vibrational state at the appropriate moment of absorption ; this would allow it to make the transfer to the minimum energy state for the conduction levels. For this reason the transition from the 4·3 ev and 5·6 ev levels to the 7·2 ev conduction band level would normally be forbidden, and these transitions are not in fact observed.

Acknowledgments

I would like to thank all those who have helped me by discussion and by reading the draft of this paper ; in particular Dr. J. H. O. Varley has given up a considerable amount of his time to general discussions, and Dr. W. M. Lomer has helped me on several specific points. I am indebted to Dr. P. Murray for placing at my disposal the facilities available in his Group, and particularly to Mr. Thorold Jones for help in the preparation of specimens.

I would also like to thank Dr. H. M. Finniston for continual interest and encouragement, and Dr. F. C. Champion of King's College, London, and Mr. O. Flint for advice at the outset of the work.

References

Boyd, C. A., Rich, D., and Avery, E., 1947, *U.S.A.E.C.*, MDDC–1508.
Day, H. R., 1953, *Phys. Rev.*, **91,** 4.
Dexter, D. L., 1956, *Phys. Rev.*, **101,** 48.
Eisenstein, A., 1954, *Phys. Rev.*, **93,** 1017.
Garlick, G. F. J., 1956, *Handbuch der Physik*, **19,** 316.
Gandy, H. W., 1955, *O.N.R. Quarterly Progress Report, June.*
Hibben, J. H., 1937, *Phys. Rev.*, **51,** 530.
Johnson, P. D., 1954, *Phys. Rev.*, **94,** 845.
Jost, W., 1953, *Diffusion* (New York : Academic Press), p. 107.
Levy, M., and Varley, J. H. O., 1955, *Proc. Phys. Soc.* B, **68,** 223.
Molnar, J. P., and Hartman, C. D., 1950, *Phys. Rev.*, **79,** 1015.
Mott, N. F., and Littleton, M. J., 1938, *Trans. Faraday Soc.*, **34,** 485.
Saksena, B. D., and Pant, L. M., 1955, *J. Chem. Phys.*, **23,** 5 ; 1954, *Proc. Phys. Soc.* B, **67,** 811.
Strong, J., and Brice, R., 1935, *J. Opt. Soc. Amer.*, **25,** 287.
Weber, H., 1951, *Z. Physik.* **130,** 392.
Woods, J., and Wright, D. A., 1955, *Proc. Phys. Soc.* B, **68,** 566.
Yamashita, J., and Kurosatwa, T., 1954, *J. Phys. Soc., Japan*, **9,** 945

The Excitation of a 2·79 MeV Level in ^{19}F by Inelastic Neutron Scattering†

By Joan M. Freeman
Atomic Energy Research Establishment, Harwell

[Received February 20, 1957]

Abstract

Gamma-rays of energy 2·594±0·015 mev have been observed following the inelastic scattering in ^{19}F of neutrons in the energy range 3·2 to 3·7 mev. They are attributed to a level at 2·791±0·015 mev which decays principally by a transition to the second excited state at 197 kev. The cross section for production of these gamma rays has been measured as a function of neutron energy and the result compared with the predictions of the Hauser–Feshbach model for different values of the spin of the level. It is concluded tentatively that the spin of the 2·79 mev level is either 9/2 or 7/2.

§ 1. Introduction

Interest in the levels of ^{19}F has received a considerable stimulus from the intermediate-coupling shell-model calculations of Elliott and Flowers (1955) and Redlich (1955); they have predicted a number of properties for the even-parity states, including the spins, which follow the sequence 1/2, 5/2, 3/2, 9/2. Paul (1956) has recently shown that very similar predictions can be made on the basis of Nilsson's rotational model (Nilsson 1955).

The data obtained from a variety of experiments concerning the positions, spins, and decay scheme of the first seven levels of ^{19}F are summarized in fig. 1.‡ The 197 kev level has been definitely established as a 5/2+ state and the 1·56 mev level is almost certainly 3/2+. The first excited state, at 110 kev, is 1/2− : it has been suggested that this state is like a ^{20}Ne nucleus with a hole in the $p_{1/2}$ shell of its ^{16}O core. The levels at 1·35 and 1·47 mev have been found both by inelastic neutron and inelastic proton scattering. Their spins and parities have not been established and the assignments shown in brackets are a guess which has been used in some calculation to be discussed below : the guess is

† Communicated by the Author.

‡ For references see the papers on gamma-rays following inelastic neutron scattering (Freeman 1956), on gamma-rays following inelastic proton scattering (Toppel *et al.* 1956), and on inelastically-scattered proton groups (Squires *et al.* 1956).

based on the suggestion that these two states may correspond to a ^{20}Ne* nucleus in its first excited state, again with a $p_{1/2}$ hole.

The interest of the present paper lies mainly in the next level, at 2·79 MeV, which is predicted to be a 9 2+ state. This level has been observed in particle emission in several experiments, the most accurate being the recent measurement of an inelastically scattered proton group by Squires *et al.* (1956): they obtained the value $2{\cdot}784 \pm 0{\cdot}008$ MeV for this level, which was the only one observed between the 1·56 MeV state and one at 3·9 MeV. In the experiments to be described here a gamma-ray of energy $2{\cdot}594 \pm 0{\cdot}015$ MeV has been observed, following

Fig. 1

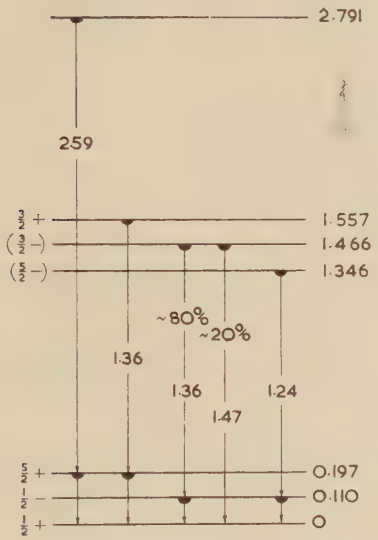

Level and decay scheme of ^{19}F.
Observed level energies and gamma-ray transitions are given in MeV.

inelastic neutron scattering, the threshold being at a neutron energy somewhat greater than 3 MeV. Since there are no other known levels from which it could arise, this gamma-ray is attributed to the 2·79 MeV level with the assumption that it is produced in a transition to the second excited state at 197 kev. This would give a value of $2{\cdot}791 \pm 0{\cdot}015$ MeV for the level, in good agreement with the measurement of Squires *et al.*

§ 2. Experimental Method and Results

The observations were made with a ring-geometry arrangement previously described (Freeman 1956). Neutrons, obtained from the T(pn) reaction with an energy spread of 70 kev, were scattered by a teflon (effectively CF_2) ring of outside diameter 10 cm, inside diameter

5·5 cm and thickness 2 cm, placed with its axis along the direction of the proton beam and its centre 36 cm from the neutron source. Gamma-rays were detected by a shielded sodium–iodide crystal, 3·8 cm in diameter and 2·5 cm thick, situated at the centre of the ring. The crystal could thus receive gamma-rays emitted from the ring within the angular range 45° to 125° with respect to the direction of incident neutrons. The neutron flux was measured with absolutely calibrated BF_3 long-counters. Gamma-ray spectra were recorded on a hundred-channel analyser, first with the teflon ring in position, and secondly with a ring of carbon, of mass chosen to produce about the same amount of elastic scattering. The spectra were then subtracted to give the

Fig. 2

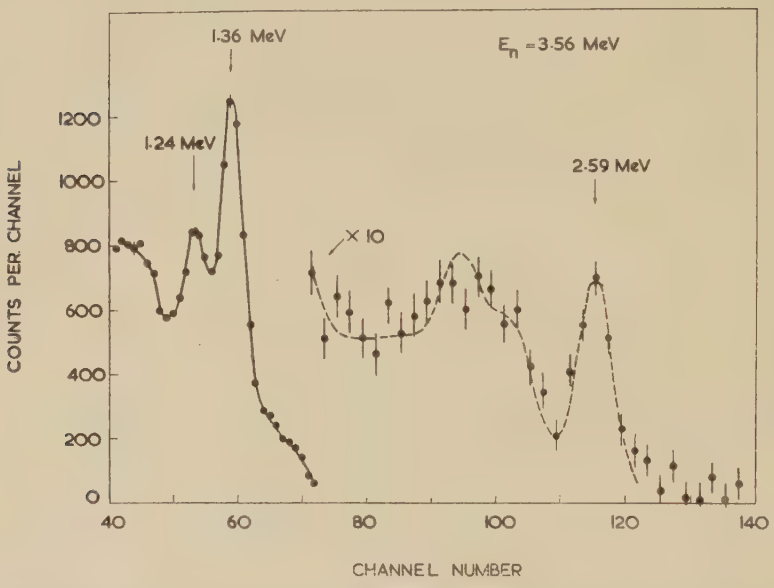

Spectrum of gamma-rays following inelastic scattering of 3·56 MeV neutrons in ^{19}F. The broken curve is the spectrum of a RdTh source of 2·615 MeV gamma-rays, fitted to the 2·594 MeV fluorine peak.

spectrum of gamma-rays due to inelastic scattering in fluorine. A typical result obtained in this way for a mean neutron energy of 3·56 MeV is shown in fig. 2. The energy of the peak at 2·594 MeV was measured by comparison with a RdTh source of 2·615 MeV gamma-rays. The broken curve shows the shape of the RdTh spectrum, adjusted to fit the 2·59 MeV peak. The Compton edge due to 2·59 MeV gamma-rays is evident, and also the position of the peak corresponding to the loss of one annihilation gamma-ray following pair-production in the crystal; the peak corresponding to loss of both annihilation gamma-rays is somewhat obscured by the rise of the spectrum at lower energies. Evident here are the peaks of 1·36 and 1·24 MeV gamma-rays following inelastic neutron scattering to the lower levels of ^{19}F.

The cross section for production of 2·59 MEV gamma-rays in the angular range of observation, at a particular neutron energy, was obtained by the following methods : (i) calculation of the efficiency of detection of the NaI crystal, (ii) comparison with a RdTh source of 2·615 MEV gamma-rays of known strength, and (iii) comparison with the yield of 1·36 MEV gamma-rays following inelastic scattering to the 1·56 and 1·47 MEV levels ; the absolute yield of 1·36 MEV radiation was measured at lower neutron energies, first by a comparison with the reaction ^{56}Fe(nn′)^{56}Fe* for which the cross section is known (Freeman 1955 a), and secondly by using the measurement by Day (1956) of the yield of 1·36 MEV gamma-rays at a neutron energy of 2·56 MEV. The total cross section for 2·59 MEV

Fig. 3

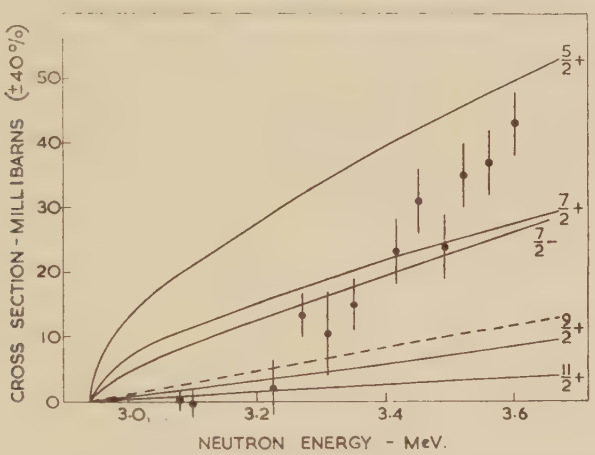

Excitation of the 2·79 MEV level in ^{19}F. The points give the observed cross section for 2·59 MEV gamma-ray production ; they represent the total cross section for excitation of the 2·79 MEV level to the extent that other modes of decay of this level can be neglected. The full curves are calculations based on the Hauser–Feshbach model for the spin assignments shown ; the broken curve is a complex potential calculation.

gamma-ray production was obtained, with an overall error estimated to be 40%, assuming the angular distribution of the gamma-rays to be isotropic to within 10%.

The yield of the 2·59 MEV gamma-rays was studied as a function of the initial neutron energy up to the maximum energy obtainable with the Harwell Van de Graaff machine. The result is shown in fig. 3. Ignoring the curves for the moment, the black circles show the observed variation in yield with neutron energy ; the errors given on the points are statistical. The ordinate scale gives the cross section for production of 2·59 MEV gamma-rays ; the total cross section for excitation of the 2·79 MEV level may be somewhat greater if gamma-ray transitions to levels other than the 197 KEV level are not negligible. The observations show that 2·59 MEV gamma-ray emission is the main mode of decay ;

transitions to the ground and first excited states are together less than 10%, but somewhat more branching to the levels at 1·35, 1·47 or 1·56 MeV could have occurred without detection. It is estimated that the values of the cross section for excitation of the 2·79 MeV level could be up to 50% higher than those given in the figure for 2·59 MeV gamma-ray production. However the main feature of the experimental results remains, namely the very slow rise in yield for the first 300 kev above the threshold (2·94 MeV in the laboratory system), which suggests a large spin difference between the 2·79 MeV level and the ground state.

§ 3. Theoretical Comparisons

An attempt has been made to determine the spin of the 2·79 MeV level by making a comparison with the Hauser and Feshbach model (1952). The basic assumption for application of this theory is that, at the given excitation energy of the compound nucleus and with the energy spread used in the incident neutron beam, many levels of the compound nucleus can be excited, so that resonance and interference effects are not encountered. The cross section for formation of a compound nucleus with neutrons of angular momentum l is assumed to be of the form $\sigma_c^{(l)}=(2l+1)\pi\lambda^2 T_l(E)$, where the $T_l(E)$ are transmission coefficients. In the decay of the compound state, competition between neutron emission to the various accessible levels of the target nucleus is considered, and the cross section for excitation of any particular level is obtained by summing over all possible l-values, channel spins, and J-values of the compound state. For our calculations the spins and parities assumed for the lower ^{19}F states were as indicated in fig. 1.

In order to test the applicability of the model to our case calculations were first made for some of the lower ^{19}F levels. In fig. 4 the upper curve shows the calculation for excitation of the 1·35 MeV level and the points represent the observed cross section based on measurements of the 1·24 MeV gamma-ray by which this level decays (Freeman 1955 b). The lower curve gives the calculated cross section for excitation of the 1·47 and 1·56 MeV levels taken together ; it was convenient to combine these since each level emits a 1·36 MeV gamma-ray (see fig. 1) and the experimental points were obtained by measuring all the gamma-rays emitted from both levels. It is clear that in the neighbourhood of the thresholds for these lower levels the model is not applicable, there being, apparently, insufficient states in the compound nucleus. However, by the time one reaches the neutron energy range 3·0 to 3·6 MeV, where the level of excitation in ^{20}F is 10 MeV, the theoretical curves seem to agree fairly well with the experimental points. This may be fortuitous, but does encourage one to apply the calculations to the 2·79 MeV level. In fig. 3 the full curves give the predictions of the Hauser–Feshbach model for different spins and parities assumed for this level. The radius of the ^{19}F nucleus was taken to be $3{\cdot}9\times10^{-13}$ cm and the strong coupling approximation was used for the transmission coefficients T_l. An examination was

then made of the effect of introducing the parameters of the complex potential model (Feshbach *et al.* 1954) into the T_l coefficients ; the broken curve in fig. 3 shows the results of one such calculation, for a square well, with $V_0=42$ and $\zeta=0{\cdot}05$ for neutron energies up to 1 MeV and $V_0=40$ and $\zeta=0{\cdot}07$ for higher neutron energies†. The conclusion is that the experimental results cannot be fitted by curves of the Hauser–Feshbach type. It seems probable, therefore, that the assumption of a statistical distribution of levels in the compound nucleus is unjustified and that relatively isolated groups of levels are influencing the shape

Fig. 4

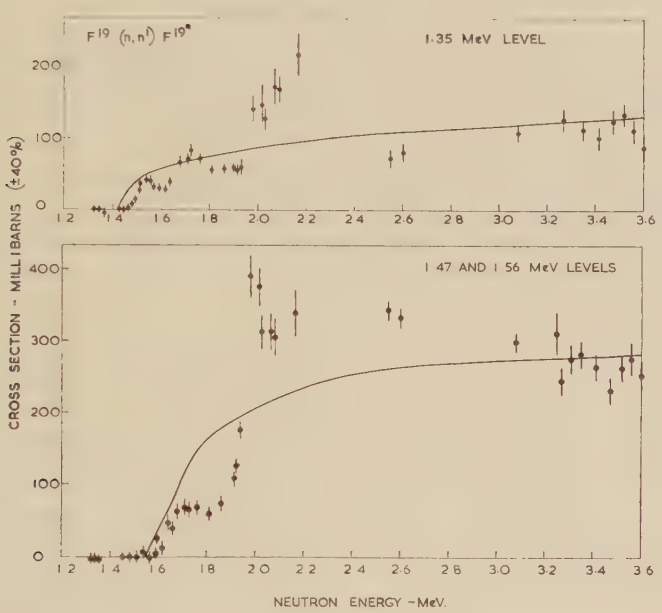

Cross section for excitation of the 1·35 MeV level in ^{19}F (upper diagram) and of the 1·47 and 1·56 MeV levels combined (lower diagram). The points were obtained from measurements of the gamma-rays and the curves from the Hauser–Feshbach formula.

of the cross section curve. In this connection it should be noted that, although the total cross section is quite smooth in this region (Hughes and Harvey 1955), Marion and Brugger (1955) have reported some resonant structure in the yield of the ^{19}F(n, α)^{16}N reaction for neutrons above 3·5 MeV in energy.

In view of the discrepancies one cannot make a definite spin assignment from the analysis of fig. 3 ; the behaviour of the cross section curve for the first 300 kev above the threshold suggests a spin equal to or greater

† I am very grateful to Dr. W. S. Emmerich of Westinghouse Research Laboratories for making available to me some of his calculations of complex potential model transmission coefficients.

than 9/2 for the 2·79 MEV level, whereas the trend at higher energies is more appropriate to a 7/2 spin. Tentatively we conclude that this level most likely has a spin of either 9/2 or 7/2 ; this would be consistent with the 9/2+ shell-model prediction.

REFERENCES

DAY, R. B., 1956, *Phys. Rev.*, **102,** 767.
ELLIOTT, J. P., and FLOWERS, B. H., 1955, *Proc. Roy. Soc.* A, **229,** 536.
FESHBACH, H., PORTER, C. E., and WEISSKOPF, V. F., 1954, *Phys. Rev.*, **96,** 448.
FREEMAN, J. M., 1955 a, *Phil. Mag.*, **46,** 12 ; 1955 b, *Phys. Rev.*, **99,** 1446 ; 1956, *Phil. Mag.*, **1,** 591.
HAUSER, W., and FESHBACH, H., 1952, *Phys. Rev.*, **87,** 366.
HUGHES, D. J., and HARVEY, J. A., 1955, *Neutron Cross Sections*, BNL 325.
MARION, J. B., and BRUGGER, R. M., 1955, *Phys. Rev.*, **100,** 69.
NILSSON, S. G., 1955, *Dan. Mat. Fys. Medd.*, **29,** No. 16.
PAUL, E. B., 1956, Amsterdam Conference, *Physica*, **22,** 1140.
REDLICH, M. G., 1955, *Phys. Rev.*, **99,** 1427.
SQUIRES, G. L., BOCKELMAN, C. K., and BUECHNER, W. W., 1956, *Phys. Rev.*, **104,** 413.
TOPPEL, B. J., WILKINSON, D. H., and ALBURGER, D. E., 1956, *Phys. Rev.*, **101,** 1485.

A Study of the Growth of Crystals from Solution when Subjected to Local Deformation†

By Anne P. Williams
Royal Holloway College, Englefield Green, Surrey

[Received January 16, 1957]

Abstract

The effect of local deformation on the growth features on crystal faces has been studied on crystals of lead nitrate and potassium di-hydrogen phosphate. New growth centres form at these points and these can be initiated where desired on the face and if strong enough will dominate over the existing centres of growth. This can be done repeatedly, and it is suggested as a possible method for controlling flawed regions in artificially grown crystals.

§ 1. Introduction

The natural growth phenomena of lead nitrate crystals when growing from aqueous solution have been described in a previous paper (Williams 1957). Following the work previously carried out on the local deformation of cadmium iodide crystals, Korndorffer *et al.* (1952), it was decided to carry out similar experiments on lead nitrate and potassium di-hydrogen phosphate crystals as these show clear layer formation on the growing faces. It was hoped that by this method some study might be made of the movement or creation of dislocations in the crystals.

The method used to observe and record the crystal growth using transmission phase contrast has already been described in the previous paper. The deforming tool was a fine glass needle. This was attached to the base of the condensing system on the microscope and could be raised and lowered with it, to enable the point to be brought slowly into contact with the upper growing surface of the crystal while under constant observation. Optical adjustment was made with the indenter raised and out of the field of view and the crystal was observed under these conditions apart from the time during indentation. The indenter being made of glass did not affect the illumination appreciably.

§ 2. Observations

Figures 1–9 (Plate) show a sequence filmed of a crystal of lead nitrate which was subjected to deformation. Before deformation the crystal was growing by the initiation of growth layers at the lower left-hand

† Communicated by the Author.

corner of the face under observation. The layer grows rapidly along the edges of the face and finally forms an enclosed pit (fig. 1 (Pl.)). This behaviour would continue throughout subsequent natural growth. As described in the previous paper it is concluded that this is growth by normal nucleation and not based on dislocation centres since these would move to the centre of the face at a later stage in the growth and this does not happen. Also, no evidence of the overlapping of a layer on one face on to another face has been found.

The crystal was then deformed and fig. 2 (Pl.) shows the fine point in contact with the surface. It appears very large relative to the crystal, but in fact contact is only made in a small area. The ' point ' must be an irregular circularly shaped section of the filament from which the point is made and the part of the rim of this which first makes contact with the crystal surface acts as the indenter. That this is so is seen in the following fig. 3 (Pl.), which is that taken immediately after the removal of the indenter, the time of contact being made as short as possible. The three black spots mark the points of contact. The natural growth layers can still be seen following their original pattern. For transmission phase contrast the high edge of a step on the surface appears dark and the low side appears bright. The next two photographs, figs. 4 and 5 (Pl.), show that the points of contact becomes an active growth centre. The old natural growth layers complete themselves on the right-hand side of the face but the next natural layer from the left is overwhelmed by a larger step from the new centre.

The new centre is complex at first, but later, fig. 6 (Pl.), it becomes steady, regularly forming layers in the form of closed loops. The sequence of photographs, figs. 6–8 (Pl.), shows the formation of one of these loops, which appears to be by the action of two screw dislocation sources of opposite hand. In fig. 8 (Pl.), the area inside the loop is quite clear of cracks etc., which shows that the deformation which was produced was very slight, yet it was completely effective in making the point of indentation the initiation centre of growth layers. It might be expected that this effect would only be a temporary one, which would die out after the damage had been healed. However layers continued to form from this point, and it provides the source of the future growth of the crystal. This behaviour has occurred on all crystals studied. Once deformed the subsequent growth is entirely from the deformation centre. When natural growth is taking place from a centre within the face before deformation, the point of deformation still becomes dominant and the natural centre dies out. This is illustrated with a deformation centre in figs. 10 and 11 (Pl.), after the crystal previously discussed has been deformed a second time and a new growth centre induced to the left of the first one. In fig. 10 (Pl.), this has just been formed and the previous centre is still active, the loop on the right having been formed by it, but a few seconds later, in fig. 11 (Pl.), the new centre is dominant and remained so for the remaining growth. This repeated initiation of

growth centres, each in turn dominant could be carried out at will, and thus one could locate the centre of growth of a crystal at any desired point.

The behaviour of the layers at the deformation centres often appears to give evidence of screw dislocation, in that they often show a spiral form. Figure 9 illustrates this on the crystal of lead nitrate already described. The interesting thing is the manner in which these shapes form. The steps on the crystal surface are formed by the bunching together of smaller layers formed at the complex centres as described in the previous paper. This also happens at the deformation centres. Figures 12–14 (Pl.) show another crystal of lead nitrate after deformation. Before deformation the growth layers formed by nucleation, as described for the previous crystal. After indentation the growth was complex for a few seconds, layers of the closed loop type forming. In fig. 12 (Pl.), the left-hand edge of the loop in the process of formation is thicker than the right-hand end and this causes incomplete joining of the layer so that the thicker turns and dominates the screw dislocation of the opposite hand leaving a spiral form on the surface of the crystal. This persists strongly for some time, all the growth taking place from the dominant screw dislocation centre. The behaviour is periodic, however, and after a certain time, about one minute, the centre becomes quiescent and the growth dies out. No more layers appear to form, the existing layers grow out and the surface becomes flat. The centre as a whole then becomes active again repeating the procedure of forming initially closed loops ; then the left-hand arm builds a thicker step and a spiral form is again set up. This periodic behaviour was observed to repeat at intervals of a few minutes. This is explained by the fact that the centre is complex and at one time the elementary layers reinforce and bunch together preferentially in one area but cancel one another in another area, as described by Frank (1949) in his description of the behaviour of several centres within an area. Such an array of dislocations must have been generated during the deformation process. The combinations of the elementary layers depends on their thickness, and the separations of the centres in the local area. At certain instants they will combine sufficiently to cause spiral growth forms, at others they will cancel and the face will appear to have stopped growing with visible layers.

§ 3. Multiple Deformation

This has already been mentioned with the first crystal of lead nitrate described. Repeated deformation is also illustrated in figs. 15–18 (Pl.), showing the effect of deformation on a crystal of potassium di-hydrogen phosphate. Figure 15 (Pl.) shows the layer formation from the first deformation centre made in the centre right where the crack mark at the point of indentation can be seen. Figure 16 (Pl.) is one taken some minutes later when an indentation had been made lower and to the left in the face. The crack mark associated with this can be seen and also

that due to the first deformation. The new centre dominates the growth on the face, though the old centre is still active, modifying the layers passing over this region. Figure 17 (Pl.) shows the effect of a third deformation in the centre of the face to the left of the first point of contact and at the same time of a fourth centre initiated at the top of the face. These are now acting together and the influence of the second centre is still seen. The last photograph shows a final deformation made at the lower edge which has dominated all previous centres. The crack marks of the old centres are absorbed into the body of the crystal. The growth centre can be changed at will in this way, the strength of the deformation determining whether the effect of previous centres will remain.

In this way it might be possible to control the growth centres on the faces of artificially grown crystals. The growth in crystal faces seem from the evidence of the experiments and previous studies on natural growth to be associated with flaws or imperfections which are propagated through the body of the crystal as growth proceeds. To control the growth centres gives a means of producing unflawed regions in the crystal which will be formed by layer deposition away from the initiating centre of growth.

When these experiments were commenced it was hoped that it might be possible to move dislocation centres of growth so that the movement and resulting slip traces might be seen. Efforts have been made to produce movement by stressing cadmium iodide crystals which exhibited spiral layer growth. These experiments have not been successful. A new centre is generally formed at the point of stress, but the spiral centres were not affected. On lead nitrate the original centres were generally overcome by layers from the new centres formed, the original centres dying out immediately. On cadmium iodide also, after some time if strong enough, growth from the new centre will cover the crystal though the later stages of growth are often very complex on this crystal. For potassium di-hydrogen phosphate the new centres took a short time to establish themselves and did not always overwhelm the old ones. No slip was ever observed. Deformation did not appear to have any effect on the stacking fault lines, which were described in the previous paper. During the deformation local movement of dislocations was probably taking place but on a small scale probably immediately masked by the subsequent growth and bunching which occurs in the formation of visible growth layers.

Acknowledgment

The author wishes to acknowledge the award of a grant by the Department of Scientific and Industrial Research which made this work possible.

References

Frank, F. C., 1949, *Disc. Faraday Soc.*, **5**, 48.

Korndorffer, A., Rahbek, H., and Sultan, F. S. A., 1952, *Phil. Mag.*, **43**, 1301.

Williams, Anne P., 1957, *Phil. Mag.*, **2**, 317.

The Thermal Expansion of Solids†

By G. C. Fletcher
Department of Mathematics, University of Exeter‡

[Received December 19, 1956]

Summary

The assumptions involved in two well-known formulae due to Grüneisen are investigated and with these assumptions an explicit formula for the volume of a solid as a function of temperature is derived. Application is made to the case of KCl and the results compared with experiment with a view to deciding whether defects are present at high temperatures. Defects in the theory and a previous investigation by Fischmeister are discussed.

§ 1. Introduction

It has been suggested that when a solid approaches its melting point lattice defects such as vacancies and interstitial atoms may occur and that these could be responsible for the fairly rapid increase in coefficients of thermal expansion α in such temperature regions. Lawson (1950) has assumed that α should be constant for a perfect lattice and therefore deduces that defects do occur in the cases of AgCl and AgBr. Gertsriken (1954), in determining the number of holes and energies of hole formation in a number of metals and alloys, has tacitly made the same assumption, as has Uno (1951) in the case of NaCl. No theoretical reasons for this are given and it seems clear that the variation of volume with temperature predicted by theory for a perfect lattice is not fully understood. Obviously this point must be clarified before any conclusions can be reached regarding the presence of defects. Fischmeister (1956) has attempted to show that the theories of Debye and Grüneisen account completely for the expansion of the alkali halides so that no defects need be present but it is shown here in § 3 that his method is too insensitive to be conclusive on the point. In §§ 2 and 6 the assumptions involved in deriving two well-known formulae due to Grüneisen (1926) are investigated from both the mathematical and physical points of view and in § 4 a relation is derived between the volume and temperature of a Debye–Grüneisen solid involving the same assumptions. Calculations are carried out for KCl and the results are compared with experiment. Factors

† Communicated by the Author.
‡ Now at Department of Mathematics, University of Sydney, N.S.W.

which might be responsible for some of the wide discrepancy between theory and experiment are discussed and possible improvements to the theory are mentioned.

§ 2. Grüneisen's Equations

Let $\Phi(V, T)$ be the potential energy of volume V of a solid at temperature T with all atoms at rest in their equilibrium positions and $\mathscr{F}(V, T)$ the free energy of the vibrations of the atoms about these positions so that the total free energy of the solid is

$$F(V, T)=\Phi+\mathscr{F}. \quad . \quad . \quad . \quad . \quad . \quad . \quad . \quad (1)$$

Then the external pressure p on the solid is

$$p=-\left(\frac{\partial F}{\partial V}\right)_T=-\left(\frac{\partial \Phi}{\partial V}\right)_T-\left(\frac{\partial \mathscr{F}}{\partial V}\right)_T$$

and the equation of state of the solid may be put in the form

$$pV+G(V, T)=\gamma E(V, T) \quad . \quad . \quad . \quad . \quad . \quad . \quad (2)$$

where E is the internal energy of the vibrations and G, γ are defined by

$$G(V, T)=V\left(\frac{\partial \Phi}{\partial V}\right)_T, \quad . \quad . \quad . \quad . \quad . \quad . \quad . \quad (3)$$

$$\gamma(V, T)=-\frac{V}{E}\left(\frac{\partial \mathscr{F}}{\partial V}\right)_T. \quad . \quad . \quad . \quad . \quad . \quad . \quad . \quad (4)$$

No assumptions have been made so far although, as mentioned later, it may not be convenient or even possible to divide the free energy of the solid into two parts Φ and $\mathscr{F}$ as defined above. Now assume (*a*) that Φ is a function of V only, independent of T, so that G is also and (*b*) that $(\partial\gamma/\partial T)_V=0$. Then, differentiating (2) with respect to T at constant volume

$$\gamma\left(\frac{\partial E}{\partial T}\right)_V=V\left(\frac{\partial p}{\partial T}\right)_V=-V\frac{(\partial V/\partial T)_p}{(\partial V/\partial p)}. \quad . \quad . \quad . \quad (5)$$

But the specific heat at constant volume, coefficient of thermal expansion and isothermal compressibility are defined as

$$C_V=\left(\frac{\partial E}{\partial T}\right)_V; \qquad \alpha=\frac{1}{V}\left(\frac{\partial V}{\partial T}\right)_p; \qquad \kappa_T=-\frac{1}{V}\left(\frac{\partial V}{\partial p}\right)_T$$

and hence (5) may be written

$$\alpha=\frac{\gamma\kappa_T C_V}{V}. \quad . \quad . \quad . \quad . \quad . \quad . \quad . \quad . \quad . \quad (6)$$

Alternatively, with assumption (*a*) only, consider the equation of state (2) when $p=0$. Let V_0 be the equilibrium volume of the solid when $T=0$ (suffix zero will always have this meaning) and expand $G(V)$ as a Taylor series, putting $V-V_0=\Delta$

$$G(V)=G(V_0)+\Delta G'(V_0)+\frac{\Delta^2}{2!}G''(V_0)+\ldots.$$

If it is assumed (*c*) that the atoms are at rest in their equilibrium positions at $T=0$, a point to be considered if quantum theory is introduced, then for equilibrium one must have

$$\left(\frac{\partial F}{\partial V}\right)_{T\ 0}=\left(\frac{\partial \Phi}{\partial V}\right)_{T\ 0}=0 \qquad \ldots\ldots (7)$$

and hence $G(V_0)$ is zero. It may easily be shown (e.g. Roberts 1940) that

$$G'(V_0)=\frac{1}{\kappa_0}\ ; \qquad G''(V_0)=-\frac{2x}{V_0\kappa_0} \qquad \ldots\ldots (8)$$

where

$$x=-\frac{V_0^2\kappa_0}{2}\Phi_0'''-1. \qquad \ldots\ldots (9)$$

Thus (2) becomes

$$G(V)=\frac{\Delta}{\kappa_0}\left[1-x\frac{\Delta}{V_0}+\ldots\right]=\gamma E.$$

To a first approximation $\Delta=\gamma E\kappa_0$: substituting this in the square brackets on the left-hand side the result obtained is

$$\frac{\Delta}{V_0}=\frac{E/Q_0}{1-xE/Q_0+\ldots} \qquad \ldots\ldots (10)$$

where

$$Q_0=V_0/\gamma\kappa_0. \qquad \ldots\ldots (11)$$

Thus assumptions (*a*) and (*b*) are necessary in order to derive eqn. (6) and (*a*) and (*c*) to derive eqn. (10). Before considering the physical meaning of these assumptions a little more may be said about eqn. (10). For a monatomic solid treated as an elastic continuum by the Debye theory

$$E=3RTD\left(\frac{\Theta}{T}\right)\ ; \qquad \gamma=-\left(\frac{\partial \ln \Theta}{\partial \ln V}\right)_T$$

where $D(\Theta\ T)$ is the Debye specific heat function. At reasonably high temperatures this function is essentially constant so that, with the assumption that γ is independent of temperature $E/Q_0=AT$ where $A=-3(\kappa_0/V_0)\gamma RD(\Theta/T)$ is approximately constant. Then

$$\frac{\Delta}{V_0}=\frac{AT}{1-xAT+\ldots}$$

and Δ/V_0 will increase faster than linearly with T. This will be true on any theory provided that for the temperature range considered

$$\gamma E=-V\left(\frac{\partial \mathscr{T}}{\partial V}\right)_T=BT$$

where B is a constant (necessarily positive) and x, as defined by (9), is positive. With regard to the latter Grüneisen (1926) assumed for two atoms a distance ρ apart a potential of the form

$$\phi=-\frac{a}{\rho^m}+\frac{b}{\rho^n} \qquad \ldots\ldots (12)$$

and obtained $x=(n+m+3)/6>0$.

§ 3. Fischmeister's Investigation

Fischmeister (1956) has investigated the validity of eqn. (10) for the alkali halides when the Debye expression $6RTD(\Theta/T)$ is used for the internal vibrational energy E per mole of a diatomic molecular solid. By inverting the equation, he obtains

$$\frac{a_0}{a_T-a_0} \simeq \frac{3V_0}{\Delta} = \frac{Q_0}{2R}\frac{1}{TD(\Theta/T)} - 3x + \ldots \quad . \quad . \quad . \quad (13)$$

where a is a linear dimension of the solid. On the theory of Debye and Grüneisen $Q_0 = V_0/\gamma\kappa_0$ is independent of temperature so that, if $a_0/(a_T-a_0)$ is plotted against $1/TD(\Theta/T)$, a straight line should be obtained, ignoring terms after the second on the right-hand side of (13). In each case, using a constant experimental value of Θ, Fischmeister finds that the experimental results for $a_0/(a_T-a_0)$ do lie on a straight line and concludes that the dilatation of the alkali halides does vary in the manner predicted by Debye and Grüneisen. There would then be no need to invoke the occurrence of lattice defects to explain the rapid increase of dilatation near the melting point.

Two points in Fischmeister's treatment may be thought to have influenced the results. The first is the approximation $a_0/(a_T-a_0) \simeq 3V_0/\Delta$ and the second is the use of a constant value for Θ over the whole temperature and volume range. In the case of KCl the calculation was repeated by the present author, correcting the first approximation and allowing Θ to vary as $V^{-5/3}$ (see (19)) but no appreciable change in the graph was noted.

There still remains the point that the temperature scale of these graphs is far from linear so that any deviation from a straight line in the important high temperature range would be difficult to detect. The question is whether this method of plotting the experimental results is capable of distinguishing them from the results of a theory which postulates no defects when there are in fact defects present. In order to test this, graphs were plotted of $a_0/(a_T-a_0)$ against $1/TD(\Theta/T)$ assuming (i) a constant coefficient of thermal expansion of $0{\cdot}00014/^\circ$C for the range $273 < T < 1000^\circ$K and (ii) a coefficient $\alpha = 6\times10^{-5} + 1{\cdot}18\times10^{-7}T$ for this range, the actual figures being so chosen that a valid comparison could be made with Fischmeister's graph for KCl. The former is the type of assumption made by Lawson (1950) for a perfect lattice and the latter corresponds to assuming that a theory for a perfect lattice will give α increasing linearly with T for medium and high temperatures and any deviation from this is due to the occurrence of lattice defects. The results are shown in fig. 1 and it is seen that the Fischmeister method shows clearly that a Debye–Grüneisen solid could not have a constant coefficient of thermal expansion but it fails to distinguish between the actual solid and one which has α linearly dependent on T, i.e. there could be an occurrence of lattice defects at high temperatures in the actual solid.

For this reason it was decided to try to obtain a direct relationship between volume and temperature for a solid, based on the theories of Debye and Grüneisen, from which a graph of z against T could be plotted for direct comparison with experiment.

Fig. 1

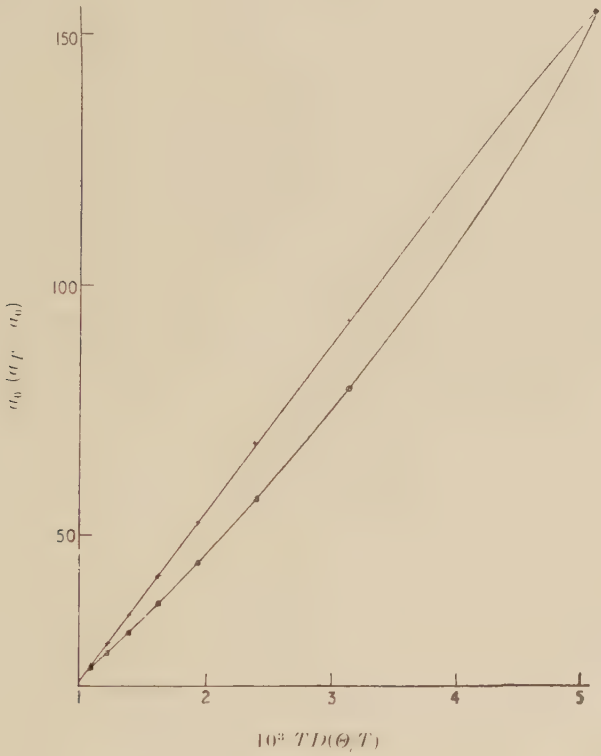

Expansion of KCl. —— Experiment (Eucken and Dannöhl 1934); ⊖⊖ Assuming $\alpha=0{\cdot}00014/^\circ$; × × Assuming $\alpha=6\times10^{-5}+1{\cdot}18\times10^{-7}T/^\circ$.

§ 4. Theory of Thermal Expansion

When $p=0$ the equation of state (2) becomes

$$G(V)=\gamma E. \qquad (14)$$

If we assume an interatomic potential of the form (12), it is easily shown (Grüneisen 1926) that for a monatomic solid

$$G(V)=V\left(\frac{\partial\Phi}{\partial V}\right)_T=\frac{mA}{3V_0^{m/3}}\left[\left(\frac{V_0}{V}\right)^{m/3}-\left(\frac{V_0}{V}\right)^{n/3}\right] \qquad (15)$$

where $A=aN^{(m+3)/3}\sigma_m$, N is the number of atoms per mole and assumption (*c*) of § 2 has been made. Provided it is assumed that no distortion of the lattice structure occurs as the volume changes, σ_m depends only on the type of structure and on m, being defined by $\sigma_m=\sum(r/\rho)^m$, where $V=Nr^3$ and the summation is over all pairs of

atoms in volume V, each pair being counted once. On Debye's theory for a monatomic solid treated as an elastic continuum E and γ are given by

$$E=\frac{9Nh}{\nu_m{}^3}\int_0^{\nu_m}\frac{\nu^3\,d\nu}{\exp(h\nu/kT)-1}, \qquad (16)$$

$$\gamma=-\left(\frac{\partial \ln \nu_m}{\partial \ln V}\right)_T \qquad (17)$$

where

$$\nu_m=\left[\frac{9N}{4\pi}\left(\frac{1}{c_l{}^3}+\frac{2}{c_t{}^3}\right)^{-1}\right]^{1/3}V^{-1/3}=CV^{-1/3}, \qquad (18)$$

c_l and c_t being the velocities of longitudinal and transverse waves respectively. It is not a good enough approximation to assume c_l, c_t independent of volume as this leads to $\gamma=\frac{1}{3}$, a value generally regarded as much too small for any solid. Grüneisen (1926), by considering the motion of one atom with all others fixed, the interatomic potential being of the form (12) with $n\gg m$, has obtained ν as a function of V for small amplitude vibrations and thereby deduces $\gamma=(n+2)\,6$. As a first approximation this seemed sufficient for present purposes and then (17) and (18) give

$$\nu_m=C_0V_0{}^{n/6}V^{-(n+2)/6}. \qquad (19)$$

From (7) and (8) it is easily shown that $A=9V_0{}^{(m+3)/3}/m(n-m)\kappa_0$: substituting (15) and (16) in (14) one obtains finally

$$\frac{J}{y^{(n+2)/2}}\left[\frac{1}{y^{m/3}}-\frac{1}{y^{n/3}}\right]=T^4\int_0^{K/Ty^{(n+2)/6}}\frac{x^3\,dx}{e^x-1} \qquad (20)$$

where $x=h\nu/kT$; $y=V/V_0$ and

$$J=\frac{2C_0{}^3h^3}{N(n-m)(n+2)\kappa_0k^4}; \qquad K=\frac{h}{k}C_0V_0{}^{-1/3}. \qquad (21)$$

§ 5. Calculation for KCl

It was decided to apply the above theory to KCl since it was one of the substances considered in Fischmeister's paper and the theory should be reasonably applicable to it for the following reasons.

(i) It is an ionic substance with the electrons tightly bound to the nuclei in the crystal so that electronic effects not considered above should be small.

(ii) An interatomic potential of the form (12) with $m\sim1$, $n\sim8$ seems to be generally accepted as a reasonable assumption for KCl: one notes incidentally that $n\gg m$.

(iii) The above theory is strictly applicable only to monatomic solids. However, if one assumes a potential (12) between like ions and one of the form $a\rho^{-m}+b\rho^{-n}$ between unlike ones with the same values of a, b, m and n, and one assumes that the two kinds of ions are of approximately equal mass as is the case for KCl, then eqn. (20) may be derived as before provided N is taken as the number of atoms in half the molar volume.

For the actual calculation the measurements of Durand (1936) of the elastic constants of KCl were extrapolated to 0°K to give $(c_{11})_0=5{\cdot}07\times10^{11}$; $(c_{12})_0=0{\cdot}6\times10^{11}$ dynes cm^2. Substituting these in the formulae

$$\kappa=\frac{3}{c_{11}+2c_{12}}\ ;\quad c_l^2=\frac{3(1-\sigma)}{(1+\sigma)\kappa\rho}\ ;\quad c_t^2=\frac{3(1-2\sigma)}{2(1+\sigma)\kappa\rho}\ ;\quad \sigma=\frac{c_{12}}{c_{11}+c_{12}} \qquad (22)$$

and assuming a value 2·07 g cm^3 for the density ρ, the following values were obtained

$\kappa_0=4{\cdot}8\times10^{-12}$ cm^2/dyne ; $\quad (c_l)_0=4{\cdot}94\times10^5$; $\quad (c_t)_0=3{\cdot}28\times10^5$ cm/sec.

Using a mean ionic weight of 37·28 g a value of 18·01 cm^3 was obtained for V_0 and then assuming $m=1$, $n=8$ gives

$$J=5{\cdot}25\times10^{10}\text{ deg.}\ ;\qquad K=344\text{ deg.}$$

For various values of y from 1 up to 1·12, eqn. (20) was then solved for T by trial and error. A graph was plotted of ln y against T, from which the coefficient of thermal expansion can be deduced since

$$\alpha=\frac{1}{V}\frac{\partial V}{\partial T}=\frac{1}{y}\frac{\partial y}{\partial T}=\frac{\partial \ln y}{\partial T}\,.$$

The variation of α with temperature is shown in fig. 2. It is seen that

Fig. 2

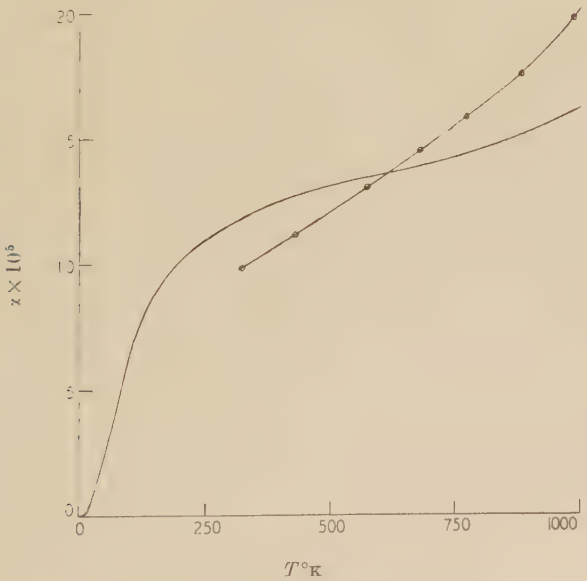

Thermal expansion of KCl.
—— Theoretical ; ⊖⊖ Experiment (Eucken and Dannöhl 1934).

it is of the same general shape as that obtained for C_v on the Debye theory as might have been expected. Moreover, it exhibits an upward curvature at high temperatures which does suggest that the Debye and Grüneisen theories as applied here will account for this phenomenon,

which is in fact observed, without postulating the presence of lattice defects. However, there is less cause for satisfaction when the curve is compared with experiment (Eucken and Dannöhl 1934) as is obvious from fig. 2 and it is worth while considering various factors which may affect the theoretical curve at least for medium and high temperatures. If one puts $J'=(n-m)J$ and $y=1+z$ in the left-hand side of (20) and expands by the binomial theorem, it takes the form

$$J'\left[\frac{z}{3}-\frac{4n+m+9}{3}z^2+\ldots\right].$$

For the right-hand side e^x-1 was expressed as a series and integration carried out term by term, giving a series valid for $T>Ky^{-(n+2)/6}$, i.e. $T>350^\circ$K in the present case. Again putting $y=1+z$ and expanding by the binomial theorem eqn. (20) may finally be reduced to a polynomial in z, whose coefficients are power series in $Q\,T$. In the present case it was found possible for $T>2K\simeq 700^\circ$K to neglect most of the terms resulting in the high temperature approximation

$$z\sim\frac{K^3T}{J'}\left(1+\frac{n+m+3}{6}\frac{K^3T}{J'}\right) \qquad . \quad . \quad . \quad . \quad (23)$$

and

$$\alpha=\frac{1}{1+z}\frac{\partial z}{\partial T}\sim\frac{K^3}{J'}\left(1+\frac{n+m}{3}\frac{K^3T}{J'}\right). \qquad . \quad . \quad . \quad (24)$$

Small changes in the individual values assumed for m and n are unlikely to affect the sum $n+m$ involved in this and in

$$\frac{\partial\alpha}{\partial T}\sim\frac{n+m}{3}\frac{K^6}{J'^2}.$$

The other important factor involved is K^3/J' and from (21) this is found to be equal to $N(n+2)\kappa_0 k/2V_0$. This does not depend critically on n, which is certainly quite large, nor is there likely to be much error in the value assumed for V_0. However, judging by Durand's own estimates of $(c_{11})_0$, $(c_{12})_0$ and κ_T at $T=303^\circ$K, it does appear that the value assumed here for κ_0 is probably too low. A larger value would increase both α and $\partial\alpha/\partial T$ at high temperatures, improving the agreement with experiment.

§ 6. Physical Nature of Assumptions

Some consideration will now be given to the physical meaning of the assumptions made by Grüneisen in deriving (6) and (10) which are also involved in the derivation of (20).

(*a*) If the volume of a solid is kept fixed and the temperature varied, some of the heat added or taken away will change the energy and therefore the distribution of the electrons in the lattice. This will result in an alteration of the interatomic potential and hence of the total potential energy Φ of the solid. Thus in general Φ will not be a function of volume only although this may be regarded as a valid approximation for certain solids at temperatures where electronic effects are generally regarded

as negligible. When it is necessary to consider the electrons specifically, e.g. in metals at low temperatures, it may be preferable to abandon the concept of a separate potential energy Φ and treat the total free energy F as a single quantity either by classical or quantum methods.

(*b*) The total internal energy of a solid is defined by

$$U=\Phi+E=F+TS=F-T\left(\frac{\partial F}{\partial T}\right)_V$$

so that $E=\mathscr{T}-T(\partial\mathscr{T}/\partial T)_V$ and by (4)

$$\gamma=\frac{V(\partial\mathscr{T}/\partial V)_T}{\mathscr{T}-T(\partial\mathscr{T}/\partial T)_V}. \qquad \ldots\ldots \quad (25)$$

It is very difficult to get a physical picture of γ from this definition or to appreciate the physical meaning of the assumption that $\partial\gamma/\partial T)_V=0$. On the Debye theory (25) reduces to the usual well-known formula and, if a wave of frequency ν_m has wavelength λ_m and velocity c_m this is

$$\gamma=-\frac{\partial \ln \nu_m}{\partial \ln V}=-\frac{\partial \ln c_m}{\partial \ln V}+\frac{\partial \ln \lambda_m}{\partial \ln V}. \qquad \ldots\ldots \quad (26)$$

The minimum wavelength λ_m must be of the order of the distance between nearest neighbouring atoms in the lattice so that it is reasonable to assume $\lambda_m \propto V^{1/3}$ and the second term then contributes the constant value of $\frac{1}{3}$ to γ. As regards the first term, if V is increased, interatomic coupling is decreased and therefore c_m is decreased and this term is positive, giving $\gamma>\frac{1}{3}$. More than this it is difficult to say without considering a specific model. The only reasons why γ should vary with temperature at constant volume are the consequent changes in the interatomic forces, already considered above, and changes in the amplitude of the atomic vibrations thereby producing a smaller or larger mean force on one atom due to its neighbours which would affect c_m.

For different types of wave, e.g. longitudinal and transverse, a ν_m and γ may be defined for each: in general they will be different from one another and will show different temperature variation as the corresponding c_m are different functions of c_{11} and c_{12} for instance (see (22)). Again, $\partial \ln \lambda_m/\partial \ln V$ should be $\sim\frac{1}{3}$ for waves in all crystallographic directions but $\partial \ln c_m/\partial \ln V$ and hence γ will vary with direction in general. Finally for crystals with atomic groups of much stronger internal coupling than that between groups the group dimensions will vary much less than the crystal dimensions. Thus γ's which may be defined for vibrations within a group should be smaller than those defined for vibrations of the crystal as a whole.

(*c*) Quantum theory shows that a simple harmonic oscillator has some vibrational energy even at absolute zero, so that the equilibrium condition there should be $(\partial F/\partial V)_{T=0}=0$ and not $(\partial\Phi/\partial V)_{T=0}=0$, which would only be true if all the atoms were at rest. This point does not appear to have been considered before and is probably unimportant when relatively crude theories of the thermal behaviour of solids are involved.

§ 7. Discussion

It has been shown that two well-known formulae due to Grüneisen for the thermal expansion of a solid depend essentially on three assumptions. These same assumptions have been made in deriving a direct relation between volume and temperature, based as closely as possible on the theories of Debye and Grüneisen. Application to the ionic solid KCl has shown that, although the experimental observations on the thermal expansion of KCl may be explicable without postulating the occurrence of lattice defects at high temperature, Debye-Grüneisen theory does not give a good general agreement with experiment. This contrasts with the conclusion of Fischmeister, whose method, however, is shown to be too insensitive to be conclusive. It is realized that the present theory is very crude in that the Debye frequency spectrum for a solid is not regarded as more than a poor approximation and also that the Debye model of an elastic continuum has been mixed with the Grüneisen atomic model but the author hopes to extend the method to more realistic models of solids by use of the lattice theory of Born and von Karman and of plasma theory, particularly in the case of metals.

Acknowledgments

This work was carried out at the Royal Aircraft Establishment, Farnborough, while the author was acting as a vacation consultant to the Ministry of Supply and he wishes to express his gratitude for the cooperation and inspiration he obtained from everyone there, and in particular Dr. L. G. Carpenter, Dr. J. N. Eastabrook and Dr. D. L. Martin. He would also like to thank his fellow consultant, Mr. H. T. Hall, for his assistance in investigating previous work on thermal expansion.

References

Durand, M. A., 1936, *Phys. Rev.*, **50**, 449.
Eucken, A., and Dannöhl, W., 1934, *Z. Electrochem.*, **40**, 814.
Fischmeister, H. F., 1956, *Acta Cryst.*, **9**, 416.
Gertsriken, S. A., 1954, *Dokl. Akad. Nauk., U.S.S.R.*, **98**, 211.
Grüneisen, E., 1926, *Handb. der Physik* (Berlin : Springer), Vol. X, p. 1.
Lawson, A. W., 1950, *Phys. Rev.*, **78**, 185.
Roberts, J. K., 1940, *Heat and Thermodynamics* (London : Blackie).
Uno, R., 1951, *Busseiron Kenkyu*, **36**, 32.

Dislocation Locking and Fracture in α-Iron†

By J. Heslop‡ and N. J. Petch
Metallurgy Department, Houldsworth School of Applied Science, University of Leeds

[Received February 11, 1957]

Abstract

The inhibition of plastic deformation by dislocation locking promotes brittleness. The influence of manganese in iron is studied in detail and it is concluded that the ductility conferred by the manganese is associated with weakened dislocation locking as well as with grain refinement. The weakening of the locking appears to be due to interaction between nitrogen and manganese atoms.

§ 1. Introduction

It now seems fairly certain that the fracture of polycrystalline metals originates in cracks formed ahead of arrays of dislocations piled up against grain boundaries (Zener 1948, Mott 1953, Petch 1953, 1953, 1956 a, Stroh 1954, Greenwood and Quarrell 1954). Brittle (cleavage) fracture probably occurs when the crack produced by a dislocation array is sufficiently large to spread catastrophically across the specimen by its own concentration of the applied stress. On the other hand, ductile fracture would seem to arise when the crack produced is too small to spread in this way; further deformation, with the formation of further cracks, is then necessary to complete the fracture.

If plastic deformation occurs in the region of high stress ahead of a dislocation array, cracking may be suppressed. Alternatively, if a crack does form, it will be a short one when its formation is accompanied by plastic deformation, since some of the energy of the array is then dissipated in plastic work. Thus, plastic deformation gives protection against fracture, or, if this does occur, ductile fracture is favoured. Since dislocation locking influences the occurrence of plastic deformation, such locking will also influence the occurrence of fracture.

If the dislocation locking is sufficiently strong, complete brittleness in a tensile test will result. Less strong locking may be wiped out by deformation prior to fracture, but even then the onset of plasticity will be delayed to a higher stress and the plastic strain at fracture will be reduced.

† Communicated by the Authors.
‡ Now at the Naval Construction Research Establishment, Dunfermline.

The possibility that the dislocation locking is wiped out by prior deformation is less in fracture from a notch, since the strain rate is higher. In such fracture, dislocation locking will reduce the amount of plasticity associated with the spread of the crack from the notch and so will increase the crack velocity. This, combined with the locking ahead of the advancing fracture will increase the probability that it eventually changes to the cleavage type.

The effect of dislocation locking partly, possibly mainly, explains the greater brittleness of the body-centred cubic metals compared to the face-centred cubic ones, for the locking is particularly strong in the body-centred cubic structure. Enhanced ductility follows removal of the locking impurity. Thus, chromium is ductile in the absence of nitrogen. Similarly, the low temperature ductility of iron is increased when the dislocations are unlocked by a prior small deformation at room temperature (fig. 1).

Fig. 1

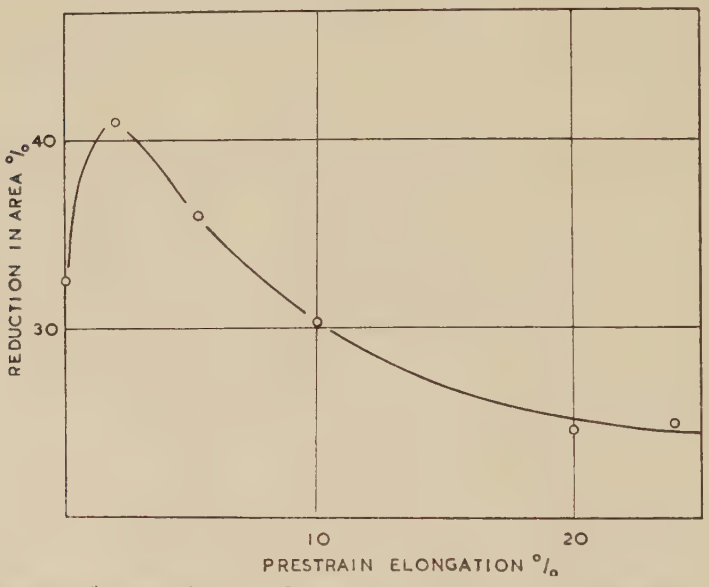

The influence of prestrain at 18°c on the ductility of mild steel at −196°c (Patwardhan and Petch, unpublished).

Technologically, the most important case of brittle fracture is that of mild steel. There, one of the principal safeguards against the occurrence of this type of fracture lies in the presence of sufficient manganese in the steel (Barr and Honeyman 1947). This has never been fully explained. Partly it is due to the finer grain size produced by the manganese and to the lower carbon content that can be used to give the same 'maximum stress' but this does not appear to be the complete answer. The present paper presents a study of the possible association of this effect of manganese with an effect on the dislocation locking.

§ 2. Measurements on Manganese Irons

The approach adopted involved an examination of the effect of Mn on the lower yield point $\sigma_{l.y.p.}$ and the fracture stress σ_f of polycrystalline iron at 18 and $-196°C$ for a wide range of grain diameter l. This permitted an evaluation of the influence of Mn on the constants σ_0, k and k^* in the relationships

$$\sigma_{l.y.p.}=\sigma_0+kl^{-1/2}, \quad . . . . . (1)$$

$$\sigma_f \quad \sigma_0+k^*l^{-1/2}, \quad . . . . . (2)$$

The form of (1) is consistent with the propagation of a Lüders band from grain to grain by the shear stress ahead of an array of dislocations held up by the grain boundary and proportional in length to l. The form of (2) is consistent with the production of fracture by the tensile stress ahead of such an array. This relationship applies to both the cleavage and ductile fracture of α-iron and k^* has practically the same value in both cases (Petch 1956 a).

The magnitudes of k and k^* are a measure of the stress required ahead of the array for the propagation of the yield or for cracking. Thus, if Mn modifies the dislocation locking, it should alter k.

Table 1. Composition of the Irons, Weight %

Mn	C	Si	P	S	N	Al
0·02	0·04	0·12	0·03	0·01	0·006	0·03
0·25	0·03	0·12	0·03	0·01	0·006	0·03
0·47	0·04	0·11	0·03	0·01	0·006	0·02
0·91	0·04	0·14	0·03	0·01	0·006	0·02
1·90	0·05	0·17	0·03	0·01	0·008	0·02

Ni, Cr, Mo and V all $<0·02$.

The constant σ_0 is a measure of the stress opposing the motion of a free dislocation through the grain and consequently opposing the compression of the dislocation array (Cracknell and Petch 1955, Heslop and Petch 1956).

Five irons were examined in which as far as possible the only composition variation was in the Mn content.

The general experimental procedure for the determination of the yield point and fracture stresses was the same as previously employed (Cracknell and Petch 1955, Petch 1956 a). The variation in grain size was obtained by the same types of heat treatment as before and the specimens were all tested in the annealed condition. Tensile specimens with 1 in. gauge length of 0·125 in diameter were used and the testing machine was driven at a cross-head velocity of 0·013 in./min. As previously, the fracture stresses were corrected to zero plastic deformation

Fig. 2

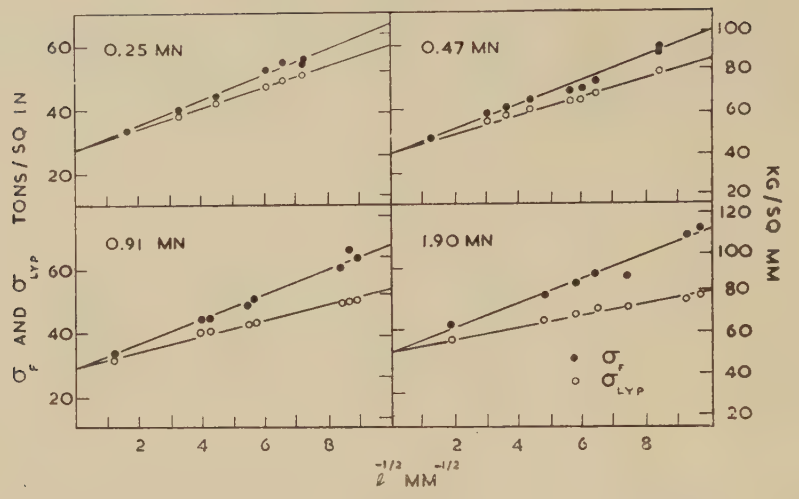

The influence of Mn on the fracture stress and lower yield point of α-iron at −196°c.

Fig. 3

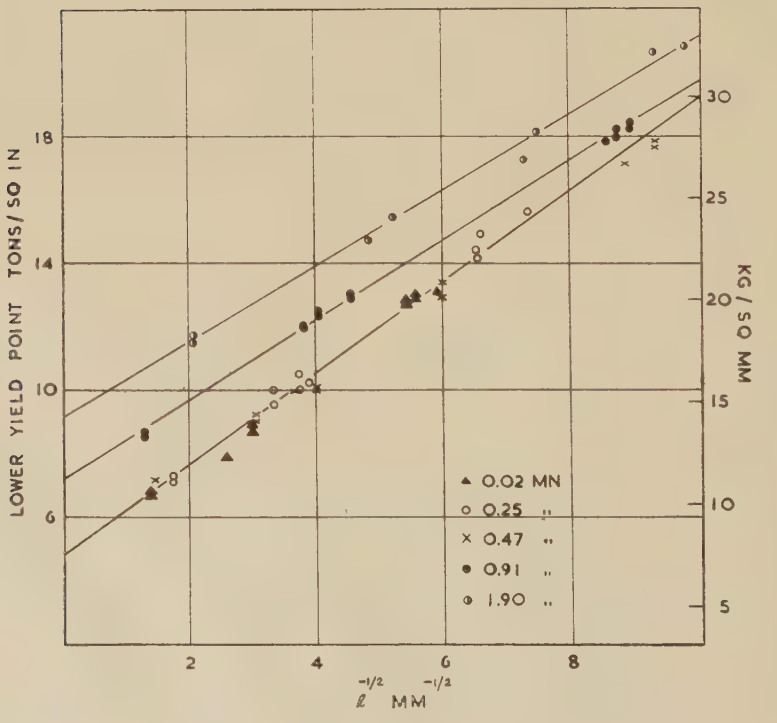

The influence of Mn on the lower yield point of α-iron at 18°c.

at −196°C and to the average plastic strain at 18°C (Petch 1956 a, b). Correction was also made for departure from uniaxial tension, if necking occurred.

Figure 2 shows the dependence of $\sigma_{l.y.p.}$ and of σ_f upon $l^{-1/2}$ for four of these irons at −196°C. Figure 3 contains $\sigma_{l.y.p.}$ at 18°C, and the values of k, k^* and σ_0 at 18° and −196°C are given in figs. 4 and 5.

It will be seen that the initial additions of Mn have no effect. After that, σ_0 increases, the fracture stress slope k^* is unaffected and the yield stress slope k decreases considerably at −196°C, but the effect is small at 18°C.

The reduction in k at −196°C increases the gap between $\sigma_{l.y.p.}$ and σ_f and a corresponding increase in ductility is observed. For example, the reduction in area at fracture was about 20% with $l^{-1/2}$ in the range 6–7 $mm^{-1/2}$ for the low manganese irons, but 45% for the 1·9% Mn iron.

§ 3. The Influence of Mn on k and k^*

The initial lack of any effect of the Mn is readily explained. The Mn combines preferentially with the carbides not in solution in the α-iron, and only when these are satisfied is there any appreciable rise in the Mn content of the α-iron itself.

Table 2. Grain Sizes of the Irons after similar Treatments

Mn (%)	0·02	0·25	0·47	0·91	1·9
Grains/mm^2	980	1350	1300	5450	9200
$l^{-1/2}$ ($mm^{-1/2}$)	5·6	6·1	6·0	8·6	9·8

The lack of an effect on the fracture stress slope k^* is also to be expected, since k^* depends on the rigidity modulus and the surface energy and neither of these should be much affected by small amounts of Mn. With some irons, manganese raises the fracture stress and increases the ductility by the prevention of intergranular brittleness, but there is no sign of this in the present case.

The really interesting point is the alteration in the yield stress slope k. It is clear that at −196°C manganese makes the propagation of yield from grain to grain at the lower yield point easier. This might arise from an effect of Mn on the distribution of sources ahead of a pile-up of dislocations, but there seems no reason for expecting this. The more probable explanation of the reduction in k is a weakening of the dislocation locking. This then would seem to be the cause of the increased ductility produced by manganese at −196°C and constant grain size.

In an impact test on notched specimens, the high strain rate in the notch makes the test near room temperature comparable to a low temperature tensile test. Thus, a lowering of the brittle ductile transition

Fig. 4

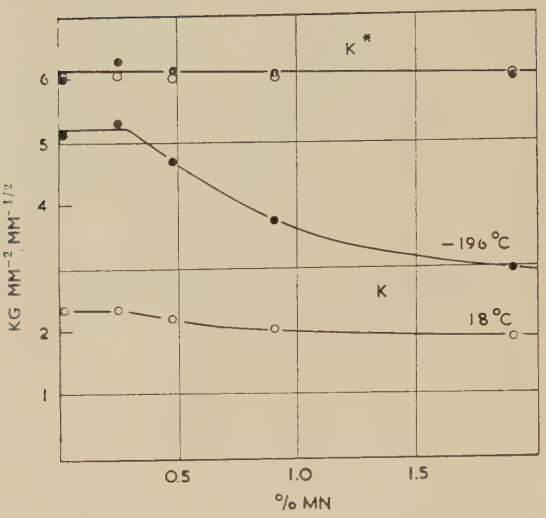

The influence of Mn on k^* and k.

Fig. 5

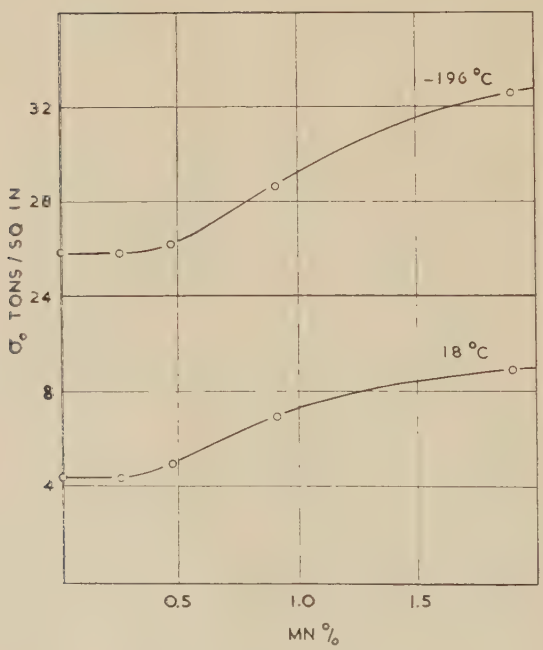

The influence of Mn on σ_0.

temperature at constant grain size by the Mn was expected and was observed in measurements using Charpy-type test pieces of 5/16 in. diameter (fig. 6).

The beneficial effect of Mn on the ductility at constant grain size is reinforced by the grain refinement that is also produced. This refinement is illustrated in table 2, which gives the grain sizes obtained in these irons after the initial ingots had received similar treatments in forging and rolling down to bars and had finally been held at 900 °C for two hours and furnace cooled.

Fig. 6

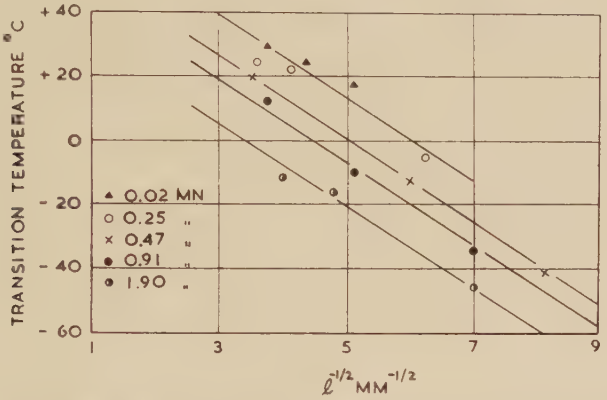

The influence of Mn and of grain diameter l on the transition temperature.

§ 4. The Influence of Mn on the Dislocation Locking

Normally, the locking in an annealed iron should be mainly due to nitrogen, since the concentration of this in solution is greater than that of carbon during the temperature range where a condensed atmosphere exists.

One way in which Mn may weaken nitrogen locking is by displacement of some of the nitrogen atoms from the interstices they occupy at a dislocation in a plain iron to neighbouring interstices. Damping measurements on iron–manganese alloys show that the free energy of a nitrogen atom is lowered by 0·12 ev when the metal atoms that surround it include a Mn one (Dijkstra and Sladek 1953). This binding of carbon to an Fe–Mn interstice is sufficiently great compared with the 0·5 ev binding to a dislocation for some scatter of the nitrogen atoms about their normal positions at a dislocation to result, with some consequent weakening of the dislocation locking.

The extent of the weakening that could arise in this way is uncertain, because of the uncertainties in the calculation of the interaction energy between nitrogen and a dislocation. However, fig. 7 can be used to illustrate what may happen. Figure 7 shows the interaction energy for a nitrogen atom in the various octahedral interstices below a positive edge dislocation lying along [211] in a (011) plane with the Burgers

vector in the [$\bar{1}$11] direction. The equilibrium position is taken to be as shown and the calculation follows Cochardt *et al.* (1955). The letters *a*, *b*, *c*, indicate the directions of the tetragonal distortion of the interstices, and the interstices where one of the metal atoms in the direction of tetragonal distortion lies within the core of the dislocation have been neglected.

Fig. 7

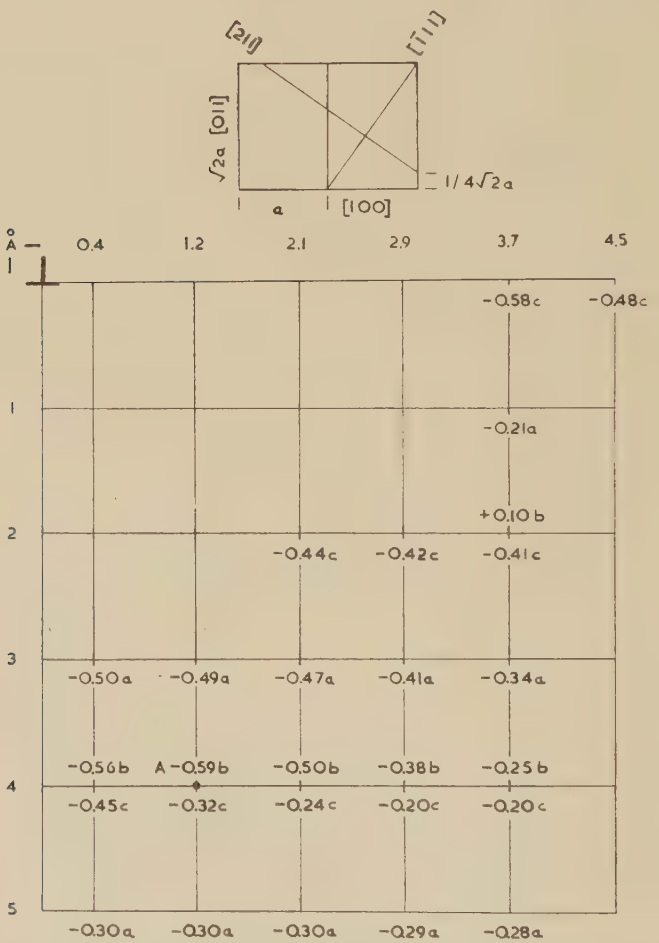

The interaction energy in ev for a nitrogen atom in the octahedral interstices below a positive edge dislocation in α-Fe.

According to this calculation, the *A* interstice with extension along *b* has the greatest interaction energy and the N atoms should normally condense there. But, there are a number of other interstices with interaction energies greater than ~0·45 ev and the N will prefer these if they are Fe/Mn interstices.

Consideration of a model shows that there are 16 metal sites per A interstice, occupation of any one of which by a Mn atom will cause displacement of the N atom from A. To a first approximation, the resultant contribution of the displaced atoms to the dislocation locking will be zero, so that, with Mn present at a concentration of $c\%$, the strength of the locking will be reduced by a factor $\{1-0{\cdot}16\,(c-0{\cdot}25)\}$ when $0{\cdot}25\%$ Mn is removed by the carbon. If the slope k is directly proportional to the strength of the dislocation locking, k will be reduced by the same factor and this gives a 28% reduction at 2% Mn. Thus, it appears that an appreciable effect on k could arise in this way, although this conclusion may well be wrong if fig. 7 is not a good approximation to the interaction energies.

Another possible explanation of the weakening of the locking by Mn is that nitrogen is removed from the dislocations and replaced by carbon and that carbon locking is weaker than nitrogen locking.

Manganese lowers the solubility of nitrogen in α-Fe (Dijkstra and Sladek 1953) and the amount left in solution might become too low for dislocation locking. This does not seem to be so, however, because the $1{\cdot}9\%$ Mn iron strain-aged at 35 °C at about the same speed as the $0{\cdot}25\%$ Mn iron and strain-ageing at 35°C is mainly due to nitrogen. Another possibility of the replacement of nitrogen at the dislocations arises because carbon does not appear to have any preference for the Fe Mn interstices (Fast 1950). If carbon and nitrogen are both present, the lowest energy state may be one with the carbon atoms at the dislocations and the nitrogen atoms in the Fe Mn interstices away from the dislocations.

Thus, replacement of nitrogen locking by carbon locking seems possible, but the suggestion that the latter is weaker has not previously been made. However, it has been found in concurrent work that deoxidation of a steel with $0{\cdot}07\%$ Al also reduces k at −196 °C (Codd and Petch, unpublished). Now Al combines with nitrogen as well as oxygen and, with this small amount of Al, replacement of nitrogen locking by carbon locking seems more probable than scatter of the N atoms about their normal locking positions. This suggests that carbon locking is in fact weaker than nitrogen locking.

Experiments to distinguish between these two possible mechanisms of lowering k by Mn have not yet produced a definite result.

§ 5. The Influence of Mn on σ_0

Cracknell and Petch (1955) have obtained an expression for the resistance to dislocation motion due to interaction with random solute atoms. This gives

$$\sigma_0 = \frac{N^{11/9}}{(\alpha\mu)^{1/3}b^{5/3}}\left[\frac{16A}{\pi}\ln\frac{1}{2r_0N^{1/3}}\right]^{4/3}, \qquad \ldots\ldots \quad (3)$$

where N is the number of solute atoms per unit volume, $\alpha\sim0{\cdot}5$ is a

constant, μ is the rigidity modulus, b is the Burgers vector, A is the constant in Cottrell's expression for the interaction energy and $r_0 \sim b$.

Treating the resistance due to random Mn, C and N atoms as independent to a first approximation, (3) can be used to estimate σ_0 due to the Mn.

From the x-ray data of Walters and Wells (1935), the degree of misfit ϵ of manganese in iron is 0·02, so A is $\sim 3 \times 10^{-21}$ dynes cm^2 and σ_0 is ~ 1 ton. in.^{2} for 1·6% Mn in the α-Fe. Thus, (3) underestimates σ_0 due to Mn in the same way that it underestimates σ_0 due to interaction with C and N (Cracknell and Petch 1955).

The temperature dependence of σ_0 due to Mn can be estimated as for carbon (Heslop and Petch 1956). If τ_i is the shear stress required for dislocation motion without thermal help and τ is the actual value required at room temperature, this calculation gives $\tau = 0{\cdot}3\tau_i$, so, in contrast to carbon, some temperature dependence of σ_0 due to Mn would be expected. Figure 5 suggests that a little temperature dependence does exist.

References

Barr, W., and Honeyman, A. J. K., 1947, *J. Iron Steel Inst.*, **157,** 239.

Cochardt, A. W., Schoek, G., and Wiedersich, H., 1955, *Acta Met.*, **3,** 533.

Cracknell, A., and Petch, N. J., 1955, *Acta Met.*, **3,** 186.

Dijkstra, L. J., and Sladek, R. J., 1953, *J. Metals*, **197,** 69.

Fast, J. D., 1950, *Rev. Metall.* **47,** 782.

Greenwood, G. W., and Quarrell, A. G., 1954. *J. Inst. Metals*, **82,** 551.

Heslop, J., and Petch, N. J., 1956, *Phil. Mag.*, **1,** 866.

Mott, N. F., 1953, *Proc. Roy. Soc.* A, **220,** 1.

Petch, N. J., 1953, *J. Iron Steel Inst.*, **173,** 25 ; 1954, *Progress in Metal Physics* 5 (London : Pergamon Press), p. 1 ; 1956 a, *Phil Mag.*, **1,** 186 ; 1956 b, *Ibid*, **1,** 331.

Stroh, A. N., 1954, *Proc. Roy, Soc.* A, **223,** 404.

Walters, F. M., and Wells, C., 1935, *Trans. Amer. Soc. Metals*, **23,** 731.

Zener, C., 1948, *Fracturing of Metals* (Amer. Soc. Metals), p. 3.

The Magnetization of Cobalt–Manganese and Cobalt–Chromium Alloys†

By J. Crangle
Physics Department, The University, Sheffield

[Received December 17, 1956]

Abstract

Magnetization measurements on the hexagonal and the face-centred cubic phases in several ferromagnetic Co-rich alloys in these systems have been made. By the use of suitable extrapolation procedures, the magnetic moments of both phases in each system at the absolute zero have been estimated. In the CoMn alloys there is a significant difference in the dependence of moment on composition between the two phases. This is not the case in the CoCr alloys, where the rate of change of moment with composition of both phases is the same.

§ 1. Introduction

In pure cobalt and in a number of cobalt-rich binary alloys, the equilibrium phase at low temperatures has a hexagonal close-packed structure, while at higher temperatures a face-centred cubic phase is stable. Both phases are ferromagnetic. Previous work (Myers and Sucksmith 1951, Crangle 1955) has shown that in pure cobalt, a definite difference exists between the magnetic moments of the two phases when extrapolated to the absolute zero of temperature. With this difference in view, the present work was undertaken to establish whether any difference in magnetic behaviour on alloying occurs between the two phases.

The two alloy systems investigated here, cobalt–manganese and cobalt–chromium, are of special interest because of the proximity of both solute elements to cobalt within the first transition series. Also a certain amount of information on the hexagonal phase was already available (Sadron 1932, Farcas 1937), and their metallurgical properties seemed suitable.

The fact that a long extrapolation is necessary in order to estimate the magnetization corresponding to the absolute zero from measurements made at the lowest temperatures at which the cubic phase is stable has hitherto deterred precision work on this phase in cobalt-rich alloys. The only previous measurements on the phase were in pure cobalt, depending on the reduced magnetization–temperature curve having the same shape over its available temperature range as that of nickel, on which low temperature data exist; and on some cobalt–copper alloys, depending on the magnetization at zero temperature varying linearly with composition.

† Communicated by Professor W. Sucksmith, F.R.S.

Preliminary observations showed that neither of these conditions obtained in the cobalt–manganese system, and that the method previously used for pure cobalt was not applicable to the cobalt–chromium system. A new extrapolation technique was therefore devised, which is applicable in favourable cases.

§ 2. Metallurgical Properties of the Alloy Systems

2.1. *The Cobalt–Manganese System*

According to Hashimoto (1937), the solid solution of manganese in cobalt occurs over a wide range of compositions, extending to at least 50% at room temperature, and to not less than 50% at higher temperatures. The temperature at which the hexagonal phase transforms to the face-centred cubic on heating falls with increasing manganese content, from about 400°C in pure cobalt to 0°C at about 25% of manganese. The Curie temperature of the cubic phase is shown by Hashimoto to fall from over 1100°C in pure cobalt to room temperature at rather less than 40% of manganese.

2.2. *The Cobalt–Chromium System*

Chromium is soluble in cobalt up to more than 30%.

In the phase diagram reproduced by Hansen (1936), the temperature of the hexagonal to face-centred cubic phase transition increases with increasing chromium content. This diagram also indicates that the Curie point decreases uniformly with increasing chromium, so that alloys containing more than about 20% of chromium are not ferromagnetic at and above room temperature. Thus the temperature range over which a ferromagnetic face-centred cubic phase is stable decreases rapidly with increasing chromium content. At 6% of chromium the cubic phase only exists at temperatures above about three-quarters of the absolute Curie temperature, compared with pure cobalt, where the phase change occurs at a temperature of about half the Curie temperature.

§ 3. Preparation and Chemical Analysis of the Alloys

Alloys having various compositions in the cobalt–manganese and cobalt–chromium systems were made by melting together appropriate amounts of cobalt and the respective solute elements in an induction furnace. Each melt weighed about 20 g. The metals from which the alloys were prepared were of high purity and the crucibles were of pure recrystallized alumina. The melting was carried out *in vacuo*, or in cases where serious metal loss by evaporation was expected, in pure argon at reduced pressure. To ensure adequate mixing, alloys were kept molten for up to ten minutes, and also each alloy was subsequently homogenized by heating at a temperature just below its melting temperature for about half-an-hour immediately after solidification.

All the alloys were analysed chemically for the amount of the solute elements, and also spectrographically for the presence of impurities. The analyses are shown in table 1.

§ 4. Experimental Methods

Measurements of magnetization in strong magnetic fields were made using experimental methods which have now become standard in this laboratory, and the established extrapolation techniques (covering the variation of magnetization with applied field) were used to obtain values of the spontaneous magnetizations of the alloys at temperatures up to their respective Curie points (see Crangle 1955). About nine different applied field strengths were generally used, between about 3 and 15 kilo-oersteds. The Curie temperatures were estimated by plotting graphs of the squares of the spontaneous magnetizations against temperature, and extrapolating the parts with steepest slope to the temperature axis. The probable error involved in the various Curie point determinations is less than $\pm 2°$C.

Table 1. Analyses

	Cobalt–Manganese †					Cobalt–Chromium‡		
% Mn by weight	1·87	3·58	4·91	9·87	17·48	—	—	—
% Cr by weight	—	—	—	—	—	2·62	4·44	5·20
% Mn atomic	2·00	3·83	5·25	10·51	18·52	—	—	—
% Cr atomic	—	—	—	—	—	2·96	5·00	5·85

† Spectrographic traces ($<0{\cdot}01\%$) were detected of Cu, Ni, Fe, and Si.

‡ Spectrographic traces ($<0{\cdot}01\%$) were detected of Cu, Fe, and Si.

In order to estimate the spontaneous magnetization of the face-centred cubic phase at the absolute zero (σ_0), an extrapolation procedure has to be followed, since the phase is not stable at low temperatures. The new procedure which has been developed is as follows.

Measurements on an alloy of composition c give values of the spontaneous magnetization σ_T at various temperatures T. When the Curie temperature θ of the alloy has been measured, the reduced temperature T/θ corresponding to each σ_T is thus known.

We may write

$$\sigma_T = \sigma_0 \, (\sigma_T/\sigma_0)_{c,\, T/\theta}.$$

Since σ_0 is unknown, $(\sigma_T/\sigma_0)_{c,\, T/\theta}$ will in general be unknown also. But it is related to the reduced magnetization of the pure solute element at the same reduced temperature by

$$(\sigma_T/\sigma_0)_{c,\, T/\theta} = (\sigma_T/\sigma_0)_{0,\, T/\theta} - \Delta$$

where Δ expresses the deviation from the Law of Corresponding States at the particular reduced temperature and composition being considered.

Δ increases with increasing T/θ in the lower temperature range: that is, Δ increases as $(\sigma_T/\sigma_0)_{0,\, T/\theta}$ deviates from unity. Since the reduced

magnetization only falls gradually with increasing temperature when T/θ is small, it is assumed that it is possible to write

$$\Delta=\alpha\{1-(\sigma_T/\sigma_0)_0\}+\beta\{1-(\sigma_T/\sigma_0)_0\}^2+\ldots$$

where α and β are constants, and to consider only the first term of this expansion when $\{1-(\sigma_T/\sigma_0)_0\}$ is small.

Thus we have that

$$\sigma_T=\sigma_0[(\sigma_T/\sigma_0)_{0,\,T/\theta}\{1+\alpha\}-\alpha].$$

It is thus to be expected that when $(\sigma_T/\sigma_0)_{0,\,T/\theta}$ is close enough to unity, σ_T will vary linearly with $(\sigma_T/\sigma_0)_{0,\,T/\theta}$. By plotting σ_T for the alloy as a function of the reduced magnetization of the pure solute element at the same reduced temperature as that to which σ_T applies, it should then be possible to estimate the true σ_0 for the alloy by extrapolation of σ_T to its value where $(\sigma_T-\sigma_0)_{0,\,T/\theta}$ becomes unity.

Table 2. Reduced Magnetization Data for Face-centred Cubic Cobalt

T/θ	σ_T/σ_0	T/θ	σ_T/σ_0
0·493	0·934	0·949	0·467
0·508	0·930	0·961	0·418
0·536	0·919	0·971	0·385
0·579	0·899	0·977	0·344
0·624	0·879	0·980	0·331
0·647	0·867	0·985	0·295
0·673	0·849	0·987	0·271
0·699	0·831	0·990	0·241
0·753	0·787	0·992	0·211
0·795	0·747	0·993	0·193
0·836	0·695	0·996	0·151
0·873	0·641	0·999	0·120
0·895	0·602		
0·911	0·571		
0·932	0·518		

Measurements on the magnetization of pure face-centred cubic cobalt exist down to about 400 °C ($T/\theta=0{\cdot}5$) (Crangle 1955), and reduced data from them are given in table 2. Intermediate values of $(\sigma_T/\sigma_0)_0$ were obtained for the various T/θ by graphical interpolation, with extrapolation to $T/\theta=0{\cdot}4$. The known magnetization data for pure nickel, which follows the same reduced curve as cobalt (Myers and Sucksmith 1951) were used as a guide to this extrapolation.

Graphs of σ_T as a function of $(\sigma_T/\sigma_0)_0$ for all the present series of alloys are shown in fig. 1. The quality of the straight lines obtained over the range shown justifies the procedure used. In the case of the 2·96% CoCr

alloy, the onset of the phase change from hexagonal to cubic on cooling was detected solely by the appearance of a definite departure from the main line which characterizes the cubic phase, at a temperature agreeing well with that determined previously by direct methods. In all the other

Fig. 1

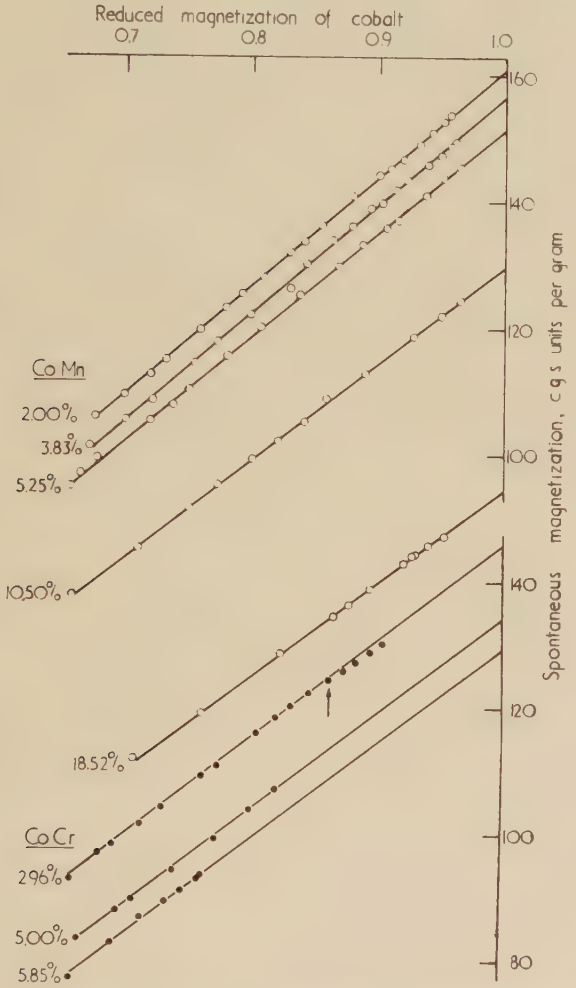

Extrapolation to the magnetization at the absolute zero for the face-centred cubic phase. The start of the phase transformation in the 2·96% CoCr alloy is marked.

alloys, the phase transformations were detectable also from marked discontinuities in the magnetization–temperature curves.

In the case of the hexagonal phases of both alloy systems, considerable magnetic hardness was found, and in order to be able to estimate intrinsic magnetizations, extrapolations to saturation conditions were necessary.

Weiss and Forrer (1929) used a method which involved the extrapolation to infinite field of a graph of magnetization against the reciprocal of the field strength. Néel (1948) gave a theoretical justification for plotting against $1/H$ when the magnetic hardness is caused by cavities or other non-magnetic imperfections in the specimen, and against $1/H^2$ when the hardness arises from magnetocrystalline anisotropy.

During the present work on the hexagonal phases, applied fields ranged between about 7 and 15 kilo-oersteds. It was found that the CoMn alloys gave better straight lines when $1/H$ was used, and in the case of CoCr, $1/H^2$ was better. The uncertainty in which parameter is correct affects the final estimates of spontaneous magnetization at the absolute zero. Values from the $1/H^2$ extrapolations are of the order of 1% lower than when $1/H$ is used. At temperatures as far below the Curie point as those at which the hexagonal phase is stable in these alloys, any error arising out of the assumption that the intrinsic magnetization is effectively identical with the spontaneous magnetization will be insignificant compared with the uncertainty in extrapolating to saturation conditions.

Values for the spontaneous magnetization of the various alloys in the hexagonal phases were estimated by making linear extrapolations of graphs of spontaneous magnetization against the square of the absolute temperature (fig. 2).

Fig. 2

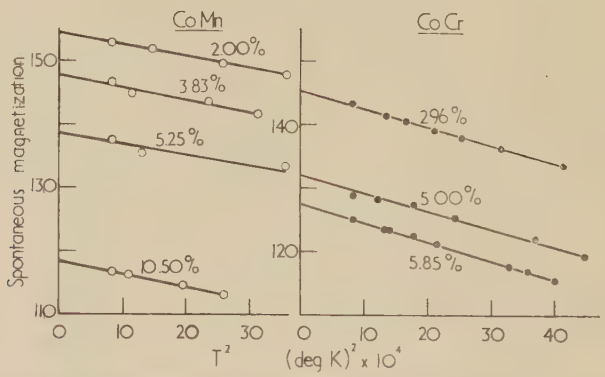

Extrapolation to the magnetization at the absolute zero for the hexagonal phase.

§ 5. Results and Discussion

It may be seen from fig. 1 that there is no difficulty in carrying out the extrapolations to σ_0 for the face-centred cubic cobalt-manganese alloys with an error of well under $\pm 1{\cdot}0$ c.g.s. units. For the cobalt–chromium alloys, however, the error is rather greater, due to the longer extrapolations.

In the case of the 18·52% CoMn alloy, the magnetization measured at any given temperature up to about 540°C appeared to be somewhat sensitive to heat treatment, depending on the rate of cooling. These effects are possibly due to an order–disorder reaction and further work is in progress to elucidate this point. The data presented here for this

alloy refer to the state produced by cooling quickly. No dependence of magnetization on heat treatment was found in any of the four alloys of lower manganese content, or in any of the cobalt–chromium alloys.

The results obtained for the hexagonal phase of the cobalt–manganese system agree well with those obtained by Sadron (1932) up to at least 10% of manganese, as may be seen from fig. 3. No data are plotted here for the 18·52% alloy because it was not possible to obtain the hexagonal phase in this alloy without some retained cubic phase being also present and the magnetization measurements were therefore displaced towards higher values. Since Sadron's data show no sign of this effect, it seems likely that there was some metallurgical difference between his alloys and the present ones, possibly of grain size, which causes different behaviour at the change of phase.

For the hexagonal phase of the CoCr system, there is agreement on the rate of change of moment with composition between the present measurements and those of Farcas (1937). Where composition overlap exists, the values of Farcas are apparently about 0·05 Bohr magnetons higher than those made here. However, this difference may not be real, largely because of the possibility of errors inherent in the method used by Farcas for estimating σ_0. Farcas apparently only made measurements at room temperature, and obtained values of σ_0 by multiplying the saturation magnetization at room temperature by a factor estimated from knowledge of the respective Curie temperatures of the alloys.

Table 3. Collected Data for CoMn and CoCr alloys

	CoMn					CoCr		
Composition, % atomic	2·00	3·83	5·25	10·50	18·52	2·96	5·00	5·85
Curie point (θ), °K	1350	1295	1243	1100	836	1275	1198	1160
Magnetic moment per atom in cubic phase (Bohr magnetons)	$1{\cdot}69_3$	$1{\cdot}64_8$	$1{\cdot}59_3$	$1{\cdot}36_2$	$0{\cdot}98_3$	1·53	1·42	1·35
Magnetic moment per atom in hexagonal phase (Bohr magnetons)	$1{\cdot}62_7$	$1{\cdot}55_6$	$1{\cdot}45_7$	$1{\cdot}24_0$	0·92†	1·53	1·38	1·34

† Probably anomalously high because of the presence of some retained cubic phase.

The numerical data for all the alloys are collected in table 3, and the magnetizations at the absolute zero (after conversion to Bohr magnetons†) are plotted against composition in fig. 3.

This work clearly shows that the rate of change of magnetic moment with alloy composition in some composition ranges of the cobalt–manganese system is sensitive to crystal structure, but that no equivalent effect occurs in the cobalt chromium system over the composition range over which observations on both phases are possible.

† The Bohr magneton was assumed to correspond to 5586 c.g.s. units per gram molecule.

The theoretical treatments of the electronic properties of transition metal alloys which have been made in the past cover a wide range of diversity, and the conclusions to be drawn from the present observations depend strongly on which picture is accepted. The opposite extremes are a simplified band theory, and theories based on the assumption that for 3d electrons in elements of the first transition series, a Heitler–London approximation is more appropriate.

Fig. 3

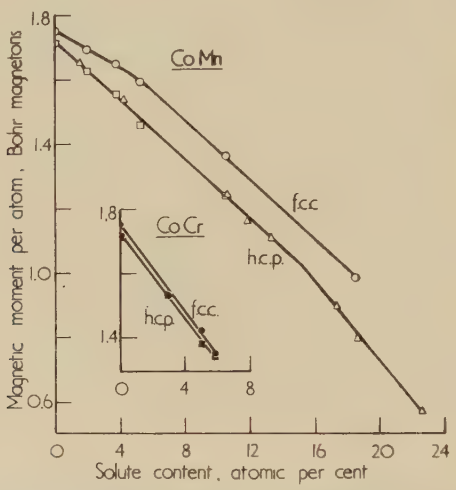

Magnetic moments of the alloys plotted as a function of composition. For the hexagonal CoMn alloys, the triangles signify Sadron's measurements, and the squares the present data.

In the simplest application of the band theory to these alloys, it is assumed that the 3d and 4s bands are common to all atoms present, and that electrons are contributed uniformly by both solvent and solute elements. The magnetic properties of any given alloy are supposed to be determined by the distribution in the 3d band between states of opposite spin of the electrons available.

On this theory, the dependence of rate of change of magnetic moment with composition on crystal structure would indicate that different schemes of electron distribution are stable states in the two phases. That is, that the energy density of states curve for the 3d band in cobalt manganese alloys is structure-sensitive.

It would be expected from this simple theory, especially since manganese and chromium are neighbours in the periodic table, that in the systems CoMn and CoCr, alloys with the same total number of 3d+4s electrons would possess the same magnetic moment. This does in fact occur in the hexagonal phases of the systems. In the cubic phases, however, there is no agreement. No simple explanation of this disagreement appears possible within this framework.

In the kind of theory which is at the opposite extreme, it is assumed that magnetic moments are localized characteristically on the various kinds of atom present in a given alloy. The magnetization of the whole is made up by compounding the effects of all the atoms. In the simplest application, the effective magnetic moments of the atoms of the solute elements may be estimated by extrapolating the graph of alloy moment plotted against composition, to 100% of solute. On this basis the following magnetic moments per atom (expressed in Bohr magnetons) may be obtained :

Manganese in face-centred cubic cobalt	
0–5% Mn	$-0{\cdot}25\pm0{\cdot}25$
Above 5% Mn	$-2{\cdot}9\ \pm0{\cdot}1$
Manganese in hexagonal cobalt	
0–16% Mn	$-2{\cdot}8\pm0{\cdot}2$
Above 16% Mn (Sadron's data)	$-4{\cdot}2$.
Chromium in face-centred cubic cobalt	$-5{\cdot}1\pm0{\cdot}5$
Chromium in hexagonal cobalt	$-4{\cdot}7\pm0{\cdot}3$

The errors quoted here are outside estimates, based on maximum errors in the magneton numbers of $\pm0{\cdot}01$ in cubic CoMn alloys, $\pm0{\cdot}02$ in all alloys in the hexagonal phase, and $\pm0{\cdot}03$ in cubic CoCr ; the lengths of the various extrapolations are taken into account.

The negative signs imply that the solute atoms are aligned in antiferromagnetic fashion with respect to the magnetization of the solvent.

In the case of the CoMn alloys, if the present simple picture is accepted, the variety of the extrapolated moments given here must mean that the effective moment of the manganese atoms depends on their detailed environment. In the face-centred cubic structure, a given atom has twelve nearest neighbours and six next nearest neighbours at a distance 1·4 times further away. Thus the composition at which, on the average, there is one other manganese atom included in the eighteen nearest or next nearest neighbours of a given manganese atom is about $5\frac{1}{2}$%. This is close to the composition at which the bend in the curve of moment against composition for the cubic phase occurs. The presence of Mn Mn interactions may then be responsible for a change in the effective moment of manganese. This argument is not very convincing, however, for in the hexagonal phase the bend found by Sadron was near 15% of manganese, where about one in six of the atoms surrounding a given manganese atom is another manganese atom. In the unit cell of hexagonal cobalt, the deviation from ideal closest packing is slight (c/a is actually 1·624, compared with 1·633 ideally). The nearest six and the six next nearest neighbours are all at very nearly the same distance away, all twelve forming a configuration very similar to that of the twelve nearest in the face-centred cubic structure. It is difficult to believe that a Mn–Mn pair made

up of atoms which are nearest neighbours would have properties very different from one made up of next nearest neighbours. The arrangement of the six further neighbours in the hexagonal structure is quite different from that of the next nearest in the face-centred cubic, and they are now as much as 1·7 times further away than the nearest neighbours.

Acknowledgments

The author wishes to record his gratitude to Professor W. Sucksmith, F.R.S. for his help and advice. Thanks are also due to the Société Générale Métallurgique de Hoboken, Antwerp, for the gift of the pure cobalt on which the alloys were based.

References

Crangle, J., 1955, *Phil. Mag.*, **46**, 499.
Farcas, T., 1937, *Ann. Phys., Paris*, **8**, 146.
Hansen, M., 1936, *Der Aufbau der Zweistofflegierungen* (Berlin : Springer).
Hashimoto, U., 1937, *Nippon Kinzoku Gakkai-Si*, **1**, 177.
Myers, H. P., and Sucksmith, W., 1951, *Proc. Roy. Soc.* A, **207**, 427.
Néel, L., 1948, *J. Phys. Radium*, **9**, 184, 193.
Sadron, C., 1932, *Ann. Phys., Paris*, **17**, 371.
Weiss, P., and Forrer, R., 1929, *Ann. Phys., Paris*, **12**, 279.

Stacking Faults in Face-Centred Cubic Metals and Alloys†

By R. E. Smallman and K. H. Westmacott
Metallurgy Division, A.E.R.E., Harwell

[Received December 12, 1956 and in revised form January 25, 1957]

Summary

Stacking faults on the (111) planes of several face-centred cubic metals and alloys have been introduced by cold work, and estimates of the stacking fault probability α, have been obtained from changes produced in the Debye–Scherrer spectrum. The faulting probability increases on alloying, from one plane in 300 in copper, to one plane in 25 for some high solute content alloys containing zinc, aluminium, tin or germanium. Both neutron irradiation (5×10^{19} n.v.t.) and 'quenched-in' vacancies have little significant effect on the faulting parameter.

Lowering the temperature of deformation increases the faulting probability but in copper the faults 'anneal-out' at room temperature after several hours. Line broadening analysis shows that the dislocation density is increased on alloying and also by lowering the deformation temperature. It is suggested that the faulting may be accounted for by the regions between separated half dislocations. Ribbons of stacking faults as given by extended dislocations and 'infinite' stacking faults produced by splitting of dislocations at high stresses are both considered and estimates of fault energy made.

Some work on segregation of solute atoms to faults is reported with particular reference to the alloys silver–gold and copper–aluminium.

§ 1. Introduction

Recent experiments have shown that solute atoms (Smallman 1955) and irradiation damage (Smallman 1957) produce similar changes in the preferred orientation normally assumed by pure face-centred cubic metals. It is thought that these texture changes may be related to alterations in the stress–strain characteristics of the pure metal: alloying, irradiation or quenching all resulting in a yield point followed by a low rate of work hardening. Overshoot of the active slip plane is also observed on alloying by Piercy *et al.* (1955) and slip line studies indicate that it is also likely to occur in irradiated (Blewitt and Jamison 1952) or quenched (Maddin and Cottrell 1955) material.

† Communicated by the Authors.

It has long been realized that stacking faults may play an important part in these work hardening phenomena since latent slip plane hardening could be accounted for by the difficulty of the dislocations on the second set of slip planes cutting through the faulted material on the first slip system (Barrett 1952 a, b). Consequently an examination has been made of the influence of solute atoms and point defects on the stacking fault tendency in copper.

§ 2. Experimental

2.1. *Method*

Paterson (1952) has shown that stacking faults on the (111) planes of a face-centred cubic metal produce a shift of the diffraction peaks as well as broadening them. It is difficult to obtain information about faulting from line broadening measurements alone as they are affected by both particle size and strain. However the peak shift is affected solely by faulting so that a direct determination of the stacking fault probability can be made. The peak shift of any one diffraction line ($\Delta 2\theta$) expressed in degrees is given by Warren and Warekois (1955)

$$\Delta 2\theta = \pm \tan\theta \cos^2\phi 270\sqrt{3}\alpha/\pi^2 h_3, \quad . \quad . \quad . \quad . \quad . \quad . \quad (1)$$

where ϕ is the angle between the reflecting normal and planes containing deformation faults, α the stacking fault probability (assumed small) and $h_3 = |h+k+l|$. The shift is positive or negative depending on whether h_3 is $3n+1$ or $3n-1$ (n is an integer); when $h_3 = 3n$ there is no shift.

For the reflection (111) and (200) the effect of stacking faults is to move the (111) peak† to higher and the (200) peak to lower angles. Substituting in eqn. (1) this change becomes for the (111) and (200) reflections

$$\Delta(2\theta_{200} - 2\theta_{111}) = -\alpha 45\sqrt{3}(2\tan\theta_{200} + \tan\theta_{111})/2\pi^2. \quad . \quad . \quad (2)$$

For metals examined with copper $K\alpha_1$ radiation this approximates to

$$\Delta(2\theta_{200} - 2\theta_{111}) = -5\alpha. \quad . \quad . \quad . \quad . \quad . \quad . \quad . \quad (3)$$

As pointed out by Warren and Warekois (1955) the Paterson analysis assumes that the faults occur independently and on only one set of (111) planes. In severely cold worked metals the faults probably occur on more than one set of (111) planes. Consequently the significance of α obtained from eqn. (3) is not clearly defined but is considered to represent the sum of the probabilities for the different sets of active (111) planes.

2.2. *Procedure*

The stacking fault probability was determined from a change in the (111) and (200) pair reflections. Pairs from the other reflections (220), (311), (222) and (400) were also examined to ascertain that the shift was

† Three components of the (111) diffraction peak, $(\bar{1}11)$, $(1\bar{1}1)$ and $(11\bar{1})$ are shifted while the fourth component remains unaffected.

due to faults but the results quoted are from the (111) and (200) separation since this gives the most accurately measurable estimate of α. The diffraction pattern was obtained with a Geiger counter diffractometer and monochromatic $K\alpha_1$ radiation. To minimize positioning errors the peaks were manually recorded on a single run.

Difficulty was originally experienced in estimating the peak positions with any certainty and two methods were unsuccessfully tried before the one finally adopted. Using the standard Geiger counter arrangement a difficulty arises due to the overlap caused by the incident radiation being a mixture of $K\alpha_1$ and $K\alpha_2$ components. The observed diffraction peaks had to be resolved graphically and the resulting values although indicating faulting were insufficiently accurate to give reliable quantitative data. A second method was to determine the position of the centre of gravity of the diffraction peak shape and use this as a measure of the peak position. The uncertainty in this method is associated with the long tails to the diffraction lines, especially in cold worked samples, which profoundly influence the value of the centre of gravity.

The method eventually adopted depended on the elimination of the $K\alpha_2$ component of the incident radiation from the diffractometer. This was achieved by using a Guinier asymmetrical quartz monochromator set to give at its focus resolution of the $K\alpha_1\alpha_2$ doublet. It was then possible with a sharp slit to cut out the $K\alpha_2$ component, and the resulting diffraction pattern is for the copper $K\alpha_1$ wavelength alone. With this experimental arrangement it was possible to determine the peak of the line to $\pm\frac{1}{2}$ minute in 2θ.

§ 3. Results

3.1

3.1.1. *Influence of Solute Atoms*

The pure metals copper and nickel and solid solutions of copper with nickel, zinc, aluminium, tin and germanium have been examined. Spectroscopically pure metals were used (Johnson Matthey and Co. Ltd.) and alloys made by melting *in vacuo* or purified argon. The stacking faults were produced by deformation by filing and the stacking fault probability obtained by comparing the peak separation for a filed sample in both the annealed and cold worked conditions. The results are summarized in table 1. Figure 1 shows a plot of the stacking fault probability against atomic composition obtained from eqn. 3, for some copper alloys. The $(2\theta_{200}-2\theta_{111})$ separation decreases as a result of cold work and this effect increases in different alloys with increasing solute content. The faulting becomes very profuse in highly alloyed materials; for example, in copper the value of $\alpha = 3{\cdot}3 \times 10^{-3}$ corresponds to an average of 1 stacking fault in every 300 (111) planes, but the addition of 17 atm.% aluminium increases this frequency to 1 in 25 (111) planes. Similarly the addition of zinc, tin or germanium has a significant effect

but the effect of an addition of nickel is negligible. The values of the copper–zinc alloys are in good agreement with those recently published by Warren and Warekois.

3.1.2. *Influence of Deformation Temperature*

The influence of deformation temperature on the stacking fault parameter was investigated by examining a sample of pure copper deformed at liquid nitrogen temperature. The copper filings produced at −196°c were transferred to a pressure die also at liquid nitrogen temperature and pressed to a flat disc. This disc was then transferred to the diffractometer also maintained at −196°c. The measured peak separation indicated an increase in faulting probability by a factor of three to four compared with a sample deformed at room temperature. The specimen was allowed to 'warm' to room temperature and the stacking fault probability and line breadth measured after various intervals of time. The stacking faults completely annealed out together with a major part of the line breadths. (See also § 4.)

Table 1. Values of Stacking Fault Probability from Peak Shift Data for Various Copper Solid Solutions

Material	Deformation temp.	Atm.% Solute	$\Delta(2\theta_{200}-2\theta_{111})$ (minutes)	$\alpha\times10^3$
Copper	Room temp.	0	1	3·3
Copper	Liq. nitrogen	0	$3\frac{1}{2}\rightarrow4$	$11{\cdot}7\rightarrow13{\cdot}3$
Nickel	Room temp.	0	$\frac{1}{2}$	1·65
Copper–Nickel	Room temp.	50	$1\frac{1}{2}$	5
Copper–zinc	Room temp.	14·0	2	7
		27·0	6	20
Copper–aluminium	Room temp.	5·7	$3\rightarrow3\frac{1}{2}$	$10\rightarrow11{\cdot}7$
		11·0	$8\frac{1}{2}$	29
		17·0	12	40
Copper–tin	Room temp.	2·5	$1\frac{1}{2}\rightarrow2$	$5\rightarrow6{\cdot}6$
		4·5	$4\frac{1}{2}$	14·5
		7·1	10	34
Copper–germanium	Room temp.	2·5	$1\frac{1}{2}$	5
		5·0	$4\frac{1}{2}$	14·5
		7·2	$9\frac{1}{2}\rightarrow11$	$31{\cdot}7\rightarrow37$

3.1.3. *Effect of Annealing on Stacking Faults*

The effect of annealing on the faulting produced by cold work was investigated in the copper–17 atm.% aluminium alloy by heating specimens for half an hour at successively higher temperatures 100°, 150°, 200°, 250° and 300°c. The faulting effects annealed out in the range 200–250°c together with a major portion of the line broadening.

3.2. *Irradiation and Quench Damage*

3.2.1. *Direct Effect of Damage*

It has been suggested by Kunz and Holden (1954) that the interstitial atoms produced by neutron irradiation agglomerate into planes producing stacking faults parallel to (111) planes. If we assume that the most likely site for an interstitial atom in the face-centred cubic lattice is that denoted by $(\frac{1}{2}, \frac{1}{2}, \frac{1}{2})$ or $(\frac{1}{2}, 0, 0)$ then an agglomeration would change the stacking sequence from the normal ABCABCABC to ABCACBCABC in the faulted structure. This is shown diagramatically in fig. 2.

Fig. 1

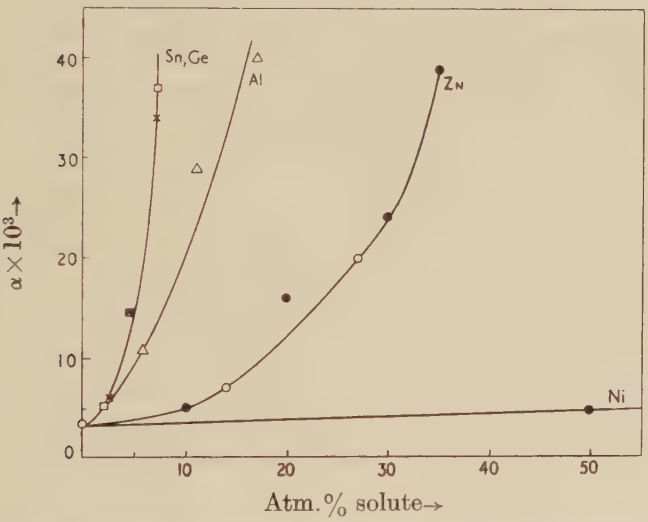

Stacking fault probability versus composition curves for α-solid solutions of copper with nickel, zinc, aluminium, tin and germanium. Full circle values for zinc are taken from Warren and Warekois.

Fig. 2

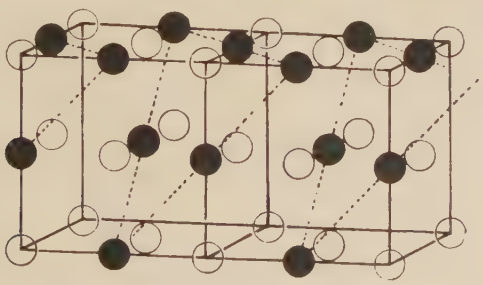

Agglomeration of interstitial atoms in the face-centred cubic lattice.

To examine this point some annealed copper filings were irradiated to a total flux of 10^{19} n.v.t. at an ambient pile temperature of 75°C. Examination of the irradiated filings showed no detectable change in peak separation indicating that any shift is less than $\frac{1}{2}$ minute of arc in 2θ. There

was, however, a small increase in strain broadening compared with the unirradiated metal. 'Quenched-in' vacancies also had a negligible effect on the stacking fault parameter as was shown by examining a specimen of annealed copper filings quenched from 1000°C.

3.2.2. *Indirect Effect of Damage*

The effect of neutron irradiation on the stress–strain curve, preferred orientation and slip line characteristics, indicates a close analogy between irradiation damage and solid solution hardening. To carry this hypothesis further, samples of copper irradiated to a total flux of 10^{19} n.v.t. and 5×10^{19} n.v.t. respectively were deformed by filing at room temperature. The resulting peak separation for the specimen irradiated to 10^{19} n.v.t. was the same as for the unirradiated sample filed at room temperature. The specimen irradiated to 5×10^{19} n.v.t. showed a slight increase on some measurements but the overall averaged peak separation was insignificant ($1'\pm\frac{1}{2}'$). Quenching a sample from 1000°C before filing at room temperature also failed to show a change in the stacking fault probability outside the experimental error.

3.3. *Line Broadening*

To correlate the changes in stacking fault probability with dislocation density the line profiles from the pure metals and alloys have been analysed in terms of particle size and strain broadening using the Cauchy line broadening relationship discussed by Williamson and Hall (1953). If β_τ is the total line breadth made up of contributions from particle size (ϵ) and strain (ξ) then, by the Cauchy relationship

$$\beta_\tau=\beta_\epsilon+\beta_\xi,$$

or

$$\beta_\tau=\lambda/\epsilon\cos\theta+2\xi\tan\theta. \quad . \quad . \quad . \quad . \quad . \quad . \quad . \quad (4)$$

Thus on a plot of $\beta_\tau\cos\theta/\lambda$ against $2\sin\theta/\lambda$ where β_τ is the correct physical breadth in radians, the intercept corresponds to the reciprocal of the effective particle size and the slope the effective strain. It is unlikely that the values of particle sizes obtained by this method are absolute owing to the assumptions involved, but are probably accurate to $\pm50\%$. However, other methods of particle size determination have similar limitations and are more time consuming (Williamson and Smallman 1955). Figure 3 shows a line broadening plot for the copper–aluminium series of alloys. The particle size and strain values for these and many other metals and alloys are summarized in table 2.

The particle size and strain values in the [100] and [111] directions are denoted by ϵ[hkl] and ξ[hkl] respectively; both change with increasing alloy content, the particle size decreasing and the strain increasing. The particle size in the high alloy content materials becomes extremely small (about 100 Å) with the exception of copper–nickel for which significantly there is little evidence of stacking faults. One surprising feature of the particle size results for the materials containing appreciable faulting, is

that the value of the dimension in the [111] direction is at least twice that in the [100] direction. The particle shape indicated by such values seems most unlikely. Moreover, the absence of such anisotropy in materials containing low stacking faults, e.g. copper and copper–nickel indicates once again that the effect is due to stacking fault broadening. These

Fig. 3

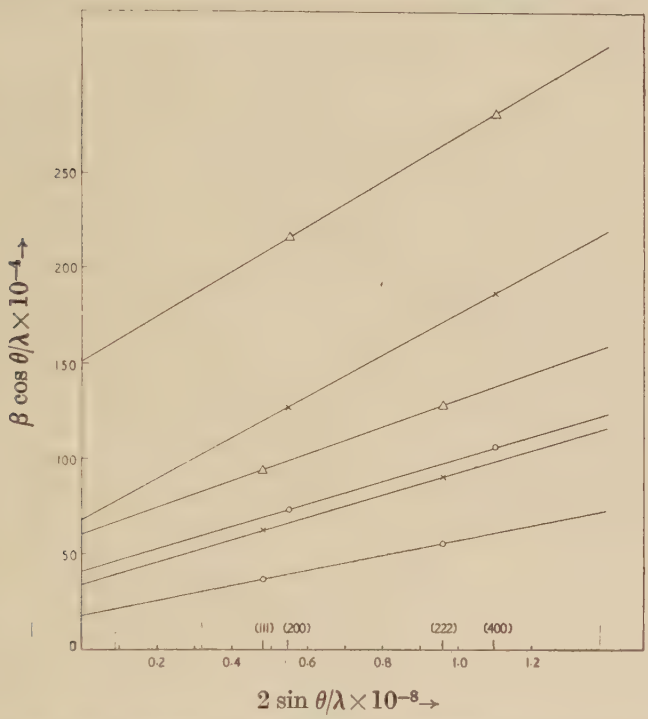

Line broadening analysis applied to copper–aluminium alloys.
○ 5·7 atm.% Al, × 11 atm.% Al, △ 17 atm.% Al.

indications are substantiated by observations during recovery (see § 4). Thus since stacking faults give rise to broadening similar to particle size broadening, the measurement of domain size from line breadths in materials containing stacking faults are incorrect. It is possible, however, knowing the stacking fault probability α to estimate the contribution to the particle size broadening, since Warren and Warekois (1955) show the effective particle size due to faults $\epsilon_{S.F.}$ to be

$$\epsilon_{S.F.}=2d_{111}/3\alpha \cos \phi. \quad . \quad . \quad . \quad . \quad . \quad . \quad . \quad (5)$$

From this equation it can be seen that the stacking fault contribution to the particle size broadening in the [100] direction is much greater than that in the [111] direction. This is partly because ϕ is smaller for the [100] directions, and partly because only three out of four (111) planes are affected, whereas all (200) planes are affected by faulting. While

eqn. (5) refers only to the effective $\epsilon_{S.F.}$ determined from line shape experiments, a similar trend may be expected for the effect on the line broadening. In the case of copper and copper–nickel filed at room temperature the contribution to particle size broadening by stacking faults is negligible, but the particle sizes observed in the alloys may be completely accounted for by fault broadening (see column 8, table 2). For example, from the measured values of α for copper–17 atm.% aluminium the stacking fault 'particle-size' in the [100] direction, $\epsilon_{S.F.}$ [100] is 61 Å, while that in the [111] direction, $\epsilon_{S.F.}$ [111], is 145 Å.

Table 2. Particle Size (ϵ) and Strain (ξ) Values for some of the Copper Based Alloys

Alloy	Treatment	Atm. % solute	ϵ[111] Å	ϵ[200] Å	ξ[111] $\times 10^3$	ξ[200] $\times 10^3$	$\epsilon_{S.F.}$[111] Å
Copper	Filed at room temp.	0	1000	1000	2	5·5	1665
Copper	Filed at −196°c	0	450	200	6	11	465
Copper	Irradiated to 10^{19}n.v.t	0	20 000	20 000	10^{-1}	10^{-1}	—
Copper-nickel	Filed at room temp.	50	1000	1000	5·5	9	1120
Copper–zinc	,,	27	250	100	4	10	280
Copper–tin	,,	7·1	250	110	7	13	170
Copper–Aluminium	,,	17·0	170	70	7	12	145
		11·0	300	150	6	11	200
		5·7	600	250	4	6	520
Copper–Germanium	,,	7·2	300	125	6	10	150

The strain values obtained are also markedly anisotropic as is expected from the differences in Young's modulus for these directions. However, the anisotropy of strain cannot be accounted for by any simple isotropic stress model as has often been assumed in the past (Smith and Stickley 1943, Warren and Averbach 1952), since the strain ratio $\xi[200]/\xi[111]$ for say copper–27% zinc is about 2·5 whereas the inverse ratio of Young's modulus is 3·5. This anisotropy is probably related to the non-uniform distribution of dislocations.

§ 4. Recovery and Segregation

The results in § 3 show that pure copper when deformed and examined at low temperatures has the faulting parameter of a highly alloyed metal. Whether this is due to a decrease in faulting energy or to the amount of deformation that can be introduced and retained, was examined from

measurements of the line breadths and stacking fault probability at liquid nitrogen temperature and after intervals of time at room temperature.

Table 3. Recovery Results for Pure Copper

Time (mins.) at room temp.	α^{-1}	$\epsilon_{[111]}$ Å	$\epsilon_{[200]}$ Å	$\xi_{[111]} \times 10^3$	$\xi_{[200]} \times 10^3$
0	75	450	200	6	11
10	85	—	—	—	—
30	100	—	—	—	—
60	120	—	—	—	—
150	150	—	—	—	—
300	200	—	600	—	4·5
600	300	—	—	—	—
5000	>600	1000	1000	0·6	0·8

The results in table 3 show that as the stacking faults 'anneal' out, so the particle size increases suggesting that the particle size broadening is due almost entirely to faults. However, the total change in broadening cannot be attributed to the removal of stacking faults alone since the strain breadth also undergoes a marked change. A remarkable feature of the recovery process is that the final breadth is not that exhibited by a specimen deformed at room temperature, but has a much smaller strain value of about 8×10^{-4}. Figure 4 shows the line shape of the (400)

Fig. 4

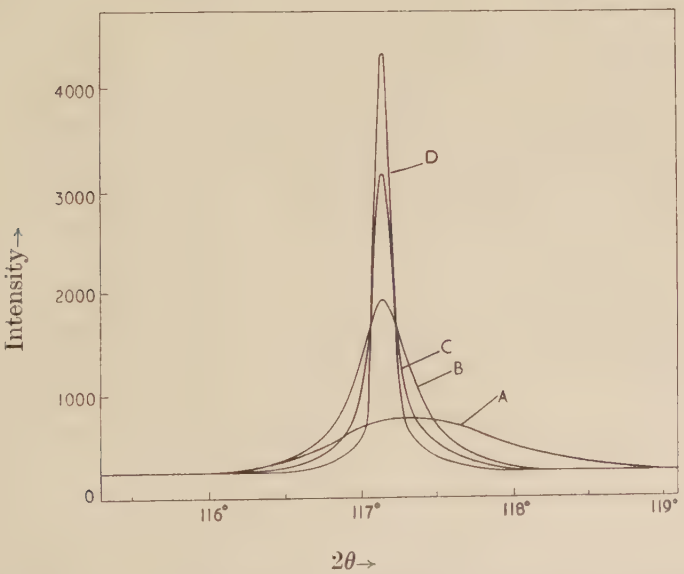

Line shape of 400 reflection, showing recovery in pure copper, A filed at −196°c, B filed at room temperature; C filed at −196°c and recovered 3 days at room temperature; D annealed at 520°c for 20 minutes.

reflection from copper after various stages of recovery. The breadth after advanced recovery is intermediate between a room temperature deformed specimen and an annealed one. An attempt was made to produce this state of recovery in a room temperature deformed sample. The closest similarity was shown by a specimen aged at 140°C for 3 hours resulting in a similar strain value of 7×10^{-4} but a larger particle size of 5×10^{-5} cm.

A similar recovery study was made with copper–17 atm.% aluminium and 50/50 atm.% silver–gold alloys. It was noticeable that recovery in both alloys was less marked. The faulting parameter for the 50/50 silver–gold alloy is shown in table 4. It is doubtful whether the exact magnitude of the increase in probability α from 9·2 to 14·7 with ageing is significant as the change was not completely reproducible. However, a decrease in parameter such as that in copper was never observed even though slight recovery of line shape was detectable.

Table 4. Recovery at Room Temperature of 50/50 Silver–Gold Alloy

Treatment	$\alpha\times10^3$	α^{-1}
Filed at room temperature	2·0	500
Filed at −196°C	9·2	108
Filed at −196°C then ' annealed ' 1 hr. at room temperature	14·7	68
Filed at −196°C then ' annealed ' 10 hr. at room temperature	11·1	90
Filed at −196°C then ' annealed ' 17 hr. at room temperature	9·2	108

It is possible that the effect may be associated with segregation of solute atoms to faults, since the solubility in the close packed hexagonal fault will be different from that in the cubic matrix, causing the faults to widen, as suggested by Cottrell (1953). The electrical resistance measurements of Aarts and Jarvis (1954) on this alloy show an increase when the specimen deformed at −196°C is allowed to warm to room temperature. If faults are responsible for electron scattering, as proposed by Broom (1952), the unusual faulting probability values would be consistent with this. The possibility of the segregation of solute atoms to faults on low temperature annealing was also examined in copper–17 atm.% aluminium by this method and by low angle scattering technique, but no change was detected.

§ 5. Estimates of Stored Energy and Dislocation Density

Values of stored energy for some of the alloys examined have been calculated from the relation

$$V=3E\overline{S^2}/2, \qquad (6)$$

where E is Young's modulus and $\overline{S^2}$ is the mean square strain. The mean square strain may be estimated from ξ, the slope of the line broadening analysis, since

$$\overline{S^2}=A\xi^2, \quad \ldots\ldots\ldots \quad (7)$$

where A is a constant dependent on the strain distribution and of order 2 for a Cauchy strain distribution, and $1/2\pi$ for a Gaussian. In table 5 an intermediate value, A equal to unity has been used. Values of about 1 cal/g. are obtained which are in good agreement with measurements made calorimetrically.

Table 5. Stored Energy and Dislocation Density Values for some of the Materials Examined

Material	Atm.% solute	Treatment	Stored Energy (cals/g)	Maximum dislocation density ρ_s
Copper	0	Filed at room temp.	0·16	3×10^{11}
Copper	0	Filed at −196°c	0·3	$1{\cdot}5\times10^{12}$
Copper	0	Irradiated	1×10^{-4}	8×10^{8}
Copper–nickel	50	Filed at room temp.	0·42	1×10^{12}
Copper–zinc	27	Filed at room temp.	0·51	1×10^{12}
Copper–aluminium	5·7	Filed at room temp.	0·21	5×10^{11}
	11·0	Filed at room temp.	0·64	$1{\cdot}5\times10^{12}$
	17·0	Filed at room temp.	0·75	$1{\cdot}8\times10^{12}$
Copper–tin	7·1	Filed at room temp.	0·83	$2{\cdot}0\times10^{12}$
Copper–germanium	7·2	Filed at room temp.	0·5	$1{\cdot}3\times10^{12}$

Dislocation density values have been estimated from the method outlined by Williamson and Smallman (1956). This depends on a knowledge of both strain and particle size and consequently cannot be fully utilized here because an exact value of the coherent domain size is masked by the overwhelming fault broadening. The dislocation density ρ_s calculated from the strain broadening is

$$\rho_s=k\xi^2/F\mathbf{b}^2, \quad \ldots\ldots\ldots \quad (8)$$

where k is a constant of order $12A$, $\mathbf{b}$ is the Burgers vector and F is a strain energy factor. The dislocation density ρ_ρ calculated from the particle size is

$$\rho_\rho=3/\epsilon^2. \quad \ldots\ldots\ldots \quad (9)$$

The inequality of eqns (8) and (9) indicates the probable dislocation arrangement and in the case of a piled up array F equals n, the number of dislocations in the pile-up, and

$$\rho_{\text{true}}=(\rho_\rho\rho_s)^{1/2}. \quad \ldots\ldots\ldots \quad (10)$$

Taking a reasonable estimate for the particle size of about 10^{-5} cm it is apparent from eqns. (8) and (9) that the dislocation arrangement is piled

up in all cases ; the pile-ups being larger for the alloys and also for pure metals on low temperature deformation.

§ 6. Discussion

In all the alloys examined the faulting probability is low for dilute solutions and increases with increasing solute concentration. It has been suggested (Barrett 1952 a, b) that the reason for this is that the difference in energy between hexagonal close packing and face-centred cubic packing is reduced as the α-phase boundary is approached. This appears to be borne out by fig. 1 since the faulting probability increases more rapidly the smaller the range of α-solid solution. Difference in atomic size between copper and the solute cannot alone account for the variation, since germanium although equally effective in producing faults has a much smaller misfit value than tin. Arranging the solutes in order of increasing valency Ni, Zn, Al, Sn, Ge the atomic misfit values $\{(1/a)da/dc\}$ are 0·025, 0·062, 0·063, 0·28 and 0·062 respectively. A correlation with all the factors affecting primary solid solution is probably more significant, but tells us little of the origin or form of the faults involved.

It is of interest to note that if the origin of the stacking faults is the region bounded by separated half dislocations the dislocation density is sufficient to account for the observed values of α. With this assumption α represents the fractional areas of the close-packed planes contained within these dislocations. Thus if ρ is the dislocation density and r the width of the extended dislocations the stacking fault probability is given by

$$\alpha=\rho r d. \quad . \quad . \quad . \quad . \quad . \quad . \quad . \quad . \quad . \quad (11)$$

For the case of pure copper deformed at room temperature $\alpha=3\times10^{-3}$, $\rho_s=3\times10^{11}$ cm^{-2} and $d=2{\cdot}55\times10^{-8}$ cm, then r is about 15 atom spacings. The equilibrium separation of partial dislocations is given alternatively by the relation (see Cottrell 1953)

$$r=\mu a^2/24\pi\gamma, \quad . \quad . \quad . \quad . \quad . \quad . \quad . \quad . \quad . \quad (12)$$

where μ is the shear modulus and γ the stacking fault energy. Thus eliminating r between eqns. (11) and (12) gives a relation connecting the dislocation density, faulting probability and faulting energy

$$\alpha=\mu a^3\rho/24\sqrt{2}\pi\gamma. \quad . \quad . \quad . \quad . \quad . \quad . \quad . \quad . \quad (13)$$

It is difficult to test this formula in practice since measurements are made on powders to obtain high deformations and also because line shifts in bulk specimens may be due to residual intergranular stresses (Greenough 1952). However fig. 5 shows α plotted against ρ for pure copper, deformed at room temperature and liquid nitrogen, and for some of the alloys. The slopes of the graphs give

$\gamma_{\text{Copper}}\simeq20$ ergs cm^{-2}, $\gamma_{\text{Copper-Nickel}}\simeq35$ ergs cm^{-2} and $\gamma_{\text{Alloys}}\simeq10$ ergs cm^{-2}.

Although these results are in good agreement with measured (Fullman 1951) and predicted (Seeger 1955) energy values it must be remembered that the physical significance of the faulting probability α is uncertain.

The non-linearity of the plot for the copper–aluminium series of alloys probably indicates the variation of stacking fault energy with alloying.

Reasonable objections to the above hypothesis may be raised on the grounds that other evidence at present available points to the existence of wide faults. The oscillation photographs taken by Barrett (1950) of supersaturated copper–5% silicon alloys show clearly sharp rods in reciprocal space. This indicates the existence of wide stacking faults

Fig. 5

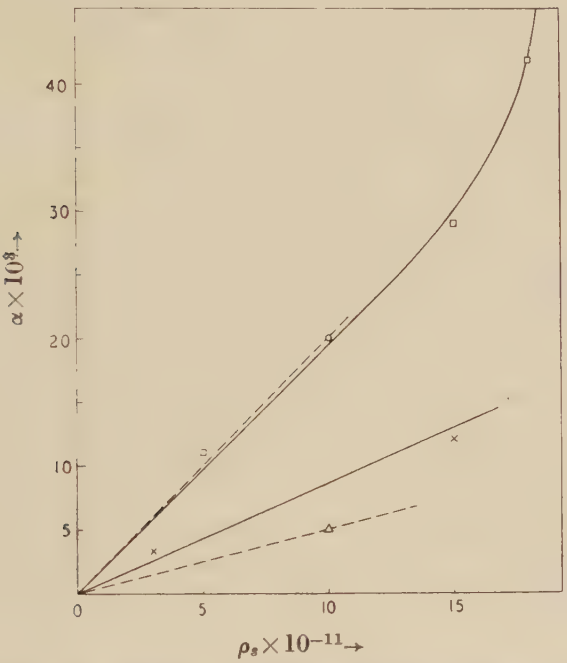

Plot of stacking fault probability versus dislocation density for × copper, △ copper–50% nickel, ○ copper–27% Zn, □ copper–aluminium.

rather than ribbons of faults as is expected from extended dislocations. As mentioned in § 2, α is derived on the assumption of infinite stacking faults and the diffraction pattern from finite stacking fault ribbons is not known. Similarly, the electron diffraction experiments of Hirsch *et al.* (1955) on gold foils show the existence of streaks indicating once again wide faults. It is possible, however, that the diffraction characteristics of wide faults may be produced by conditions which are expected to occur within a heavily deformed metal. For example, if a pile-up of dislocations against a barrier occurs then the addition of many stacking fault ribbons could lead effectively to rods in reciprocal space and the apparent existence of wide faults. On the other hand wide stacking faults may be produced similar to those shown in stainless steel by the electron microscope (Hirsch, private communication). The high

stresses present in the metals and alloys examined would certainly be sufficient to completely separate the partial dislocations. A stress σ acting normal to the Burger's vector [110] will repel the two partial dislocations completely provided

$$\sigma \cdot \mathbf{b}_{(211)} > \gamma,$$

that is

$$\sigma > 2\sqrt{6}\gamma/a. \quad . \quad . \quad . \quad . \quad . \quad . \quad . \quad . \quad . \quad (14)$$

For copper, when $\gamma = 20$ ergs cm^{-2} and $\mu = 4 \times 10^{11}$ dynes cm^{-2} the stress σ is about $\mu/160$ dynes cm^{-2}. This corresponds to a strain of 6×10^{-3} which is less than the values indicated by the line broadening measurements. It is also significant that a measurable α is only found when the strains are of the order of magnitude necessary to split dislocations completely. In copper annealed for 5000 minutes at room temperature the strain is much less than that required by eqn. (14), and in this case α is no longer measurable. An order of magnitude estimate of the stacking fault energy γ is possible from eqn. (14), provided the stress σ for which α is zero is known. Extrapolating to zero α the results for copper deformed at liquid nitrogen and also at room temperature, gives $\xi = 4 \times 10^{-3}$ and even this averaged strain yields γ about 14 ergs cm^{-2}. It is difficult to obtain more than an order of magnitude of γ since the line broadening measurements only give averaged strains. It is also possible that some splitting of the dislocations might occur near the head of a pile-up (Friedel 1955) when the average stress is lower than that given by eqn. (14), although from the line broadening analysis it appears that in recovered copper the dislocation distribution is unpiled.

Recovery at room temperature, of a specimen deformed at liquid nitrogen temperature, allows a major portion of the broadening to ' anneal out ' for the pure metal. The final ' recovered ' breadth is larger than that of a well annealed sample but smaller than that of a specimen deformed at room temperature. This indicates that the lower the deformation temperature the easier it is to recover at a given temperature. Moreover, the values of strain 7×10^{-4} and particle size 10^{-5} cm observed indicates that the dislocation distribution is essentially random. This is of interest since in copper deformed and examined at room temperature the dislocation distribution is piled-up. It therefore appears that the barriers causing a pile-up of dislocations at liquid nitrogen temperature are dispersed on ' annealing ' at room temperature. This process seems quite reasonable since the phenomenon of work softening discussed by Cottrell and Stokes (1955) relies on the combined influence of temperature and stress to unlock the barriers at the head of piled-up groups. As discussed above, with the dislocation density and arrangement known to exist in the recovered specimen any faulting would be negligible.

The inability of neutron irradiation or quenching to produce peak shifts directly, tends to indicate the absence of extrinsic faults, since, although the Paterson analysis is not worked out for this specific fault,

the effect on the diffraction pattern is expected to be similar to that for deformation faults. In addition, the low strain broadening introduced by irradiation, about 10^{-4}, indicates that few deformation faults in excess of those in the annealed state are produced and are therefore well below the limits of detection. Considering the indirect effect of irradiation, i.e. irradiation followed by deformation, it is believed that irradiating to a total flux of 5×10^{19} n.v.t. will produce mechanical behaviour analogous to that of an alloy containing 10% zinc (estimated from preferred orientation changes determined by the authors). Moreover, it is unlikely that the faulting energy is lowered as with alloying ; therefore any increase in faulting is on the borderline of detection.

Acknowledgments

We would like to thank Dr. H. M. Finniston, Dr. A. H. Cottrell and Dr. P. B. Hirsch for useful discussions during the course of this work.

References

Aarts, W. H., and Jarvis, R. K., 1954, *Acta Met.*, **2**, 87.
Barrett, C. S., 1950, *Trans. A.I.M.E.*, **188**, 123 ; 1952 a, *Structure of Metals* (New York : McGraw-Hill), p. 371 ; 1952 b, *Imperfections in nearly perfect crystals* (New York : John Wiley).
Blewitt, T. H., and Jamison, R. E., 1952, *Phys. Rev.*, **85**, 641.
Broom, T., 1952, *Proc. Phys. Soc.* B, **65**, 871.
Cottrell, A. H., 1953, *A.S.M. Relation of properties to microstructure.*
Cottrell, A. H., *Dislocations and Plastic Flow in Metal Crystals* (Oxford), p. 74.
Cottrell, A. H., and Stokes, R. J., 1955, *Proc. Roy. Soc.* A, **233**, 17.
Friedel, J., 1955, *Phil. Mag.*, **46**, 1169.
Greenough, G. B., 1952, *Progress in Metal Physics*, **3**, 196.
Hirsch, P. B., Kelly, A., and Menter, J. W., 1955, *Proc. Phys. Soc.* B, **68**, 1132.
Kunz, F. W., and Holden, A. N., 1954, *Acta Met.*, **2**, 816.
Maddin, R., and Cottrell, A. H., 1955, *Phil. Mag.*, **46**, 735.
Paterson, M. S., 1952, *J. Appl. Phys.*, **23**, 805.
Piercy, C. R., Cahn, R. W., and Cottrell, A. H., 1955, *Acta Met.*, **3**, 331.
Seeger, A., 1955, *Phil. Mag.*, **46**, 1194.
Smallman, R. E., 1955, *J. Inst. Metals*, **84**, 10 ; 1957 (to be published).
Smith, C. S., and Stickley, E. E., 1943, *Phys. Rev.*, **64**, 191.
Warren, B. E., and Warekois, E. P., 1955, *Acta Met.*, **3**, 473.
Warren, B. E., and Averbach, B. L., 1952, *Imperfections in nearly perfect crystals* (New York : John Wiley).
Williamson, G. K., and Hall, W. H., 1953, *Acta Met.*, **1**, 22.
Williamson, G. K., and Smallman, R. E., 1955, *Acta Cryst.*, **7**, 574.
Williamson, G. K., and Smallman, R. E., 1956, *Phil. Mag.*, **1**, 34.

The Breakdown of Parity Conservation in the π–μ–e Decay and a Test of the Two Component Neutrino Theory†

By G. B. Chadwick, S. A. Durrani, L. M. Eisberg, P. B. Jones, J. W. G. Wignall and D. H. Wilkinson
Cavendish Laboratory, Cambridge

[Received April 9, 1957]

Abstract

6149 complete π–μ–e events have been measured in nuclear emulsion. 3021 events were in ordinary Ilford G5 emulsion and 3128 were in G5 emulsion containing twice the usual amount of gelatin relative to halide. The angular correlation between the initial directions of motion of μ-meson and electron, after possible edge effects have been eliminated, is of the form $1-(0{\cdot}149\pm0{\cdot}033)\cos\theta$ in ordinary emulsion and $1-(0{\cdot}190\pm0{\cdot}033)\cos\theta$ in diluted emulsion. This demonstrates conclusively the breakdown of parity conservation and charge conjugation in both steps of the π–μ–e process. It is shown that, with the aid of other data, the partial quenching of the μ-meson's initial spin orientation may be eliminated from these data and the true correlation of the fundamental process obtained: it is $1-(0{\cdot}283\pm0{\cdot}060)\cos\theta$. This asymmetry is consistent with the prediction of the two-component neutrino theory with

$$(|f_A|^2+|f_V|^2)^{-1}(f_Vf_A^*+f_Af_V^*)=0{\cdot}85\pm0{\cdot}18.$$

§ 1. Introduction

The hypothesis of Lee and Yang (1956) that parity may not be conserved in β-interactions has been tested in a series of experiments, notably those of Wu *et al.* (1957) and Garwin *et al.* (1957). In particular several groups of observers have examined the π–μ–e decay chain using nuclear emulsions (Friedman and Telegdi 1957, Castagnoli *et al.* 1957, Biswas *et al.* 1957, Bhowmik *et al.* 1957). If parity and charge conjugation are both violated in both links of this chain then the angular distribution of electrons from μ-mesons of spin $\frac{1}{2}$ will be of the form $1+\alpha\cos\theta$ where θ is the angle between the directions of emission of μ-meson and electron. While indications of violation of parity and charge conjugation appear unambiguous in some experiments, the results so far obtained using nuclear emulsions are not so certain.

† Communicated by the Authors.

A specific objective of our emulsion experiment was to determine the coefficient α which measures the asymmetry in order to compare it with the predictions of particular models for the π–μ–e decay. The only detailed model so far proposed is that based on the 2-component neutrino theory of Salam (1957), Lee and Yang (1957), Landau (1957) and Touschek (1957). This model predicts an extreme value of $\alpha = -\frac{1}{3}$ if electrons of all energies are detected without discrimination. It also suggests that the asymmetry in the electron emission should be strongly dependent upon the energy of the electron. Now while from the experiment of Garwin *et al.* one may infer a distribution of the form $1+A\cos\theta$ with considerable accuracy the asymmetry coefficient so determined cannot be immediately related to the desired α of the fundamental process. This is because : firstly, the angular resolution so far achieved is poor and one must know how the electron detection sensitivity varies as a function of position across the face of the detector before a proper folding-in of this resolution function can be achieved ; secondly, the sensitivity of the detector varies with the electron energy in a manner which is not easy to determine with certainty ; thirdly, the degree of polarization of the μ-meson beam in terms of that for the fundamental process is not known. These difficulties are overcome by using emulsions : the angular resolution is very precise ; all electrons are detected without regard to energy ; since the complete π–μ–e chain is observed it is sure that the polarization of the μ-meson is as high as is allowed by the fundamental process. It appears at first sight, however, that these advantages are useless because the asymmetry observed for μ-mesons stopping in nuclear emulsion is appreciably lower than that observed for other substances such as carbon (see Garwin *et al.* 1957). It is therefore apparent that some ' quenching ' or loss of memory of the initial μ-meson spin orientation takes place in emulsion and so it seems that measurements in emulsion, despite the advantages listed above, cannot yield the true asymmetry coefficient α of the fundamental process. We shall show, however, that this is not so, and that the emulsion data may be analysed to give the desired true asymmetry coefficient if we make use also of the *relative apparent* asymmetry coefficients observed at Columbia for carbon and nuclear emulsion. We do not make use of the Columbia asymmetry measurements directly in obtaining our result but rather use them to deduce the degree of quenching taking place in nuclear emulsion.

The aim of the present experiment is therefore two-fold : to establish clearly the π–μ–e asymmetry in nuclear emulsions ; and to obtain a value for the true asymmetry coefficient α integrated over the whole electron spectrum.

§ 2. Experimental Method

The Columbia workers observed a weaker asymmetry in nuclear emulsion than in carbon and certain hydrocarbons. They also found

that this weaker asymmetry did not depend on the time, after the stopping of the μ-meson in the emulsion, at which they observed the electron. This last observation suggests that some μ-mesons stopped in emulsion are ' quenched ' very quickly and lose their initial polarization while others retain their spin direction for at least some microseconds. It is natural to associate the first class of mesons with those that stop in one component of the emulsion, probably the halide, and the second class with those stopping in the other component, the gelatin. This argument suggested to us that it may be possible to observe a stronger asymmetry if the content of gelatin in the emulsion were increased relative to halide. Such an enhanced asymmetry is obviously highly desirable if emulsions are to be used for similar studies of non-conservation of parity for rare particles such as the K-mesons. We therefore carried out the experiment using both ordinary Ilford G5 emulsions and identical emulsions in which the proportion of gelatin to halide is increased by a factor two (twice diluted or $\times 2$ emulsion). The two sets of emulsions were prepared at the same time from the same batches of halide and gelatin and they contained the same additives—stabilizers and so on. In order to achieve a good grain density on the minimum-ionizing electron tracks and also to minimize distortion the emulsions were not stripped but were exposed on their glass backing. The ordinary G5 emulsions showed a density for fast electrons of 30 blobs per 100 μm ; the density for the $\times 2$ emulsions was 27 blobs per 100 μm.

The emulsions were exposed to a flux of about $10^4 \pi^+$ mesons per cm^2 at the Liverpool University synchrocyclotron. The incident pion energy was about 35 Mev. The emulsions were contained in a steel box with a lining of mu-metal. The magnetic field at the position of the emulsions was measured with a flipcoil to be 0·15 gauss. This magnetic field is so weak that its effect in depolarizing the μ-mesons before they decay is completely negligible (the precession is by 1·6° in one mean life). It is sufficient, however, to effect a very large depolarization of any triplet ' muonium ' atoms (μ^+–e^-) which may be formed (a precession of about 160° in one mean life). It is nevertheless likely that such atoms would be depolarized very quickly by internal magnetic fields in so complicated a structure as nuclear emulsion.

Before processing, the total thickness, emulsion plus glass backing, was measured at several points on each plate using a dial gauge. These total thickness measurements were repeated at the same points on the processed emulsions and the thickness of the processed emulsion itself was measured at the same points under the microscope immediately afterwards. By combining these measurements we know the original thickness of the unprocessed emulsion at several points on each plate and so know the shrinkage factors accurately for the processed emulsions. The original thickness of the ordinary G5 emulsion was about 610 μm ; that of the $\times 2$ emulsion was about 480 μm (although both nominal thicknesses were 600 μm).

The emulsions were scanned using air objectives under low magnification and π–μ vertices were sought. The apparent ending of each μ-meson was examined under the same low magnification and if it appeared to end in the body of the emulsion the whole event was examined under high magnification using oil objectives. It is felt that the μ-mesons ending more than about 30 μm from either surface (in the unprocessed emulsion) would be detected as ending in the emulsion in the low power examination. We consider only complete π–μ–e events lying within a single emulsion and so we are sure of the initial direction of motion of the μ-meson whose ultimate decay we also observe.

The μ-mesons frequently suffer strong scattering but because they are very non-relativistic their spins are not rotated appreciably by these (purely electric) deviations. The angle θ which we want to measure is therefore that between the initial directions of the μ-meson and decay electron tracks.

The readings taken for each event were : the angles (read to 1°) of the μ-meson and electron tracks projected in the plane of the emulsion ; and depth measurements (read to 1 μm) for the π–μ vertex, the point along the μ-meson track whose projection on the plane of the emulsion was 50 μm from the π–μ vertex, the μ–e vertex and the point 50 μm in projected distance along the electron track ; in addition depth measurements were made for the top and bottom surfaces of the emulsion at each μ–e vertex so that the shrinkage factor was continuously monitored and we knew the closest approach of each μ–e vertex to an emulsion surface. Sometimes smaller projected distances than 50 μm had to be used for the μ-meson track because of scattering. Smaller projected distances were also used for a few very steep electron tracks as a precaution against the effects of distortion.

From these measurements and from the known original unprocessed thicknesses $\cos\theta$ was computed. The computation was programmed for EDSAC, the electronic digital computor at Cambridge University. Because of our knowledge of the original emulsion thicknesses the determination of $\cos\theta$ is rather accurate and introduces no appreciable error into our final analysis of the asymmetry.

Measurements were made on 3021 complete π–μ–e events in ordinary G5 emulsion and on 3128 complete events in the twice diluted emulsion.

§ 3. Analysis of the Results

These events should not be analysed directly because one may suspect a bias in favour of backward-moving electrons for those μ-mesons which stop very close to either emulsion surface. This bias has two origins : firstly, in many cases the decay electron can be seen even under the low power used for scanning and, if the electron is emitted into the body of the emulsion, this may draw attention to events in which the μ-meson stops so close to one surface that it might have been rejected as having left the emulsion had the decay electron been emitted, unnoticed, through

the surface of the emulsion ; secondly, when the μ-meson is identified as stopping in the emulsion, but close to a surface, there is a greater chance of failing to find the electron, under oil, if it is emitted out of the surface than if emitted (generally backwards) into the body of the emulsion. Because of this possibility of bias we analysed the results in two groups according to the distance of the μ–e vertex from the nearer surface. The first group, called the ' centre group ', is those events for which the μ–e vertex is further than 50 μm from either surface of the (unprocessed) emulsion. The second group, the ' surface group ', is the remainder. The figure 50 μm was chosen because it was felt to be a generous upper limit to the distance from a surface at which a stopping μ-meson might be mistakenly rejected as having left the emulsion in the low power scan to find the events. A warning sign that more detailed analysis is needed would be that this surface group of events show an anomalous apparent preference for backward emission of the electron.

In the ordinary G5 emulsion the centre group consisted of 2789 complete events, while 3 μ-mesons which ended in the same region of the emulsion did not give decay electrons which could be identified with certainty. The corresponding figures for the twice diluted emulsions were 2731 and 11. These numbers of missed electrons are so small as to have a completely negligible effect on the reliability of the results.

The best way to analyse the results was considered carefully. The method chosen was to assume that the distribution was of the form $1+A\cos\theta$ and to compute the mean value of $\cos\theta$, which is equal to $A/3$. It may be shown that, when the number N of events is large and when A is small, the answer given by this method approximates very closely to the maximum likelihood estimate and that the standard deviation in A so deduced is $\sqrt{(3/N)}$.

The results of this analysis are presented in table 1.

Table 1. Analysis of the π–μ–e Angular Distribution in the form $1+A\cos\theta$. Centre Group means Events whose μ–e Vertex is more than 50 μm from either Surface of the Unprocessed Emulsion ; the Surface Group is the Rest

Emulsion	Group	Events	A
G5	centre	2789	$-0{\cdot}149\pm0{\cdot}033$
G5	surface	232	$-0{\cdot}198\pm0{\cdot}11$
$\times2$	centre	2731	$-0{\cdot}190\pm0{\cdot}033$
$\times2$	surface	397	$-0{\cdot}090\pm0{\cdot}087$

We see at once that the asymmetry is established with virtual certainty. The second observation is that the events of the surface groups do not show a stronger backwards asymmetry than the bulk of the events in the corresponding centre groups. This, together with the generous nature

of the 50 μm thickness of the surface zones† and the fact that we miss only $\frac{1}{4}$% of the electrons from the centre zone‡ makes us feel confident that the values of A displayed in table 1 for the centre groups are not biassed. These A values for the centre groups we shall use later, rejecting all events in the 50 μm surface groups.

We also note that the asymmetry observed for the twice diluted emulsions is a little stronger, though scarcely significantly so, than that for the ordinary G5 emulsion. This is at any rate consistent with the idea

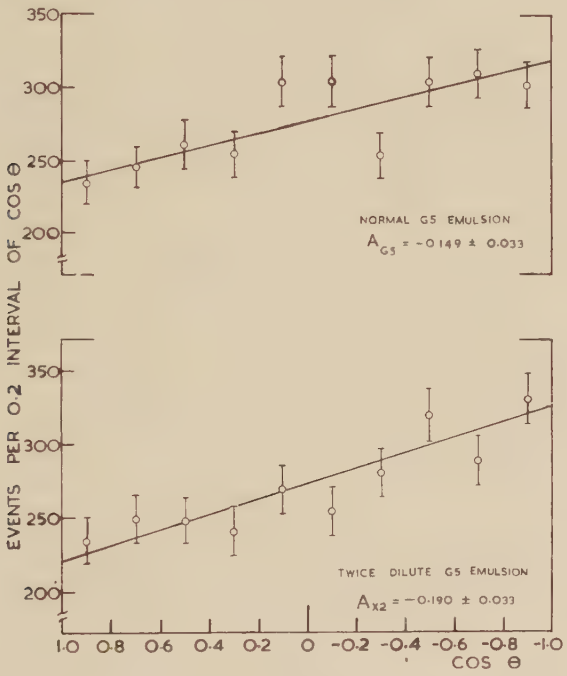

Angular distribution of the π–μ–e decays observed in ordinary G5 emulsion (top graph) and in twice-diluted emulsion, containing only half as much halide relative to gelatin (bottom graph). The errors shown are the square roots of the numbers of events represented by the points and the full lines correspond to the asymmetry coefficients displayed in table 1 for distributions of the form $1+A\cos\theta$, where θ is the angle between the initial directions of motion of the μ-meson and electron. The events shown here are only those of the centre groups for which the μ–e vertex is at least 50 μm from either surface of the unprocessed emulsion.

† Even when the analysis was repeated for surface zones of only 25 μm no significantly stronger backward asymmetry emerged.

‡ In a very few cases what appeared to be a decay electron was displaced by a few microns from the end of the μ-meson track. Scattering of the electron through a large angle very close to its origin is most unlikely and it is conceivable that we are here witnessing the diffusion of a neutral muonium atom prior to its decay. We are informed by Professor G. Bernardini that a similar phenomenon has been noticed by workers in Rome.

that the quenching of the μ-meson spin orientation takes place chiefly in the halide. In the figure we display the angular distributions themselves, grouping the events in 0·2 intervals of $\cos\theta$. The distributions are well-behaved and quite consistent with the assumed form of $1+A\cos\theta$.

For comparison the results of other workers using emulsions (see § 1) (in all cases ordinary G5) are gathered in table 2.

Table 2. Asymmetry Coefficients for π–μ–e Decay as Measured by other Workers using Nuclear Emulsions

Authors	Events	A
Bhowmik *et al.*	1562	$-0{\cdot}08\pm0{\cdot}05$
Biswas *et al.*	2003	$-0{\cdot}095\pm0{\cdot}044$
Castagnoli *et al.*	1028	$-0{\cdot}222\pm0{\cdot}067$
Friedman and Telegdi	1300	$-0{\cdot}12\ \pm0{\cdot}05$

§ 4. The True Asymmetry Coefficient

Our first objective, the demonstration of a clear asymmetry, is reached and we now consider how we may infer the true asymmetry coefficient of the fundamental π–μ–e distribution: $1+\alpha\cos\theta$. This we are obviously unable to do without calling on some other data from which we may determine the fraction γ of the μ-mesons which are quenched in the emulsion and lose their polarization before decaying.

As we remarked earlier the Columbia experiments may not be interpreted directly for a variety of reasons; they may be used, however, to give a quite accurate indication of the relative initial quenching in carbon and G5 nuclear emulsions. If, furthermore, we may assume that there is little quenching in carbon we may use the Columbia data to determine the quenching γ in emulsion, which, again following the Columbia data, we take to be rapid compared with the lifetime of the μ-meson. We would then have the true asymmetry coefficient $\alpha=A/(1-\gamma)$ where A is our apparent coefficient of table 1. The assumption that quenching is weak in carbon is likely to be a good one because just the same apparent asymmetry is observed for a variety of substances at Columbia and also at Liverpool (Cassels *et al.* 1957) including carbon and copper which certainly differ widely in their structure. It would be very surprising if the quenching were appreciable but accurately the same in such different substances. It is also known (Cassels *et al.* 1957) that with very good accuracy no loss of memory of the μ-mesons' spin orientation in carbon takes place over periods as long as 4 microseconds. Since carbon is a pure substance the most reasonable conclusion is that the quenching in it is small. We make this assumption.

The Columbia workers measure the emission of electrons in a fixed counter as the μ-mesons precess in a magnetic field. This emission shows a succession of maxima and minima as the magnetic field is changed

because of the asymmetric emission of the electron relative to the μ-meson's spin orientation. Call the observed peak-to-valley ratio for this emission R_c when the μ-mesons are stopped in carbon and R_e when they are stopped in nuclear emulsion. One may now easily show that, irrespective of the bad geometry, lengthy time gate and unknown energy response of the detecting equipment, and of the unknown degree of polarization of the μ-meson beam,

$$\gamma = 1 - \frac{R_e - 1}{R_e + 1}\frac{R_c + 1}{R_c - 1}.$$

We use the results $R_c = 1{\cdot}86 \pm 0{\cdot}07$ and $R_e = 1{\cdot}40 \pm 0{\cdot}07$ to deduce $\gamma_{G5} = 0{\cdot}45 \pm 0{\cdot}11$.

Before considering this result we turn to the problem of determining $\gamma_{\times 2}$, the quenching in the twice diluted emulsion of the second half of the experiment. This we may do, continuing our hypothesis that the quenching takes place chiefly in the halide. We do not need to assume, however, that all μ-mesons which stop in the halide are quenched. We find

$$\frac{\gamma_{\times 2}}{\gamma_{G5}} = \frac{1 - 0{\cdot}86(1-p)}{2 - 0{\cdot}86(2-p)}.$$

In the expression 0·86 is the proportion by weight of halide in ordinary G5 emulsion and p is the mass stopping power of halide relative to gelatin. p may be deduced from the standard datum that the number of particles ending their tracks in halide and gelatin in ordinary G5 emulsion stand in stopping ratio 7 : 3. This gives $p = 0{\cdot}38$ so $\gamma_{\times 2}/\gamma_{G5} = 0{\cdot}77$ and $\gamma_{\times 2} = 0{\cdot}35 \pm 0{\cdot}10$. The final result is, however, extremely insensitive to this assumed stopping ratio and changes in it over a factor of two produce changes in α small compared with errors from other sources. We have increased the error in the above value of $\gamma_{\times 2}$ to allow for this uncertainty in the stopping ratio.

We now use these values of γ to correct our observed centre group A values of table 1 to find the true asymmetry coefficient α. We display the results in table 3.

Table 3. The Observed Asymmetry Coefficients A, the Quenching Factors γ, and the Deduced True Asymmetry Coefficients α for the Two Types of Emulsion. The Mean Value of α Quoted Allows for the Fact that the Error in γ is Common to the Two Emulsions

Emulsion	A	γ	α
G5	$-0{\cdot}149 \pm 0{\cdot}033$	$0{\cdot}45 \pm 0{\cdot}11$	$-0{\cdot}271 \pm 0{\cdot}080$
×2	$-0{\cdot}190 \pm 0{\cdot}033$	$0{\cdot}35 \pm 0{\cdot}10$	$-0{\cdot}292 \pm 0{\cdot}067$
		Mean value $\alpha = -0{\cdot}283 \pm 0{\cdot}060$	

Our best value $\alpha=-0{\cdot}283\pm0{\cdot}060$ has been worked out allowing for the common errror in γ (which is more serious than those in the A values).

We now consider the effect of errors in our assumptions. Even if as much as 20% of the μ-mesons are rapidly quenched in the carbon of the Columbia experiment, instead of none as we have assumed, our final result for α would be made more negative by less than the above standard error. Again, even if it is unplausibly contended that the quenching in nuclear emulsion is complete for the gelatin phase instead of zero as we have assumed then our final value for α becomes more negative just to the limit of its present standard error. The two values for α derived from the two different emulsions are then in much poorer agreement, however, and this in itself argues for the correctness of our more reasonable assumption that the gelatin phase does not quench strongly relative to the halide phase. Finally the result is very insensitive to the assumption that some μ-mesons are quenched immediately in nuclear emulsion and that the rest retain their memory until they decay. Even if we make the diametrically opposite assumption, which is certainly contrary to the evidence of the Columbia experiments, namely that there is no immediate quenching and that all their lowered asymmetry in emulsion is due to a gradual loss of polarization exponentially with time, our result for α merely becomes more negative by 0·02 which is well within the error limits. This fortunate insensitivity is due to a happy choice of the time gate in the Columbia experiment. We see that our result for α is surprisingly insensitive to the assumptions made in deriving it. It is consistent with the extreme value $\alpha=-\frac{1}{3}$ allowed by the two-component neutrino theory and relaxation of any of our assumptions moves the experimental result into better agreement with that extreme theoretical value. Alternatively we may accept the two-component theory† and use our result to determine its parameter ξ (Lee and Yang 1957) which measures a relationship between the axial vector and vector couplings.

$$\xi=(|f_A|^2+|f_V|^2)^{-1}(f_V f_A{}^*+f_A f_V{}^*).$$

We find $\xi=0{\cdot}85\pm0{\cdot}18$.

Acknowledgments

We thank Professor J. M. Cassels and Professor H. W. B. Skinner of Liverpool University who very kindly allowed us to make the exposure

† We have throughout, in speaking of the two-component theory, had in mind the process $\mu\rightarrow e+\nu+\bar{\nu}$ because of its better prediction of the Michel parameter than such a process as $\mu\rightarrow e+2\nu$. Should these two processes in fact be mixed we are not able, of course, to say anything about ξ from our results. Their separation would have to await an accurate demonstration that the Michel parameter is less than $\frac{3}{4}$, a demonstration of double β-decay without neutrinos, a demonstration of the reactions $\nu+p\rightarrow n+e^+$ or $\bar{\nu}+n\rightarrow p+e^-$ or an accurate determination of the energy dependence of the effect discussed in this paper although this also involves one in a discussion of possible derivative couplings.

to the π^+-meson beam. We thank Dr. H. E. Daniels for considerable help with the statistical aspects of the analysis. We thank especially Dr. A. J. Oxley who wrote the programme for EDSAC and who was ever-helpful in processing the data ; we also thank Dr. M. V. Wilkes who allowed us the use of this machine.

G. B. Chadwick, S. A. Durrani, P. B. Jones and J. W. G. Wignall wish to thank respectively the following bodies for grants : the Shell Petroleum Company ; Gonville and Caius College, Cambridge ; the D.S.I.R. ; the Royal Commissioners of the 1851 Exhibition.

References

Bhowmik, B., Evans, D., and Prowse, D. J., 1957, in press.

Biswas, N. N., Ceccarelli, M., and Crussard, J., 1957, *Nuovo Cimento*, **5**, 756.

Cassels, J. M., O'Keeffe, T. W., Rigby, M., Wetherell, A. M., and Wormald, J. R., 1957, in press.

Castagnoli, C., Franzinetti, C., and Manfredini, A., 1957, *Nuovo Cimento*, **5**, 684.

Friedman, J., and Telegdi, V. L., 1957, in press.

Garwin, R. L., Lederman, L. M., and Weinrich, M., 1957, *Phys. Rev.*, **105**, 1415.

Landau, A., 1957, *Nuclear Phys.*, **3**, 127.

Lee, T. D., and Yang, C. N., 1956, *Phys. Rev.*, **104**, 254.

Lee, T. D., and Yang, C. N., 1957, in press.

Salam, A., 1957, *Nuovo Cimento*, **5**, 299.

Touschek, B. F., 1957, *Nuovo Cimento*, **5**, 754.

Wu, C. S., Ambler, E., Hayward, R. W., Hoppes, D. D., and Hudson, R. P., 1957, *Phys. Rev.*, **105**, 1413.

CORRESPONDENCE

Cold Neutron Scattering in Aluminium

By L. S. Kothari and K. S. Singwi
Atomic Energy Establishment, Apollo Pier Road, Bombay 1, India

[Received February 4, 1957 and in revised form March 4, 1957]

Zimmerman and Palevsky (1955) have reported that the scattering cross section of cold neutrons in aluminium calculated on the incoherent approximation is about 10% lower than their observed value at temperatures in the neighbourhood of 880°K. According to these authors, when correction to the incoherent approximation is applied using formula (42) of Kothari and Singwi (1955, hereafter referred to as I), the discrepancy increases still further. In view of this we thought it necessary to re-examine this problem carefully.

There can arise three possible sources of error in the calculation of the scattering cross section : (i) the use of the Debye frequency spectrum ; (ii) assumption of a constant Debye temperature Θ ; and (iii) an incorrect evaluation of the correction to the incoherent approximation. We shall now examine each of these separately.

(i) Squires (1956) has recently calculated the frequency spectrum of aluminium from its elastic constants and has shown that so far as the total scattering cross section is concerned one gets almost the same results whether one uses the exact spectrum or the one given by Debye. This, therefore, rules out (i) as a significant source of error.

(ii) Owen and Williams (1947), from their x-ray diffraction studies in aluminium, have concluded that the Debye temperature Θ decreases with increasing temperature. Variation of Θ with temperature calculated from their experimental results is shown in fig. 1. It is seen that Θ changes by about 12% in going from 300° to 800°K. Taking account of this variation and using eqn. (40) of I, which has been derived on the incoherent approximation, we have recalculated the scattering cross section as a function of temperature for 8 Å neutrons. In fig. 2, curve A represents the scattering cross section derived by assuming a constant value of Θ, whereas curve B represents the same quantity calculated by taking account of proper variation of Θ. At 800°K, a 12% change in Θ produces nearly a 12% increase in the cross section.

(iii) It appears that formula (42) of I does not give the correction to the incoherent approximation correctly, and therefore, we have not used this in the present calculations. We evaluate the one-phonon cross section both by summing over the reciprocal lattice vectors (Weinstock 1944) and also by replacing the sum by an integral (eqn. (30) of I with

Fig. 1

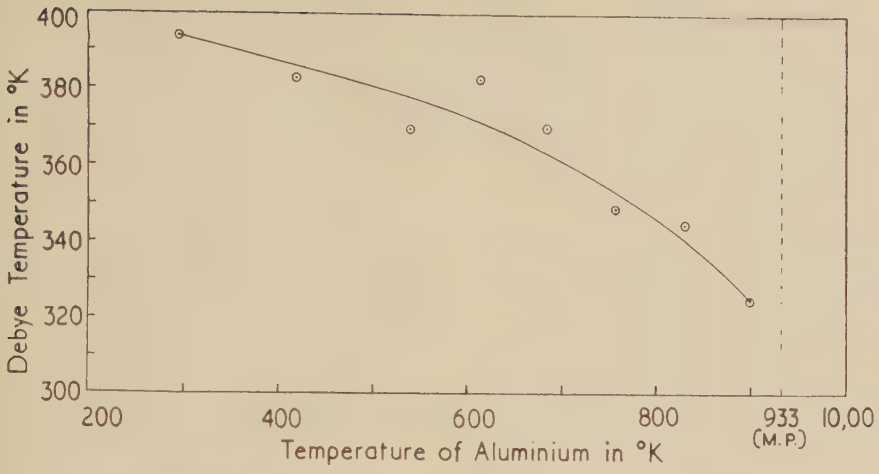

Debye temperature as a function of temperature of aluminium. Circles denote the values computed from the experimental data of Owen and Williams (1947).

Fig. 2

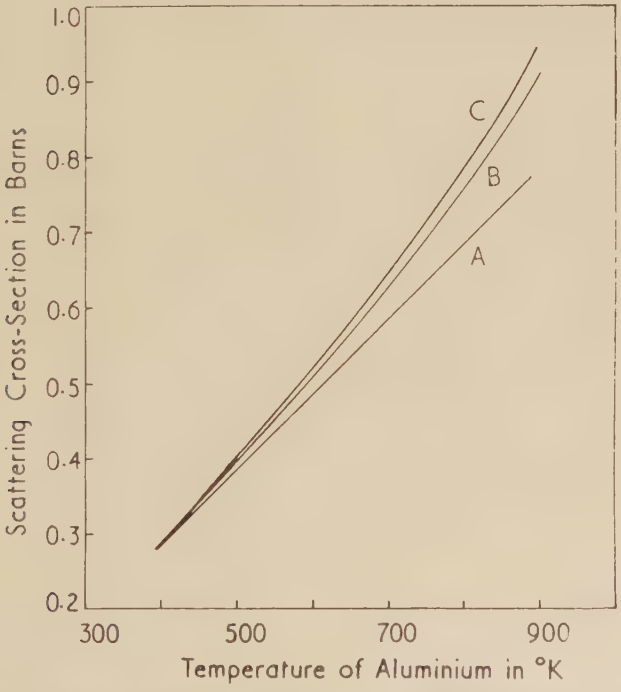

Scattering cross section of 8 Å neutrons in aluminium as a function of temperature. Curve A: multi-phonon cross section calculated on the incoherent approximation using a constant value of Θ (Θ=394°K). Curve B: same as curve A but using values of Θ as given by fig. 1. Curve C: obtained by adding to curve B correction to the incoherent approximation.

$l=1$). The difference of these two values gives us the correction to the one-phonon incoherent cross section. At 800°K this correction is about +4%, and will decrease rapidly with the order of phonon process. And since the contribution of the multi-phonon processes to the total cross section is nearly 30% at this temperature, the correction to the incoherent multi-phonon cross section will not alter the final results by more than one per cent. We may, therefore, justifiably assume that the correction to the one-phonon incoherent cross section also represents the correction to the total incoherent cross section. Further, the correction has been evaluated for a fixed value of Θ. The effect of the variation of Θ on the correction being negligible, has not been considered.

It may be mentioned that in evaluating the sum over the reciprocal lattice vectors we have used formula (51) of Weinstock (1944) but unlike him we have retained the Debye–Waller factor within the sign of integration over his variable λ, and have carried out the integration numerically.

If we now add to the cross section represented by curve B of fig. 2, the correction discussed above, we get curve C which gives the final values of the calculated cross section.

Apart from the statement of Zimmerman and Palevsky (1955) the only published value of the total cross section $\sigma_t=\sigma_s+\sigma_a$, for aluminium in the temperature range considered is at 800°K (Hughes and Harvey 1955) and is 1·83 barn. If we subtract from this the value of the absorption cross section, σ_a, for 8 Å neutrons, $\sigma_a=1{\cdot}02$ barn, the scattering cross section is $\sigma_s=0{\cdot}81$ barn. The calculated cross section (curve C of fig. 2) at this temperature is 0·79 barn. Thus the present theory and experiment agree to within 3% at this temperature. It may be mentioned that even if we take the correction to the incoherent approximation properly but neglect the variation of Θ with temperature, the calculated value of the cross section at 800°K is 15% lower than the observed value. In other words at high temperatures the effect of the variation of Θ with temperature on the cross section is more important than the correction to the incoherent approximation.

Although the theory has been found to agree well with experiment at 800°K, it would be desirable to have more experimental data available on the scattering of cold neutrons in the high temperature range.

Acknowledgment

Our thanks are due to Mr. R. C. Bhandari for his help in the calculations.

References

Hughes, D. J., and Harvey, J. A., 1955, BNL 325.
Kothari, L. S., and Singwi, K. S., 1955, *Proc. Roy. Soc.* A, **231**, 293.
Owen, E. A., and Williams, R. W., 1947, *Proc. Roy. Soc.* A, **188**, 509.
Squires, G. L., 1956, *Phys. Rev.*, **103**, 304.
Weinstock, R., 1944, *Phys. Rev.*, **65**, 1.
Zimmerman, R. L., and Palevsky, H., 1955, *Phys. Rev.*, **98**, 1162 (abstract).

A Search for Natural Radioactivity in Vanadium

By R. N. Glover† and D. E. Watt‡
Department of Natural Philosophy, The University, Glasgow, W.2

[Received January 23, 1957]

Mass spectrometer measurements by Johnson (1952) have indicated that the odd–odd nucleus ^{50}V has an energy of $2{\cdot}39 \pm 0{\cdot}12$ Mev available for decay to ^{50}Ti and $1{\cdot}19 \pm 0{\cdot}12$ Mev for decay to ^{50}Cr. Its spin has been measured to be 6 (Kikuchi *et al.* 1952, 1953, Baker and Bleaney 1952). β-decay should occur to the ground state of ^{50}Cr with spin change $\Delta I = 6$, since its first excited state is at 9·5 Mev (Endt and Kluyver 1954). Only one excited state of ^{50}Ti exists below 2·5 Mev, namely a $2+$ level at 1·58 Mev (Pieper 1952). Hence an electron capture transition with $\Delta I = 4$ accompanied by a γ-ray of energy 1·58 Mev might be expected.

Unsuccessful attempts to detect activity have been made by Sheline (1954), Strome (1954) and Selig (1954). The longest minimum half-lives have been quoted by Heintze (1955). However, the ferrovanadium source used was stated to be contaminated. Also in deducing the minimum half-life for K-capture no allowance appears to have been made for the facts that firstly, only a small fraction of the 4·5 kev x-rays could escape from a thick source (27% from a 10 mg/cm^2 source) and secondly, in only 25% of the K-capture transitions are x-rays emitted, Auger electrons, which would be absorbed in the source, being emitted in the remaining 75%. Hence the minimum K-capture half-life which can be deduced from Heintze's experiment is considerably shorter than the quoted value of 3×10^{14} yr.

A search for β-rays was carried out using the proportional counter, the apparatus and its underground site having been previously described (Glover and Watt 1957). The source of vanadium pentoxide was of average thickness 10 mg/cm^2. For the background a similar source of chromium oxide was used. The difference between source + background and background counting rates over a period of 8 hours was $+113 \pm 137$. Assuming a detectable limit of thrice the statistics and an isotopic abundance of 0·25% (White *et al.* 1956), then, taking into account β-ray absorption in the thick source, the half-life for emission of β-rays of energy >50 kev must be $>2{\cdot}4 \times 10^{14}$ yr. In case the β-rays were emitted predominantly with very low energy as in the ^{87}Rb spectrum, the measurements were extended so that pulses of energy $>1{\cdot}5$ kev could be detected, but no activity was observed.

† Present address: Naval Section, A.E.R.E., Harwell.
‡ Present address: A.W.R.E., Aldermaston.

Using the 10 mg/cm^2 source the K x-ray region was closely examined, the difference between the source+background and background counting rates over 8 hr being $+45\pm47$. Assuming the same detectable limit, then, allowing for absorption in the source of the x-rays which would be produced in only 25% of the transitions, the K-capture half-life must be $>4\times10^{13}$ yr.

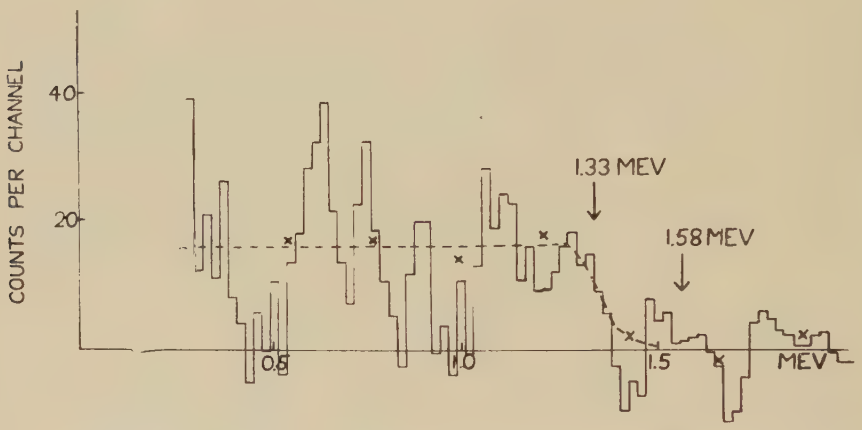

The γ-ray spectrum of ^{50}V. Each cross denotes the average excess counting rate over a group of ten channels centred about its position.

A search for γ-rays was undertaken with the scintillation spectrometer shielded by 4 in. lead lined with 4 in. steel. The 2 in. NaI crystal was surrounded by 110 g of vanadium pentoxide and by the same mass of chromium oxide for the background run. The source+background and background counting rates above an energy of 200 kev were consistent over several periods adding up to 10 hr the totals being 28503 ± 169 and 27644 ± 166 respectively, an excess of 859 ± 237. Since this excess counting rate was only 3% of the total background, the statistics were very poor as can be seen from the figure. There is no appreciable peak near 1·58 Mev but it seems significant that the spectrum drops sharply near 1·33 Mev, the energy at which the Compton edge would be expected. Also the result obtained from averaging the excess counting rate in each group of ten channels (see figure) suggests that the counts below 1·33 Mev are spread evenly over the spectrum, as would be expected for a Compton distribution. Failure to detect β-activity eliminates the possibility of β-contamination. The α-activity of both the vanadium pentoxide and chromium oxide was found to be only 2 c.p.m., the minimum level of impurity we have found to be attainable. Although tests have been carried out on the oxides of six different elements which gave this α-rate of 2 c.p.m., no γ-activity has been found to be associated with the α-activity. Therefore, it is unlikely that the activity is due to any impurity. By surrounding the crystal with a similar mass of potassium

bicarbonate in the same geometry, the γ-activity was estimated to correspond to an electron capture half-life for ^{50}V of $(4{\cdot}0 \pm 1{\cdot}1) \times 10^{14}$ yr.

Comparison of this half-life with the lower limit attainable in the proportional counter search for K x-rays shows the impossibility of detecting these x-rays using a thick source of unenriched material. It is estimated that if the search for x-rays was carried out using a minimum of 250 mg of vanadium pentoxide, 50 times enriched in ^{50}V, then a significant counting rate should be obtained.

Acknowledgments

The authors wish to acknowledge helpful discussions with Dr. G. M. Lewis, and the interest and encouragement of Professor P. I. Dee.

One of us (R.N.G.) acknowledges the receipt of a maintenance grant from the Department of Scientific and Industrial Research; the other (D.E.W.) of a Strang–Steele Scholarship.

References

Baker, J. M., and Bleaney, B., 1952, *Proc. Phys. Soc.* A, **65**, 952.
Endt, P. M., and Kluyver, J. C., 1954, *Rev. Mod. Phys.*, **26**, 147.
Glover, R. N., and Watt, D. E., 1957, *Phil. Mag.*, **2**, 49.
Heintze, J., 1955, *Z. Naturforsch.*, **10 a**, 77.
Johnson, W. H., 1952, *Phys. Rev.*, **87**, 166.
Kikuchi, C., Sirvetz, M. H., and Cohen, V. W., 1952, *Phys. Rev.*, **88**, 142; 1953, *Ibid.*, **92**, 109.
Pieper, G. F., 1952, *Phys. Rev.*, **88**, 1299.
Selig, H., 1954, *Thesis*, Carnegie Inst. Tech.
Sheline, R. K., 1954, quoted by Selig.
Strome, F. C., 1954, *Thesis*, University of Michigan.
White, F. A., Collins, T. L., and Rourke, F. M., 1956, *Phys. Rev.*, **101**, 1786.

A Search for Electron Capture in ^{176}Lu

By R. N. Glover† and D. E. Watt‡
Department of Natural Philosophy, The University, Glasgow, W.2

[Received January 23, 1957]

Recent investigations by Arnold and Sugihara (1953), Arnold (1954) and Dixon *et al.* (1954) have conclusively confirmed the β^--decay scheme of naturally radioactive ^{176}Lu first suggested by Goldhaber and Hill (1952) on the basis of unpublished work by Scharff-Goldhaber (1952). Since ^{176}Lu is an odd-odd nucleus and the middle member of the isobaric triplet ($^{176}Yb_{70}$, $^{176}Lu_{71}$, $^{176}Hf_{72}$), decay by electron capture

† Present address: Naval Section, A.E.R.E., Harwell.
‡ Present address: A.W.R.E., Aldermaston.

might also be expected. However, it was not observed by Scharff-Goldhaber (1952) nor by Arnold (1954), the latter concluding that its intensity was certainly $<10\%$ of that of the β-rays. From an examination of the L x-ray peak, Dixon *et al.* (1954) tentatively proposed that $3\pm1\%$ of the disintegrations took place by electron capture. The ground state spin of ^{176}Lu being 10, it is unlikely that electron capture occurs to the ground state of ^{176}Yb, since its spin is zero. Hence a search was undertaken for γ-rays or conversion electrons which could be attributed to an electron capture branch.

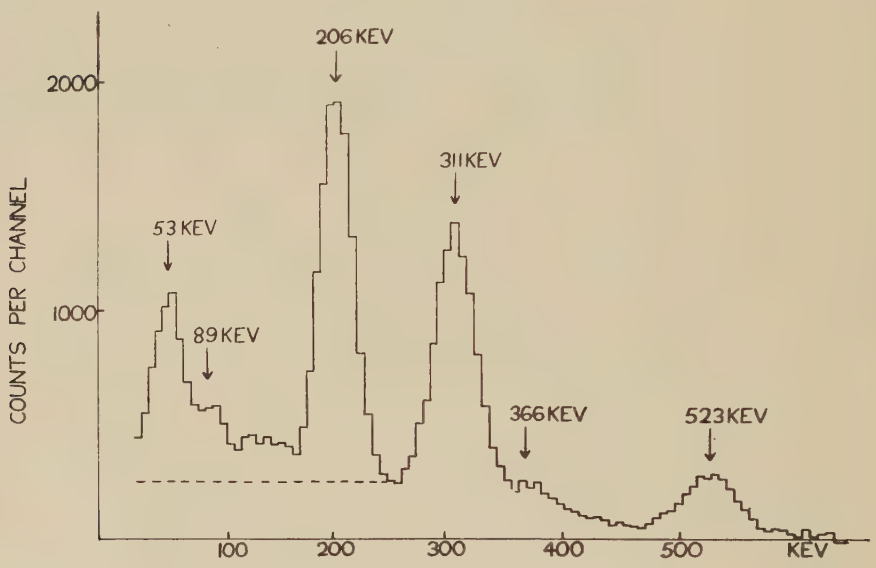

The γ-ray spectrum of ^{176}Lu.

Both the scintillation and proportional counters were located 90 ft underground as described previously (Glover and Watt 1957). The γ-ray spectrum from 500 mg of lutecium oxide placed on top of the 2 in. NaI crystal is shown in the figure. The source counting rate was 700 c.p.m. compared with the background of 80 c.p.m. The energies of the γ-rays were accurately determined to be 206 ± 5 and 311 ± 7 kev in good agreement with the values of 203 and 306 kev found by Arnold (1954). The peak at 523 ± 10 kev was due to simultaneous detection of these two γ-rays by the crystal. Similarly that at 366 kev corresponded to addition of the 311 kev γ-ray and a 55 kev x-ray. The addition peak for the 206 kev γ-ray and an x-ray would occur in the valley between the two γ-ray peaks and was obscured in the present spectrum. The incompletely resolved peak close to the K x-ray peak was due to 89 kev γ-rays which were not internally converted. There was, therefore, no indication of any peak not attributable to the known γ-radiation.

120 mg of Lu_2O_3 was spread over an area of 800 cm^2 of the proportional counter lining giving a uniform source of thickness 0·15 mg/cm^2. The anticoincidence Geiger ring was not required. The pulses were fed along a 400 ft cable to the Hutchinson–Scarrott kicksorter. There was no indication of any electron peaks other than those known to be due to internal conversion of the 89 kev γ-ray.

The half-life was estimated from the observed γ-ray spectrum. Allowance was made for the Compton distribution due to the 206 kev γ-ray (see figure). Then the remainder of the counts in the spectrum represent the total number of 311 kev γ-rays detected by the crystal either alone or in coincidence with a 206 kev γ-ray or an x-ray. A source of potassium chloride was placed in the same geometry and its spectrum taken. Knowing the specific γ-activity of potassium and calculating the average thickness of the crystal, the geometry was deduced using a value of μ_m, the mass absorption coefficient in NaI for 1·46 Mev γ-rays, interpolated from the tables given in the Appendix to Siegbahn (1955). Hence, using the value of μ_m for 311 kev γ-rays obtained from the same tables, the half-life was calculated to be $(2{\cdot}1\pm0{\cdot}2)\times10^{10}$ yr. This is in excellent agreement with the value of $(2{\cdot}15\pm0{\cdot}10)\times10^{10}$ yr. found by Arnold (1954) also from examination of the γ-ray spectrum, but not with that of $(4{\cdot}6\pm0{\cdot}3)\times10^{10}$ yr. obtained by Dixon *et al.* (1954) from examination of the β-spectrum. The half-life was also calculated from our observed β-spectrum, but an α-rate of 40 c.p.m. was obtained from the source. In the course of investigations on the natural radioelements with $Z<80$ it has been found necessary to check the purity of all sources, measurement of their α-activity, which is due to slight contamination by natural radioelements of the uranium and thorium series, being the most sensitive method. High α-rates have often been found to be associated with contamination, either β or γ, and hence the half-life calculated from the ^{176}Lu β-spectrum ($2{\cdot}8\times10^{10}$ yr.) cannot be considered significant.

It is concluded that there is no evidence of γ-rays or conversion electrons which could be associated with an electron capture branch and that the branching ratio of $(3\pm1)\%$ proposed by Dixon *et al.* (1954) might rather be regarded as an upper limit. There appears to be a marked disagreement between the half-lives reported from γ- and β-ray measurements. Unfortunately for the reason given above, it was not possible in the present investigation to determine the β-ray half-life.

Acknowledgments

The authors are indebted to Professor P. I. Dee for his interest and to Dr. G. M. Lewis for useful discussion throughout the course of these experiments.

One of us (R.N.G.) acknowledges the receipt of a maintenance grant from the Department of Scientific and Industrial Research ; the other (D.E.W) of a Strang–Steele Scholarship.

References

Arnold, J. R., 1954, *Phys. Rev.*, **93**, 743.
Arnold, J. R., and Sugihara, T., 1953, *Phys. Rev.*, **90**, 332.
Dixon, D., McNair, A., and Curran, S. C., 1954, *Phil. Mag.*, **45**, 683.
Glover, R. N., and Watt, D. E., 1957, *Phil. Mag.*, **2**, 49.
Goldhaber, M., and Hill, R. D., 1952, *Rev. Mod. Phys.*, **24**, 222.
Scharff-Goldhaber, G., 1952, reported by Goldhaber and Hill (1952).
Siegbahn, K., 1955, *β- and γ-ray Spectroscopy* (Amsterdam: North-Holland Publishing Co.).

On the Surface Free Energy and Specific Heat of a Metal

By R. Stratton
Metropolitan Vickers Electrical Co. Ltd., Manchester, 17

[Received January 3, 1957]

The surface contributions to the lattice and free electron specific heats of metals were derived by Montroll (1950) (to be referred to as M) in a paper which has only recently come to the author's attention. The lattice contribution has however been calculated on a different basis, Stratton (1953 a) (to be referred to as S), and the electron contribution can be similarly derived by extending to non-zero temperatures the calculation, Stratton (1953 b) (to be referred to as I) on the surface free energy of a metal in the normal state at absolute zero of temperature.

Since our method differs in some important details from that employed by Montroll the calculations are briefly presented although the results differ from those given by Montroll only by numerical factors which are not large enough to produce any changes of magnitude. The opportunity will also be taken to correct an arithmetical error in the derivation of the ratio (μ) of the surface free energy difference (Δf) between the superconducting and normal states, to the corresponding bulk term, Stratton (1953 c) (to be referred to as II).

(*a*) Comparing the expressions for the total number of elastic modes with angular frequency less than ω given in M (eqn. (3)) and S (eqn. (68)) it will be seen that the term $\frac{1}{4}C_2^{-1}$, or $\frac{1}{4}(C_l^{-2}+2C_t^{-2})$, in the former is replaced by $(\frac{1}{2}+Y_0^2-I_3)C_t^{-2}$ in the latter (C_l and C_t are the velocities of longitudinal and transverse elastic waves respectively, Y_0 and I_3 are functions of Poisson's ratio σ defined in S).

The difference arises because periodic boundary conditions are assumed in M so that the elastic waves can be separated into longitudinal and transverse modes whereas it is shown in S that for a free surface the normal modes have both transverse and longitudinal components. (Similar conclusions would hold for a fixed surface.) The results in M can thus be used if C_2 is replaced by

$$\frac{\frac{1}{4}C_t^2}{\frac{1}{2}+Y_0^2-I_3}=\frac{(5-6\sigma)C_2}{8(1-\sigma)(\frac{1}{2}+Y_0^2-I_3)}=L(\sigma)C_2. \quad . \quad . \quad . \quad (1)$$

For the three values of σ considered in S, $\sigma=0, \frac{1}{4}, \frac{1}{2}$: $L(\sigma)$ is given by 0·51, 0·69, 2·04, respectively. In particular the ratio between the bulk T^3 and surface T^2 term in the specific heat will be multiplied by the factor $L(\sigma)$.

(*b*) The density of electron states whose wave number k lies in the range k, $k+dk$ is given by (I, eqn. (20 *a*))

$$\rho(k)dk=(V/\pi^2)[1+d/L_z][1-\pi/(4kL_z)]k^2dk \quad . \quad . \quad . \quad . \quad (2)$$

where V is the volume of a thin flat plate of thickness $2L_z$ and d is the distance separating the position of the lattice and potential barrier surfaces. (It has also been assumed that the potential barrier height is infinite since, as the calculations in I show, a finite barrier causes a correction to the surface free energy of only a few per cent.) The second term in square brackets represents a correction due to states with the z-component of the wave number vector equal to zero, which are included in integrals over wave number space with weight $\frac{1}{2}$ but should be excluded. The corresponding expression for the density of states given, without derivation, in M differs from eqn. (2) in that d is zero and there is a positive sign inside the second square bracket.

At a temperature T the total number of electrons is given by

$$N=\int_0^\infty \frac{\rho(k)dk}{1+\exp\,[(E-\zeta)/\boldsymbol{k}T]} \quad . \quad . \quad . \quad . \quad . \quad . \quad (3)$$

where ζ is the Fermi energy, E is the electron energy and $\boldsymbol{k}$ is Boltzmann's constant. Substituting for $\rho(k)$ from eqn. (2) and expanding the integral in the usual way, neglecting terms of $0[(\boldsymbol{k}T/\zeta_0)^4]$, gives

$$N=\frac{k_m{}^3}{3\pi^2}V\left[1+\frac{\pi^2}{8}\left(\frac{\boldsymbol{k}T}{\zeta_0}\right)^2+\frac{1}{L_z}\left\{d-\frac{3\pi}{8k_m}+d\frac{\pi^2}{8}\left(\frac{\boldsymbol{k}T}{\zeta_0}\right)^2\right\}\right] \quad . \quad (4)$$

where k_m is the maximum wave number corresponding to ζ and the suffix 0 denotes values at $T=0$. Contrary to the assumption that $d=0$ in M it has been emphasized in I that d must be chosen so as to make k_m (or ζ) surface independent, i.e. the term involving V/L_z in eqn. (4) must vanish. Hence

$$d=(3\pi/8k_m)[1-(\pi^2/8)(\boldsymbol{k}T/\zeta_0)^2] \quad . \quad . \quad . \quad . \quad . \quad . \quad (5)$$

and

$$\zeta=\zeta_0[1-(\pi^2/12)(\boldsymbol{k}T/\zeta_0)^2] \quad . \quad . \quad . \quad . \quad . \quad . \quad . \quad . \quad (6)$$

Since k_m in eqn. (5) still involves T we have by using eqn. (6)

$$d=(3\pi/8k_{m0})[1-(\pi^2/12)(\boldsymbol{k}T/\zeta_0)^2]. \quad . \quad . \quad . \quad . \quad . \quad (7)$$

In a similar manner the internal energy

$$U=\int_0^\infty \frac{E\rho(k)dk}{1+\exp\,(E-\zeta)/\boldsymbol{k}T} \quad . \quad . \quad . \quad . \quad . \quad . \quad (8)$$

turns out to be

$$U=\frac{3}{5}N\zeta_0\left[\left\{1+\frac{5}{12}\pi^2\left(\frac{\boldsymbol{k}T}{\zeta_0}\right)^2\right\}+\frac{\pi}{16k_{m0}L_z}\left\{1+\frac{7}{6}\pi^2\left(\frac{\boldsymbol{k}T}{\zeta_0}\right)^2\right\}\right] \quad . \quad (9)$$

where ζ and d have been replaced from eqns. (6) and (7) respectively.

Thus the specific heat is

$$C_V = \frac{1}{N}\frac{dU}{dT} = k\frac{\pi^2}{2}\frac{kT}{\zeta_0}\left[1+\frac{7}{40}\frac{\pi}{k_{m0}L_z}\right]. \quad . \quad . \quad . \quad . \quad . \quad (10)$$

The value of C_V found in M, expressed in the same form as eqn. (10), has the factor $1/8=0{\cdot}125$ instead of $7/40=0{\cdot}175$. (N.B. The result in M can be found by putting $\zeta_0=\hbar^2k_{m0}{}^2/2m=(\hbar^2/2m)(3\pi^2N/V)^{2/3}$ and $L_z{}^{-1}=S/V$ where S is equal to the surface area).

(*c*) The last term in the equation immediately following eqn. (54) in II should be omitted. This requires the following replacements of numerical factors : $\frac{1}{8}\pi$ by $\frac{1}{4}\pi$ in eqn. (55), $\frac{1}{4}\pi$ by $\frac{1}{8}\pi$ in eqn. (56), π by $\frac{1}{2}\pi$ in eqn. (57) and 1·9 by 0·24 in eqns. (65) and (67). Thus the values of Δf and μ for mercury become 0·07 erg cm^{-2} and $1{\cdot}2\times10^{-7}$ cm respectively.

Acknowledgments

The author wishes to thank Dr. R. W. Sillars for commenting on the manuscript, Dr. Willis Jackson, F.R.S., Director of Research and Education, and Mr. B. G. Churcher, Manager of the Research Department, Metropolitan-Vickers Electrical Co. Ltd., for permission to publish this letter.

References

Montroll, E. W., 1950, *J. Chem. Phys.*, **18**, 183.
Stratton, R., 1953 a, *Phil. Mag.*, **44**, 519. (S) ; 1953 b, *Ibid.*, **44**, 1236, (I) ; 1953 c, *Ibid.*, **44**, 1247, (II).

A New Method for Decorating Dislocations in Crystals of Alkali Halides†

By D. J. Barber, K. B. Harvey and J. W. Mitchell
H. H. Wills Physical Laboratory, University of Bristol

[Received January 4, 1957]

§ 1. Introduction

Linear imperfections within transparent crystals which could, with little doubt, be recognized as dislocations were first observed in crystals of silver chloride and silver bromide by Hedges and Mitchell (1953). Amelinckx *et al.* (1955) and Amelinckx (1956) then showed that dislocations could be made visible in crystals of sodium chloride by heating the crystals in contact with sodium—a method for rendering imperfections visible which had previously been employed by Rexer (1931, 1932 a, b). Boesman *et al.* (1956) next found that a trace of silver halide had to be

† Communicated by the Authors.

present in the alkali halide before dislocations could be reliably decorated by the Rexer method. This method does, however, suffer from the disadvantage that the crystals have to be heated, in contact with sodium, to about 100°c below the melting point so that annealing structures alone can be observed. Decoration of dislocations at considerably lower temperatures has since been achieved by Van der Vorst and Dekeyser (1956) who have heated mixed crystals of sodium chloride with a few per cent of silver chloride in hydrogen at 500°c for periods of 24 hours or more. Silver then separates along the dislocation lines near the surfaces of the specimens.

The purpose of this note is to describe another method for decorating dislocations in crystals of alkali halides at relatively low temperatures.

§ 2. Experimental Method

The method consists in heating crystals of alkali chlorides and bromides with the corresponding gold halide ($HAuCl_4$, $HAuBr_4$) in evacuated, sealed-off tubes. Specimens are cleaved from large single crystals and deformed by compression or bending. They are placed in a hard glass tube together with a small quantity of the gold halide and the tube is evacuated and sealed off. The gold halide is next melted at the lowest possible temperature and the tube is slowly rotated until the specimens are covered with a very thin layer of it. The tube is then heated to a constant temperature in the range between 500°c and 750°c for a period of up to four hours and allowed to cool to room temperature. The specimens are not coloured when the tube containing them is removed from the furnace at the high temperature. A deep blue-green or blue-violet coloration develops during cooling to room temperature. After being taken from the tube, they are cleaved into thin plates which are mounted in Canada Balsam on 3 in. × 1 in. slides for microscopic examination. It has been found that the dislocations are decorated with gold by this method to a depth below the surface which depends upon the particular alkali halide and the time of heating. The definition of the dislocations depends upon the rate of cooling. Under favourable conditions, the decoration is quite continuous along the dislocation lines and there is very little separation of particles of colloidal gold elsewhere. The mechanism of decoration, which is of considerable interest, will be discussed in a more detailed paper. It appears that the configuration of dislocations which is present in the crystal at the end of the period of heating in the furnace is made visible, with little modification, by the precipitation of gold along the dislocation lines during cooling.

§ 3. Experimental Observations

Our principal aim in this work was to develop a method for decorating dislocations on slip planes in slightly strained cleavage bars of potassium bromide. This aim has been accomplished. It is hoped that the new

observations will facilitate the interpretation of the far more complex behaviour of dislocations on slip planes in crystals of silver bromide (see Mitchell 1957).

Figure 1 (Plate) is a photomicrograph (×1250) showing individual dislocations on slip planes in a crystal of potassium bromide. The crystal was very slightly deformed by bending and then heated with gold bromide in a sealed tube at 550°c for four hours. It was then cleaved into plates, 0·4 mm in thickness, with surfaces normal to the axis of bending. The dislocation lines were found to be decorated throughout the crystal by the precipitation of gold uniformly along them. The points in the photomicrograph are defined by the passage of dislocations through the focal plane of the microscope. They represent approximately equally spaced edge dislocations which are parallel to each other on any particular glide plane. Phenomena due to the climb of dislocations are not observed at this temperature. Some relaxation must occur, however, because the strain birefringence associated with the deformation disappeared when a specimen was annealed at a much lower temperature. Almost identical observations have been made with similarly deformed crystals of sodium chloride heated with gold chloride for four hours at a temperature of 650°c.

The climb of edge dislocations in crystals of sodium chloride begins about 600°c and many interesting details of the behaviour of individual dislocations and of arrays of dislocations during climb have been observed. These properties cannot be adequately illustrated with photomicrographs and three dimensional wire models which can be photographed are being made.

Figure 2 (Plate) (×1250) shows two walls of dislocations in a crystal of sodium chloride which was heavily deformed by bending and then polygonized by heating at 700°c for four hours. The lines at the top and bottom of the photomicrograph are the traces of glide planes upon which individual dislocations cannot be resolved. Similar configurations have been observed by Amelinckx in crystals of sodium chloride, containing a trace of silver chloride, which had been deformed and heated in contact with sodium.

Specimens of sodium chloride, lightly deformed by bending and then heated with gold chloride for four hours at 650°c have been found to contain many groups of closed dislocation loops with a common axis coinciding with one of the twelve ⟨110⟩ directions of the crystal. A typical system is illustrated in fig. 3 (Plate) (×4650) in which (*a*), (*b*) and (*c*) were taken with the focal plane above, coinciding with, and below the axis of the system. The trace of a slip plane appears in the left hand part of the field. We assume, as a working hypothesis, that these are derived from segments of edge dislocations by climb as discussed by Bardeen and Herring (1952). We believe that the source is associated with a cavity in the crystal which, in fig. 3 (*b*) (Plate), appears as a dark spot near the centre of the system with a loop expanding from it on the

left-hand side. Many thousands of these systems have been examined, some with one or two closed loops, and many with twenty or more loops.

A close relationship has been observed between these systems of closed loops and helical dislocations which appear, at least superficially, to be of the same type as those first observed in crystals of calcium fluoride heated in sodium and described by Dekeyser and his co-workers. A typical helical dislocation in a crystal of sodium chloride, which had been heated to 650°C for four hours, is illustrated in figs. 4 (*a*), (*b*) and (*c*) (Plate) (×3150). This helical dislocation appears to have been derived from a system of closed loops associated with a central source (shown as a dark spot in fig. 4 (*b*) (Plate) as a result of interaction with a dislocation which extended from the slip band, the trace of which is shown in the left-hand part of the field, to an adjacent slip band, which was located at a distance of approximately 8 times the width of the photomicrograph to the right. The resulting dislocation was followed continuously throughout its length. It was approximately straight from the slip band to the point where it entered the field on the right. It then followed a helix, the turns of which first contracted in radius to the position of the assumed assumed source, and then expanded again. The large individual loops of the helix, which are clearly shown in fig. 4 (*b*) (Plate), are consistent with inherent instability.

The decoration of dislocations with gold is such that they may be studied with high power microscope objectives in the bright field illumination provided by a large aperture condenser. This has not previously been possible with crystals of alkali halides. Figures 3 and 4 (Plate), which were taken with Kodak Panchromatic Microfile film using bright field red illumination, give some indication of the detail which can be observed.

§ 4. Conclusion

This method will supplement those already employed by Dekeyser and his co-workers. It allows observations of the dislocations associated with deformation structures to be made and permits details of the behaviour of dislocations during climb to be deduced. The fact that decoration is continuous along the dislocation lines is a particularly valuable feature.

Note added in proof.—It has been found since the submission of this paper that dislocations in crystals of rock salt may be very conveniently decorated with gold simply by heating them to between 600 and 700°C for four to six hours in a sealed tube containing a spiral of thin gold wire and chlorine at a pressure of 300 mm Hg (measured at room temperature). The gold precipitates along the dislocation lines at about 400°C during the cooling of the specimen and makes the configuration of dislocations which was present at that temperature visible.

References

Amelinckx, S., 1956, *Phil. Mag.*, **1**, 269.
Amelinckx, S., Van der Vorst, W., Gevers, R., and Dekeyser, W., 1955, *Phil. Mag.*, **46**, 450.
Bardeen, J., and Herring, C., 1952, *Imperfections in Nearly Perfect Crystals* (New York : John Wiley), p. 277.
Boesman, E., Remaut, G., and Dekeyser, W., 1956, *J. Chem. Phys.*, **25**, 359.
Hedges, J. M., and Mitchell, J. W., 1953, *Phil. Mag.*, **44**, 223.
Mitchell, J. W., 1957, *Report on Lake Placid Conference on Dislocations* (New York : John Wiley).
Rexer, E., 1931, *Z. Phys.*, **70**, 159 ; 1932 a, *Ibid.*, **75**, 777 : 1932 b, *Ibid.*, **76**, 735.
Van der Vorst, W., and Dekeyser, W., 1956, *Phil. Mag.*, **1**, 882.

Diffusion of Zinc in Zinc Oxide

By J. P. Roberts and C. Wheeler
Royal Aircraft Establishment, Farnborough, Hants.

[Received February 26, 1957]

In the absence of large single crystals, tracer measurements of diffusion in zinc oxide have been confined to polycrystalline material (Miller1941, Lindner *et al.* 1952) and to vapour exchange experiments on small crystals (Secco and Moore 1955, Münnich 1955, Spicar 1956). The results show considerable dispersion.

We have concluded from work referred to below that diffusion of zinc in dense polycrystalline zinc oxide is predominantly along grain-boundaries up to at least 1300°C. This supports the previous inference of Lindner *et al.* (1952) and suggests a reason why, apart from any question of non-stoicheiometry, agreement between data from polycrystalline material evaluated only in terms of uniform diffusion and data from single crystals is not to be expected.

We determined by a sectioning method the profile of diffusion of zinc-65 in sintered material (density $<93\%$, grain-size 10–$10^2\,\mu$, purity usually $>99{\cdot}9\%$) at 800–1300°C in oxygen and in argon. The tracer was initially confined to a surface layer ($\sim 1\,\mu$). After heating, the diffusion zone was progressively ground away. The residual gamma activity (A_r) of the specimen was measured at various depths (x) (Roberts *et al.* 1956). The figure shows typical results.

Constant $\partial \log A_r/\partial x$, as observed here, is to be expected if grain-boundary diffusion is predominant because the penetration of tracer then approximately obeys a simple exponential law, as predicted (Fisher 1951, essentially supported by Whipple 1954, Borisov and Lyubov 1955) and as observed in several investigations of metals. Confirmation of predominant grain-boundary diffusion in the present material was obtained by autoradiography.

From $\partial \log a/\partial x$ (where a is the activity per unit thickness at x), which here equals $\partial \log A_r/\partial x$, Fisher's theory allows evaluation of $D^{1/2}/\delta D'$, where D, δ and D' are respectively average values of the volume diffusion coefficient, grain-boundary width and grain-boundary diffusion coefficient. (The shape of our curves near $x=0$ was governed by surface roughness, which the friability of the material prevented us from reducing consistently below about ± 10 μ.) For diffusion in 1 atmos. oxygen, observations up to the present give

$$D^{1/2}/\delta D' = 10^{4\mp 2} \exp\left(\frac{+24 \pm 12 \text{ kcal mole}^{-1}}{RT}\right) \text{sec}^{1/2} \text{ cm}^{-2}.$$

We are investigating the reason for the appreciable scatter, also found with polycrystalline material by Lindner *et al.* (1952), and the result will be published later. The range of $D^{1/2}\delta D'$ values obtained is however no greater than one order of magnitude at all temperatures used (the reversed signs of the uncertainties in the above equation will be noted) and it is possible to make certain deductions now.

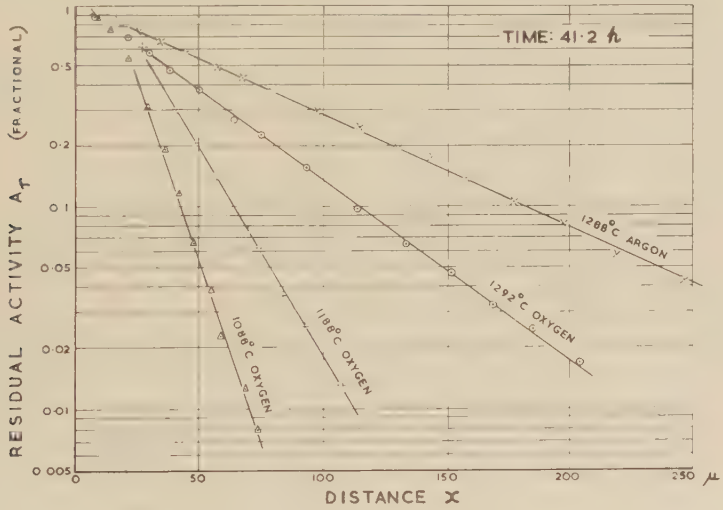

Diffusion of zinc-65 in polycrystalline zinc oxide.

No measurements on single crystals in oxygen have been reported, but in 1 atmos. oxygen it is likely that

$$D = 10^{-1} \exp\left(\frac{-89 \text{ kcal mole}^{-1}}{RT}\right) \text{cm}^2 \text{ sec}^{-1}$$

approximately. (The most probable value of activation energy given by Spicar (1956) from crystals in zinc vapour is combined with $D \sim 10^{-13}$ cm^2 sec^{-1} at 1300°c, deduced from our autoradiography.) With the usual assumption that $\delta = 5 \times 10^{-8}$ cm at all temperatures,

$$D' = 10^{3\mp 2} \exp\left(\frac{-69 \pm 12 \text{ kcal mole}^{-1}}{RT}\right) \text{cm}^2 \text{ sec}^{-1},$$

giving D' within one order of magnitude between 800 and 1300°C. The ratio of grain-boundary volume activation energy is $0{\cdot}77 \pm 0{\cdot}13$, which is reasonable.

$D^{1/2}/\delta D'$ in 1 atmos. argon ($<10^{-2}$ mm Hg oxygen) (see figure) was smaller than in 1 atmos. oxygen by up to an order of magnitude between 800 and 1300°C. The fractional excess zinc content of some of our sintered material at 1300°C, measured by a chemical method developed in this laboratory (Allsopp 1957), changed from 3×10^{-6} in 1 atmos. oxygen to 2×10^{-5} in 1 atmos. argon, suggesting a connection between $D^{1/2}/\delta D'$ and composition. Since composition might be expected to affect D more than D', the present results imply that *under our conditions* D may decrease with increasing excess zinc. This picture is less easily reconciled with the commonly assumed model of zinc oxide containing interstitial zinc than with a model involving only anion and cation vacancies.

References

Allsopp, H. J., 1957, *The Analyst* (in the press).

Borisov, V. G., and Lyubov, B. Ya., 1955, *Fizika Metallov i Metallovedenie*, **1**, 298.

Fisher, J. C., 1951, *J. Appl. Phys.* **22**, 74.

Lindner, R., Campbell, D., and Åkerström, Å., 1952, *Acta Chem. Scand.* **6**, 457.

Miller, P. H., 1941, *Phys. Rev.* **60**, 890.

Münnich, F., 1955, *Naturwissenschaften*, **42**, 340.

Roberts, J. P., Hutchings, J., and Wheeler, C., 1956, *Trans. Brit. Ceram Soc.* **55**, 75.

Secco, E. A., and Moore, W. J., 1955, *J. Chem. Phys.* **23**, 1170.

Spicar, E. G., 1956, *Thesis* (Dr. rer. nat.), Technische Hochschule, Stuttgart.

Whipple, R. T. P., 1954, *Phil. Mag.* **45**, 1225.

Circular Polarization of γ-rays : Further Proof for Parity Failure in β Decay

By H. Schopper

Cavendish Laboratory, Cambridge†

[Received March 14, 1957]

Lee and Yang (1956) suggested several experiments for testing the conservation of parity in weak interactions. Two of these have been performed (Wu *et al.* 1957, Garwin *et al.* 1957‡) and have shown that parity is not conserved. Results of a third experiment (thought impracticable by Lee and Yang) are reported here. They confirm the expectation that the γ-rays emitted after β-decay at an angle θ relative to the β-particle should show circular polarization proportional to $\cos\theta$.

† Permanent address : Physikalisches Institut, Erlangen, Germany. This work was performed during a visit to the Cavendish Laboratory.

‡ The author would like to thank Dr. D. H. Wilkinson for providing preprints of these papers and for other valuable information.

Circular polarization of γ-rays can be detected through the Compton scattering by polarized electrons in magnetized iron. Of the three possible experimental arrangements [transmission (Gunst and Page 1953), back scattering (Clay and Hereford 1952) and forward scattering (Wheatley *et al.* 1955)], forward scattering seemed most favourable here.

The scattering cylinder (see figure) was thick enough ($\frac{1}{2}$ in.) to make the scattering by the magnetizing coil negligible. The mean scattering angle was about 55° which is the optimum for a quantum energy of 1·28 Mev. The effect is not smeared out appreciably by the geometry used. No influence of the stray field on the electrons was observed. β-γ coincidences were counted on a standard fast-slow circuit (resolving time 0·1 μ sec). Pulse height selectors in the slow circuits allowed discrimination against back-scattered γ-rays, annihilation radiation and slow β-particles. Random coincidences could be counted by inserting a delay of about 0·5 μ sec in the β-line.

E and P expressed as parts per hundred

—	E for $\theta=180°$	P	α Exper.	α theor.	E for $\theta\sim90°$
^{60}Co	+2·16 ±0·36	+26 ± 4	−0·41 ±0·07	−1/3	+0·67 ±0·49
^{22}Na	−2·33 ±0·52	−28 ±6	+0·39 ±0·08	+1/3	−0·80 ±0·76

The magnetic field was reversed every 5 minutes in order to eliminate drifts in the coincidence resolution. Any variations in detection sensitivity—in particular those caused by the reversal of the magnetic stray field (change of single counting rates $\lesssim 1\%$)—were eliminated by forming R, the number of coincidences divided by the product of the single counts. Let us define the polarization effect $E = 2(R_1 - R_2)/(R_1 + R_2)$ where R_1 and R_2 refer to the magnetization pointing toward and away from the source, respectively. The observed effects at 180° are shown in the first column of the table. ^{60}Co and ^{22}Na were chosen because they have allowed β-transitions with $\Delta J = 1$, which should give maximum effect. ^{60}Co emits two γ-rays in a 4–2–0 cascade; in that special case the polarization of the second γ-ray is the same as that of the first (Tolhoek and Cox 1953). Hence the results can be discussed as if Co^{60}—like ^{22}Na—emitted only one γ-ray.

The polarization of the γ-rays is shown in the second column, computed from $E = -2fP\,\sigma_p/\sigma_0$, where f is the fraction of oriented electrons in the iron (0·08 at the measured flux density of 20 000 gauss) and σ_p and σ_0 are the polarization-dependent and independent parts, respectively, of the differential Compton cross section ($\sigma_p/\sigma_0 = 0{\cdot}52$ for the geometry used).

As a check, some measurements were done at 90°. A small effect (of the order of the statistical error) was found (column 5); actually the average angle was somewhat larger than 90°. On counting random coincidences, no effect greater than the statistical error ($\sim 1\%$) was observed.

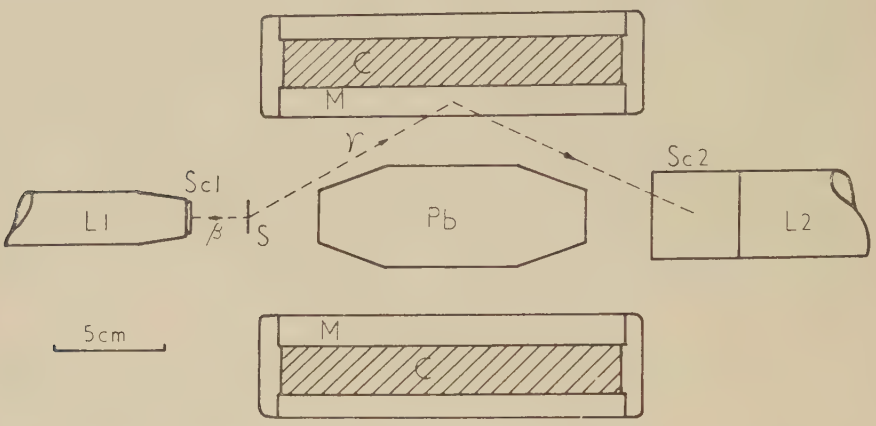

Sc1 β-counter (plastic scintillator), Sc2 γ-counter (NaI(Tl)—crystal), L1 and L2 Perspex light guides, S source, M cylindrical magnet with magnetizing coil C, Pb lead absorber.

Calculations by Skyrme (private communication†), based on the two-component theory give $P = \alpha(v/c)\cos\theta$, where α depends on the type of the β- and γ-transition (and is zero for pure Fermi interaction). Theoretical values of α are given in column 4 of the table.

The experimentally determined sign for ^{60}Co fits the experiment of Wu *et al.* The different signs for ^{60}Co and ^{22}Na prove that the antineutrino emitted together with a negatron has the opposite screw sense from the neutrino which accompanies the positron decay. The experimental values of α are somewhat higher than the theoretical ones but the deviations are within the experimental errors.

Acknowledgments

I am very grateful to Professor O. R. Frisch for enabling me to perform this experiment and for his continued interest and helpful suggestions, and to many colleagues of the Cavendish Laboratory, in particular Dr. S. D. Bloom for lending me the coincidence circuit and for discussions on the electronics. My stay in England was made possible by a grant of the German Ministry of Atomic Affairs.

† I am indebted to Dr. Skyrme and Dr. Mandl for giving me the results of their calculation before publication, and for helpful discussions.

Note added in proof: In the meantime, ^{24}Na (allowed transition, $\Delta I=0$) has been investigated; only a small asymmetry $E=+0{\cdot}56\%\pm0{\cdot}38\%$ was found. The thoery (K. Alder, B. Stech and A. Winther, private communication) predicts a large asymmetry except for practically pure Fermi or Gamov–Teller transitions; our result means that

$$C_T^2|M_{GT}|^2/(C_T^2|M_{GT}|^2+C_S^2|M_F|^2)$$

is either $>99\%$ or $<2\%$. In cases where both interactions are present in comparable amounts it would be possible to find the relative sign of C_S and C_T. I wish to thank D. J. Chandlin for helpful discussions.

References

Clay, F. P., and Hereford, F. L., 1952, *Phys. Rev.*, **85**, 675.

Garwin, R. L., Lederman, L. M., and Weinrich, M., 1957, *Phys. Rev.*, **105**, 1415.

Gunst, S. B., and Page, L. A., 1953, *Phys. Rev.*, **92**, 970.

Lee, T. D., and Yang, C. N., 1956, *Phys. Rev.*, **104**, 254.

Tolhoek, H. A., and Cox, J. A. M., 1953, *Physica*, **19**, 101, 673.

Wheatley, J. C., Huiskamp, W. J., Diddens, A. N., Steenland, M. J., and Tolhoek, H. A., 1955, *Physica*, **21**, 841.

Wu, C. S., Ambler, E., Hayward, R. W., Hoppes, D. D., and Hudson, R. P., 1957, *Phys. Rev.*, **105**, 1413.

The Weak Lines in the Radium D Gamma Spectrum

By A. C. L. Barnard† and B. C. Haywood‡

University of Birmingham

[Received January 15, 1957]

Prior to 1939 the decay of radium D (^{210}Pb) was regarded as a simple and well understood β-decay to the 46·5 kev level of ^{210}Bi (the β_{46} transition). However Lee and Libby (1939) showed that only about three-quarters of the disintegrations follow this mode, and this prompted re-examination of the RaD γ-spectrum. Results reported between 1939 and 1954§ showed a number of weak lines, summarized by Wu *et al.* (1953) as follows.

Energy (kev)	46·5	42·6	37±0·5	31±0·8	23·2±0·6	16·1±0·4	7·3±0·7
Intensity %	2·8±0·6	0·2±0·1	0·2±0·1	0·4±0·2	~1	—	~10

Wu succeeded in showing that the lines at 7·3, 16·1 and 23·2 kev originated from secondary, atomic processes, but no conclusion was offered on the 31, 37 and 42·6 kev lines. Ignoring these, a decay scheme

† Now at A.E.I. Ltd. Research Laboratory, Aldermaston Court.

‡ Now at A.E.R.E., Harwell.

§ The summarized results of 16 papers in this period are tabulated by Fink *et al.* (1956).

was postulated in which $(92\pm5)\%$ disintegrations go through the 46·5 kev level, a ground-to-ground β-transition (β_0 transition, maximum β energy $\sim$65 kev) being suggested as accounting for the remaining $(8\pm5)\%$ disintegrations. Fink *et al.* (1956) are repeating some measurements with the object of showing that β_{46} accounts for all disintegration, but Stanners and Ross (1956) claim to have detected the β_0 transition in $(15{\cdot}5\pm3{\cdot}5)\%$ of the disintegrations.

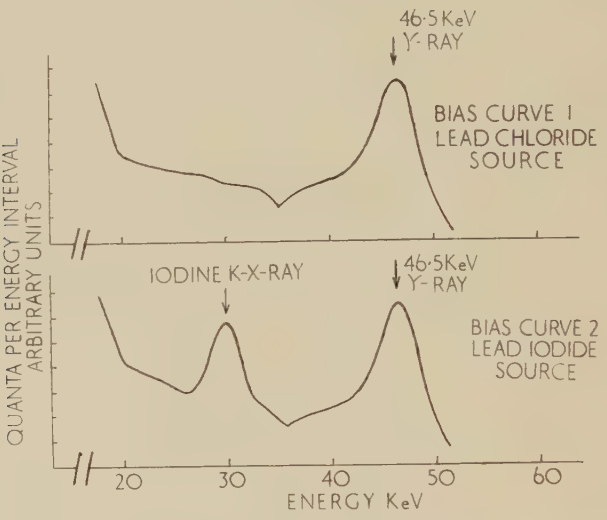

Dependence of gamma spectrum of radium D on chemical form of source. (Curves uncorrected for counter efficiency.)

The weak γ lines have been the subject of conflicting reports in which both energies and intensities have varied considerably. For example, Ewan and Ross (1952) put an upper limit of $0{\cdot}1\%$ on the intensity of the 31 kev line reported earlier, whereas Damon and Edwards (1954) report a definite line at 31 kev. Fink *et al.* (1956) suggest that the radiation in the 31 kev region originates from the selective action of an aluminium absorber on the β-bremsstrahlung from RaE (if present) but the effect of this is to introduce only an extremely broad, low hump starting at 20 kev and merging into the 46·5 kev peak. The reports suggest that a more definite peak has been seen by some workers. In another paper Fink and Robinson (1956) suggest that the 42 kev line could be caused by Compton scattering of the 46·5 kev quanta.

The comparatively intense line which had been reported at 7 kev was shown both by Wu *et al.* and by West (quoted in Jaffe and Cohen 1953) to arise from fluorescence induced in nearly copper, iron or nickel (e.g. brass counter walls) by radiation from the source. This effect is now well known, but the similar effect, fluorescence induced in atoms present in the source (either as impurity or as a chemical constituent) has not been mentioned in the literature.

Electrons from the conversion of 46·5 kev quanta are emitted in $(85\pm5)\%$ of the disintegrations, about 75% of these conversions being in the L-shell, and unconverted quanta of this energy in about 7% of the disintegrations (Wu *et al.* 1953). This is much smaller than the conversion coefficient derived theoretically by Gell-Man *et al.* (1952) but corrections to the theory by Sliv (1951), Sliv and Listengarten (1952), Rose (1955), Ward and Mihelich (1956) and Church (1956) give better agreement. The β_0 transition will produce low energy electrons in some cases, but it seems that β or γ radiation of energy greater than 30 kev is emitted in about 90% disintegration. Such radiation could induce K-fluorescence in atoms up to Sm (atomic number, $Z=62$) but the intensity would be greatest below $Z=54$, the highest element that can be excited by the L-conversion electrons.

This effect in source atoms was noticed in this laboratory in 1954, and is illustrated in the figure. Bias curve 1 was obtained with an argon-filled, thick window (1·5 mm glass) proportional counter, and a solid external RaD source in the form of lead chloride, mounted on a 250 mg cm^{-2} copper tray. Bias curve 2 is for a lead iodide source, under identical conditions, and shows the iodine K–x-ray very prominently. The intensity of this line is about 20% of that of the 46·5 kev line, using theoretical values for the efficiency of the counter at the two energies.

In the literature the chemical form of the source and the chemical separation procedures are frequently inadequately described when the detection of a very weak line is claimed. It is not therefore possible on the basis of published information, to say whether or not some of the radiations reported could arise from fluorescence in a chemical component or impurity in the source, but the general inconsistency might well arise from a factor such as this, not usually specified and probably varying from experiment to experiment. In particular a line in the region of 31 kev could be caused by the fluorescence of a Ba ($Z=56$) impurity, although this could not be excited by the L-conversion electron group.

Acknowledgments

The authors wish to thank Professor W. E. Burcham for his interest, Dr. S. C. Curran, F.R.S., for helpful comments, Dr. P. Reasbeck for the chemical processing of the source and the Department of Scientific and Industrial Research for maintenance grants.

References

Church, E. L., 1956, *Bull. Amer. Phys. Soc.*, **1**, 330.
Damon, P. E., and Edwards, R. R., 1954, *Phys. Rev.*, **95**, 1698.
Ewan, G. T., and Ross, M. A. S., 1952, *Nature, Lond.*, **170**, 760.
Fink, R. W., and Robinson, B. L., 1956, *Rev. Sci. Instrum.*, **27**, 712.
Fink, R. W., Warren, G. W., Edwards, R. R., and Damon, P. E., 1956, *Phys. Rev.*, **103**, 651.

Gell-Man, H., Griffith, B. A., and Stanley, J. P., 1952, *Phys. Rev.*, **85**, 944.
Jaffe, A. A., and Cohen, S. G., 1953, *Phys. Rev.*, **89**, 454.
Lee, D. D., and Libby, W. F., 1939, *Phys. Rev.*, **55**, 252.
Rose, M. E., 1955, *Beta and Gamma Ray Spectroscopy* (Amsterdam : North Holland Publishing Co.), p. 905.
Sliv, L. A., 1951, *J. Exp. Theor. Phys.*, **21**, 77.
Sliv, L. A., and Listengarten, M. A., 1952, *J. Exp. Theor. Phys.*, **22**, 29.
Stanners, W., and Ross, M. A. S., 1956, *Proc. Phys. Soc.* A, **69**, 836.
Ward, T. J., and Mihelich, J. W., 1956. *Bull. Amer. Phys. Soc.*, **1**, 330.
Wu, C. S., Boehm, F., and Nagel, E., 1953, *Phys. Rev.*, **91**, 319.

The Axial Ratio of Zinc, and of the Eta and Epsilon Brasses

By F. R. N. Nabarro
University of the Witwatersrand, Johannesburg

[Received February 2, 1957]

Some years ago, Nabarro and Varley (1952) discussed the equilibrium of a hexagonal metallic lattice, taking into account only the energy of central forces between each ion and its twelve nearest neighbours, and the Fermi energy of a gas of two free electrons per atom. They calculated the energy as a fraction of a, the distance between nearest neighbours in the basal plane, and b, the distance between nearest neighbours in neighbouring hexagonal planes. It was shown that any reasonable central force always leads, on this model, to the existence of a mechanically stable close packed structure with $a=b$. Some central forces lead to a second mechanically stable structure, which is always prolate, with $a<b$. A detailed discussion was given of a particular case in which the prolate structure had $b=1{\cdot}2a$, and its binding energy exceeded that of the close packed structure by 0·23 kcal/mol.

It was pointed out that the axial ratio of zinc, and of the η brasses, differed from the value corresponding to close packing by an amount much greater than that usually observed to arise from Brillouin zone effects, and it was suggested that these alloys, including pure zinc, were prolate structures which could not be considered as being formed by perturbation of the close packed structure. This view is supported by the fact that the increase in mean atomic volume in passing from the ϵ to the η phase much exceeds the increases in passing from α to β, from β to γ, or from γ to ϵ (Owen and Pickup 1933). On the other hand, the ϵ brasses, which form when zinc is alloyed with 2–3% of copper (2·7% at 380°c), may be regarded as perturbed close packed structures.

Since the ionic radii of zinc and copper are not very different, it seems reasonable to represent the addition of copper to zinc in our model by a reduction in the number of electrons per atom, with no change in the

central force. With two electrons per atom, the central force considered by Nabarro and Varley leads to a prolate structure. In the absence of an electronic contribution, the only mechanically stable structure is close packed. We therefore expect that a reduction in the number of electrons per atom will cause the energy of the prolate structure to increase relative to that of the close packed structure. Below a certain electron/atom ratio the prolate structure becomes thermodynamically unstable, while at a still lower electron/atom ratio the prolate structure is not even mechanically stable.

Computations using the central force law assumed by Nabarro and Varley have been completed by Mr. G. Hawkes and Mr. and Mrs. R. Innes, and the resulting mechanically stable structures are shown in the following table, which uses the arbitrary units of the earlier paper.

Electrons per atom	Close packed structure		Prolate structure		
	$a=b$	Binding energy	a	b	Binding energy
2·00	1·0826	0·243178	1·0000	1·2000	0·245245
1·99	1·058	0·248903	0·9988	1·1980	0·250791
1·98	1·029	0·254941	0·9974	1·1958	0·256365
1·97	1·0140	0·261300	0·9965	1·1932	0·261962
1·96	1·0126	0·267718	0·9953	1·1908	0·267588
1·95	1·0114	0·274165	0·9935	1·1896	0·273239

The prolate structure is the more tightly bound when the electron/atom ratio exceeds about 1·962, and less tightly bound when this ratio is smaller. Thus the model predicts a sudden change of axial ratio as the concentration of copper increases. The two phases have the same energy at a concentration of 3·8% of copper, and the transformation is characterized by a slight increases in a and a large decrease in b. In fact, the two-phase ϵ-η region in brass extends from 2·7 to 13·2% copper, and the transformation $\eta \rightarrow \epsilon$ is characterized by a slight increase in a and a large decrease in b. Numerical agreement is not good, largely because the central force assumed leads to an unreasonably large axial ratio for pure zinc. Moreover, our model, which neglects Brillouin zone effects, can give no deviations from exact close packing in the ϵ phase, gives the wrong sign for the small variation of a with composition in the η phase, and does not give the observed rapid variation of b with composition in the η phase.

It seems clear that the changes of lattice parameters within either the ϵ or the η phase can be accounted for only by taking into consideration the effects of the Brillouin zone, and probably other factors. On the other hand, the Brillouin zone effects will not account for the transition

from ϵ to a highly prolate structure, although they may modify the behaviour of this transition considerably. While the model discussed here is primitive, and arbitrary in its details, it predicts a transformation of the type observed, and thus illustrates a phenomenon which is likely to be important in the theory of the systems Zn Cu and Cd Ag.

References

Nabarro, F. R. N., and Varley, J. H. O., 1952, *Proc. Camb. Phil. Soc.*, **48**, 316.

Owen, E. A., and Pickup, L., 1933, *Proc. Roy. Soc.* A, **140**, 179.

ERRATUM

In the February issue of the *Philosophical Magazine*, Vol. 2, No. 14, p. 245, the name of the author was incorrectly printed. It should read O. Krisement.

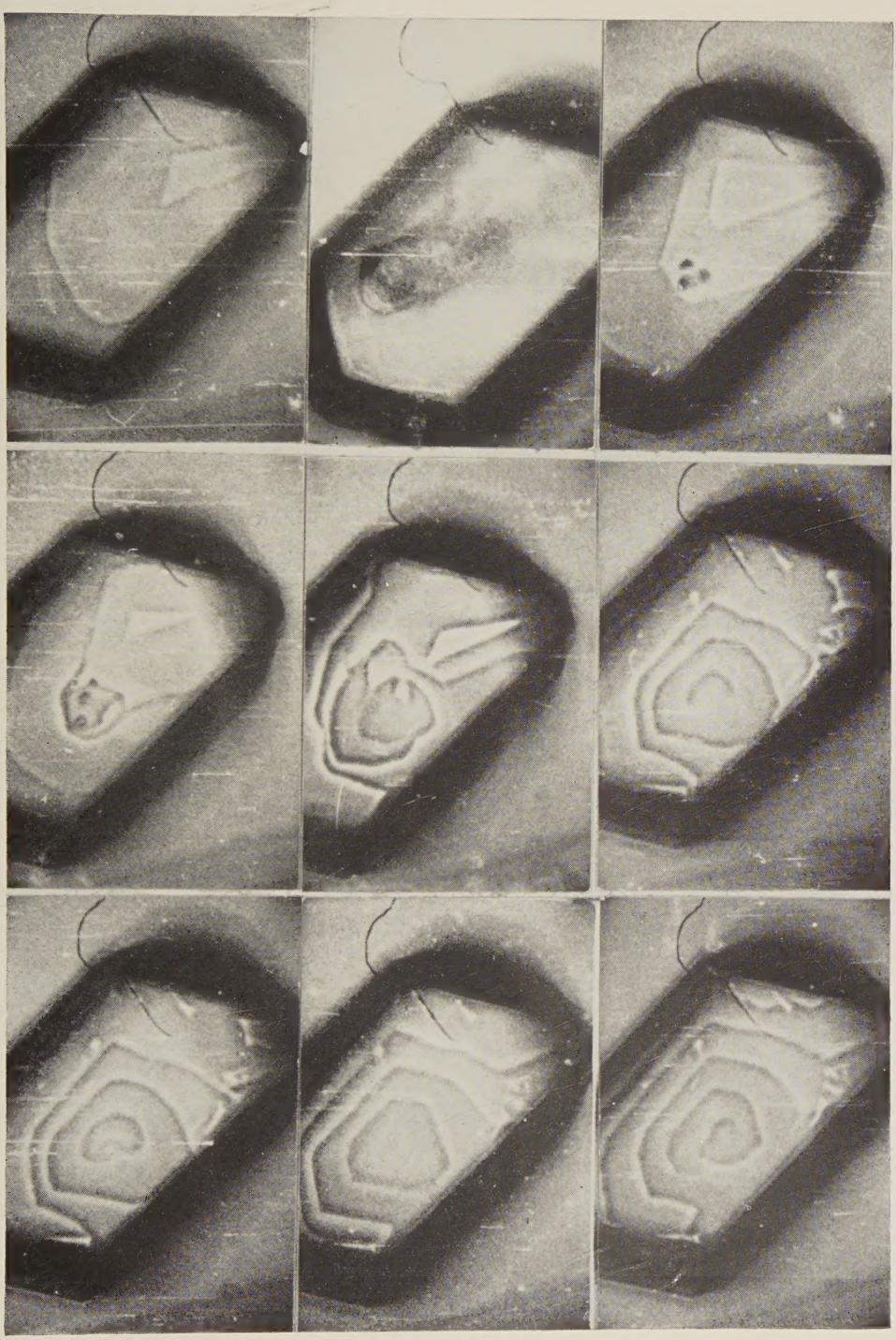

First row: Figs. 1, 2, 3. Second row: Figs. 4, 5, 6.
Third row: Figs. 7, 8, 9. (×400)

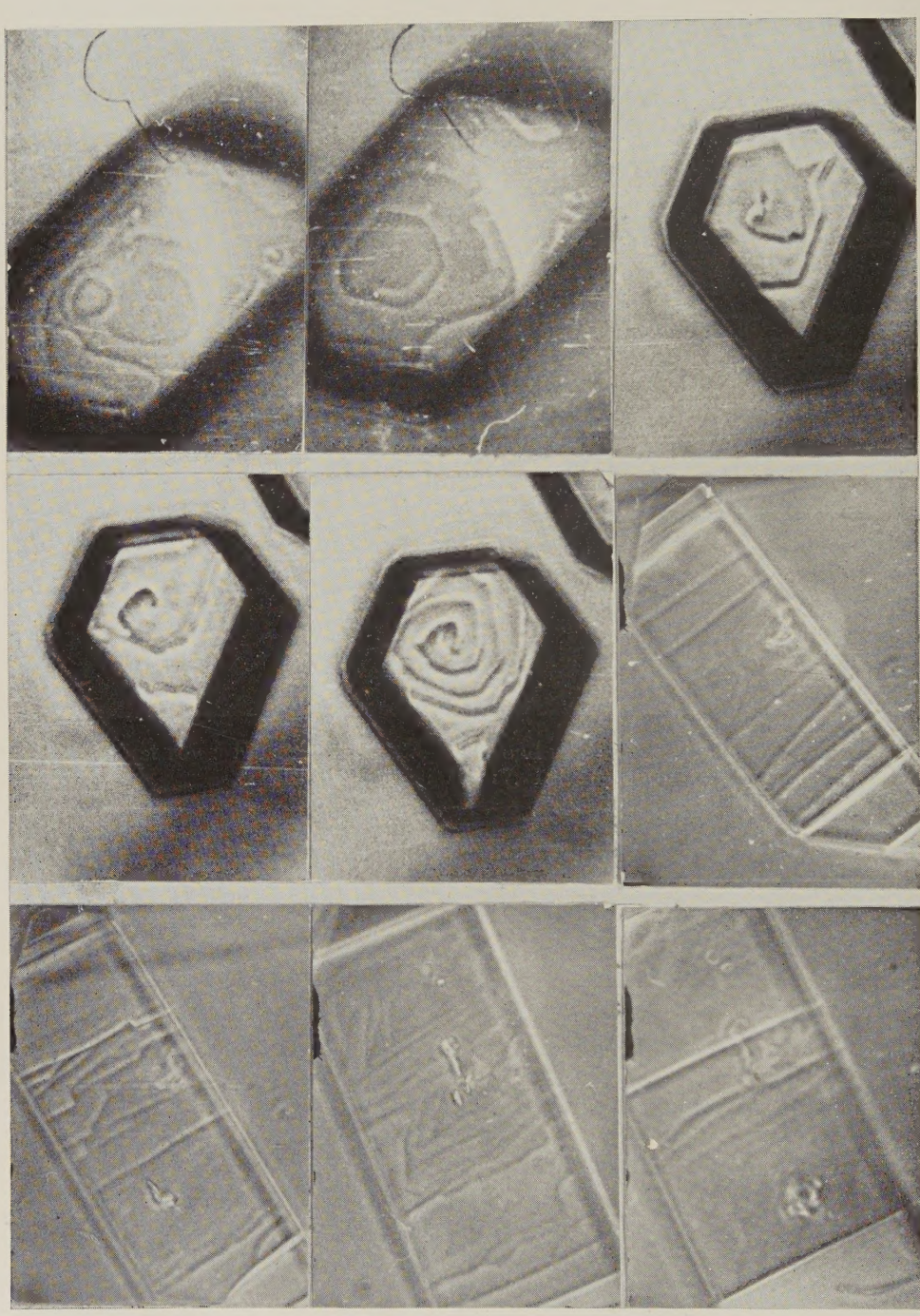

First row: Figs. 10, 11, 12. Second row: Figs. 13, 14, 15.
Third row: Figs. 16, 17, 18. (×400)

Fig. 1

Edge dislocations on slip planes in a crystal of potassium bromide made visible by decoration with gold.

Fig. 2

Two dislocation walls in a polygonized crystal of sodium chloride.

Fig. 3

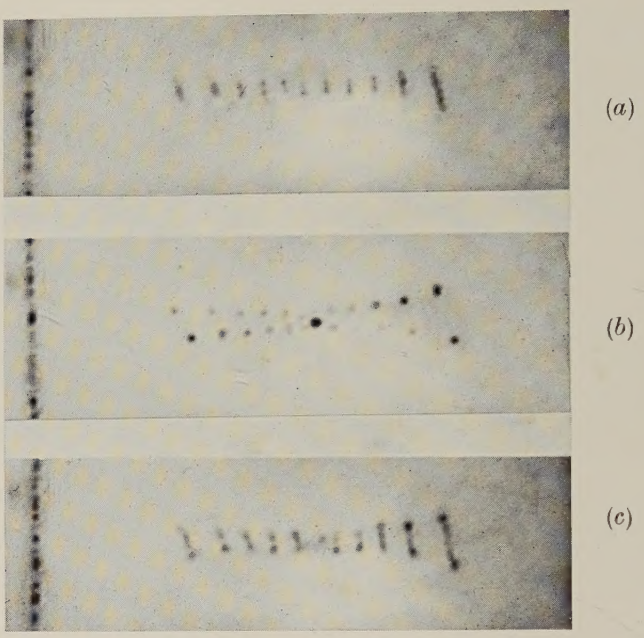

A source of closed dislocation loops in a crystal of sodium chloride.

Fig. 4

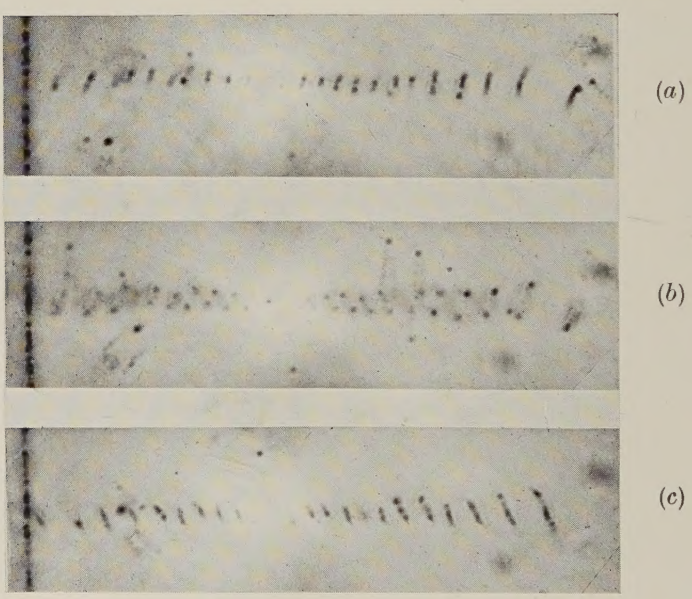

A helical dislocation in a crystal of sodium chloride.

NOTE.—In figs. 3 and 4, (*a*), (*b*), and (*c*) were taken with the focal plane of the microscope, above, coinciding with, and below the axis, of the system or of the helix respectively.